

Supersymmetry on a space-time lattice

Dissertation

Zur Erlangung des akademischen Grades
doctor rerum naturalium (Dr. rer. nat)

vorgelegt dem Rat der Physikalisch-Astronomischen
Fakultät der Friedrich-Schiller-Universität Jena

von Dipl.-Phys. Tobias Kästner
geboren am 18.07.1979 in Eisenach

Gutachter:

1. Prof. Dr. Andreas Wipf, Jena
2. Dr. habil. Karl Jansen, Berlin
3. Prof. Dr. Simon Catterall, Syracuse, NY, USA

Tag der letzten Rigorosumsprüfung: 13. Oktober 2008

Tag der öffentlichen Verteidigung: 28. Oktober 2008

For Elena & Anja
My little research fellow & my true love

Contents

1	Introduction	1
2	Numerical methods in lattice field theories	4
2.1	Lattice regulated field theories	4
2.2	Symmetries in lattice field theories	6
2.3	Physical properties from the lattice	7
2.3.1	Determination of Masses	7
2.3.2	Continuum limit & finite size effects	8
2.4	Fermions	9
2.4.1	The fermion determinant	9
2.4.2	Fermionic correlation functions	10
2.5	Monte Carlo simulation for lattice field theories	11
2.5.1	Importance sampling and Markov chains	11
2.5.2	The Hybrid Monte Carlo algorithm	13
3	Supersymmetric Quantum mechanics	15
3.1	The Model and its symmetries in the continuum	15
3.1.1	Definition and terminology	15
3.1.2	Hamiltonian formalism	16
3.1.3	Ward identities	19
3.2	Construction of (improved) lattice models	21
3.2.1	Free Theory	21
3.2.2	Interacting Theory	23
3.2.3	The Nicolai map	24
3.3	Lattice fermions	29
3.3.1	Wilson fermions	30
3.3.2	SLAC fermions	32
3.4	Numerical analysis	33
3.4.1	Free theory	34
3.4.2	Masses	35
3.4.3	Ward identities	38
4	The $\mathcal{N} = (2, 2)$, $d = 2$ Wess-Zumino model	43
4.1	The continuum model	43
4.1.1	Definition and terminology	43
4.1.2	Supersymmetries and the Nicolai map	45
4.2	Construction of the lattice actions	47
4.2.1	Complex formalism	47
4.2.2	Real formalism	48
4.2.3	Wilson Fermions	49
4.2.4	Twisted Wilson Fermions	50

4.2.5	Slac Fermions	51
4.3	Discrete symmetries	52
4.3.1	Continuum model	53
4.3.2	Lattice models	54
4.3.3	Wilson and Twisted Wilson fermions	56
4.3.4	Comparison and Summary	56
4.4	Taming the fermion determinant	57
4.4.1	The Reweighting algorithm	58
4.4.2	The Naive Inversion algorithm	61
4.4.3	The Pseudo Fermion algorithm	64
4.5	Tuning the simulations	66
4.5.1	Symplectic integrators of higher order	67
4.5.2	Fourier acceleration	70
4.5.3	Higher order integration schemes and Fourier acceleration	75
4.6	A closer look at the improvement term	77
4.6.1	Presence of Supersymmetry	77
4.6.2	Limitations for the improved models	81
4.7	Mass spectrum	90
5	Summary & Outlook	96
A	Summary (in german)	101
B	Own Publications	104

List of Figures

1	Spectrum of the supersymmetric Hamilton operator in SQM	18
2	Wilson Masses for the $d = 1$ WZ model	36
3	Slac Masses for the $d = 1$ WZ model	37
4	Ward identities for the free $d = 1$ WZ model	40
5	Ward identities for the interacting $d = 1$ WZ model using Wilson fermions	41
6	Ward identities for the interacting $d = 1$ WZ model using Slac fermions .	42
7	Masses from different lattice fermions in the $\mathcal{N} = (2, 2)$, $d = 2$ WZ-model	52
8	Classical potential for the $\mathcal{N} = (2, 2)$, $d = 2$ WZ-model	53
9	Histogram of $\log \mathcal{R}$ in the $(2, 2)$, $d = 2$ WZ-model	60
10	Cumulative distribution functions in the $\mathcal{N}(2, 2)$, $d = 2$ WZ-model	62
11	Comparison of 2nd order Leap Frog with 4th order Omelyan integrator .	69
12	Comparison of τ_{int} for std. LF and Four. acc. LF algorithm	71
13	τ_{int} as a function of m_L	72
15	Comparison of acceptance rate of std. and Four. acc. LF integrator . . .	75
16	Twopoint function from std. and Four. acc. 4th order integrator	76
17	Bosonic action computed from Slac fermions	79
19	Comparison of Wilson and Slac fermions w.r.t. the bosonic action	81
20	Fourier mode analysis for the improved model from an unphysical ensemble	82
21	[Normalized bosonic action of the unimproved model with Slac fermions .	83
22	Reduced improvement term for different lattice sizes	83
23	Analysis of the reduced improvement term for Slac and Wilson fermions .	84
24	Coupling between Wilson and improvement term	85
25	Probability distribution of ΔS_R (Slac 15×15 , $m_L = 0.7$)	86
26	Unimproved bosonic action from improved ensemble	87
27	Relation between ΔS_R , the fermion determinant and the lattice mean of φ_1	88
29	Impact of finite size effects on the extraction of fermion masses	91
30	Influence of higher excited states on the correlator	92
31	Continuum extrapolation from different lattice fermions	92
32	Comparison of mass degeneracy between improved and unimproved model	93
33	Comparison of lattice results with (continuum) perturbation theory . . .	94

List of Tables

- 1 Lattice models belonging to the $d = 1$ WZ-model 33
- 2 MC results for the continuum effective mass in the $d = 1$ WZ-model . . . 38
- 3 Possible Nicolai variables for the $\mathcal{N} = (2, 2)$, $d = 2$ WZ-Model 46
- 4 Lattice models for the $\mathcal{N} = (2, 2)$, $d = 2$ WZ-model 57
- 5 Expectation value of the bosonic action from the Reweighting method. . . 59
- 6 Bosonic action computed with the Naive inversion algorithm 63
- 7 Comparison of τ_{int} for std. LF and Four. acc. LF integrator 74
- 9 Bosonic action for Slac and Wilson fermions(quenched and dynamical) . 78
- 10 Comparison with mass formula of perturbation theory 93
- 11 Particle masses for the $\mathcal{N} = (2, 2)$, $d = 2$ WZ- model 95

1 Introduction

Supersymmetry is seen by many physicists as one of the most promising roots of extending high-energy physics beyond the well established standard model of particle physics. Despite its formidable success to describe the observed phenomenology, the deep insights into the formation of matter and into the principles by which fundamental interactions can be understood the standard model nonetheless leaves some important questions unanswered. By precisely balancing bosonic and fermionic degrees of freedom supersymmetry is capable to protect scalar masses from radiative corrections and to explain the observed hierarchy of scales in the standard model. Unification scenarios of gauge interactions also favor supersymmetric extensions since only then the running coupling constants unify properly at high energy scales. However, it is also clear that supersymmetry must be broken at some (hitherto inaccessible) scale since it has not yet been observed. Many physicists hope to see first signs of supersymmetry in the next generation collider experiments at the LHC, where physics up to a scale of a few TeV will be assessed. Moreover, in a cosmological context the heavy superpartners may constitute a promising candidate of dark matter as predicted by high precision measurements of the cosmic microwave background, e.g. COBE and (more recently) WMAP.

The standard model is build upon symmetries which comprise space-time symmetries as well as internal symmetries. In going beyond the standard model one certainly wants to maintain these guiding principle, and rather try to generalize symmetries already present. However, the celebrated Coleman-Mandula theorem [1] states that space-time and internal symmetries cannot be combined in a non-trivial manner. The loop-hole utilized by supersymmetry is to extend the notion of symmetry in a fundamental way. While the space-time symmetry generators obey the Lorentz algebra which involves commutators, supersymmetry generators extend this algebra to include anticommutators as well, i.e. the symmetry algebra becomes graded or a superalgebra. Since operators obeying anticommutation relations are normally referred to as spinors so are the supersymmetry generators. Indeed, they transform as spinors under the Lorentz group and carry spin one-half. An immediate consequence is that, if supersymmetry generators act on fields, they relate those with integer spin to those with half-integer spin. The first ever field theory furnishing a representation of such a superalgebra has been the well-known Wess-Zumino model [2] in four dimensions with two scalar fields and one Majorana spinor. Since then a wide variety of supersymmetric theories have been found and classified, e.g. supersymmetric gauge theories, supersymmetric sigma models or more general supersymmetric theories with extended supersymmetries.

Most remarkably, it turns out that the dynamics of supersymmetric quantum field theories is under much better control as compared to their non-supersymmetric counterparts. For instance, in supersymmetric theories with chiral fields parts of the classical action (the so-called F-terms) do not become renormalized. This allows for a much better understanding of the low-energy effective action of supersymmetric theories, as has been demonstrated most convincingly by Seiberg and Witten in their calculation

of the low-energy effective action of the four-dimensional $\mathcal{N} = (2, 2)$ Super Yang-Mills theory [3, 4]. It was due to the power of holomorphy and duality that in this theory a true understanding of genuine non-perturbative phenomena such as confinement or the condensation of magnetic monopoles has been achieved. Moreover, it was argued long ago by Witten that (in four dimensions) supersymmetry cannot be broken spontaneously by perturbative effects [5]. Hence, a non-perturbative approach to supersymmetric quantum field theories is very desirable. A natural candidate for this is to use lattice-regularization. However, there are many obstacles to overcome, some of them more subtle than for lattice gauge theories. Addressing those obstacles, both conceptual and technical and suggesting some solutions is the main focus of this thesis.

Once a lattice formulation of a supersymmetric field theory has been achieved its numerical evaluation poses yet another challenge. Monte Carlo simulations in supersymmetric contexts will inevitably have to include dynamical fermions, and hence a careful analysis of suitable algorithms becomes necessary. In this regard low dimensional supersymmetric lattice theories provide an excellent laboratory for the study of lattice fermions and corresponding dynamical simulations. Predictions from supersymmetry may be taken for granted and the effects or quality of a specific fermion algorithm may then be tested against this prediction (numerically or otherwise). Alternatively once efficient algorithms have been established further predictions may be confirmed numerically. For instance, the light hadron spectrum of four-dimensional supersymmetric Yang-Mills theory was determined on the lattice [6, 7] and compared with earlier results based upon an effective lagrangian approach [8].

In this thesis the lattice regularization of the one- and the two-dimensional $\mathcal{N} = (2, 2)$ Wess-Zumino model is discussed both analytically and by means of numerical simulations. A specific construction of lattice actions that preserve part of the continuum supersymmetry is described. For the first time in this context¹ the (non-local) Slac fermions have been utilized. Improvements of standard Wilson fermions are suggested and compared with the original Wilson fermions as well as with the Slac fermions.

For the two-dimensional field theory a new algorithm is constructed and found to be superior to the techniques applied previously. Thus, hitherto unfeasible lattice sizes could be analyzed, resulting in a significant improvement in precision upon previously published numerical data. Practical problems arising from the use of supersymmetrically improved lattice actions are reported for the first time and identified as a real obstruction for their use in Monte Carlo simulations. Possible remedies are discussed and compared to the supersymmetrically improved lattice models.

This thesis is organized as follows. In Sec. 2 a brief overview of lattice field theories and related numerical methods is given. The one-dimensional Wess-Zumino model is presented in Sec. 3. Problems due to a naive lattice regularization are discussed at length, and a construction scheme for a supersymmetric (or improved) lattice action is given. This leads to six different lattice models which are analyzed numerically in

¹Part of the results presented in this thesis have already been published in [9].

the remainder of Sec. 3. Next, in Sec. 4, the two-dimensional $\mathcal{N} = (2, 2)$ Wess-Zumino model will be discussed, including in brief the construction of an improved action. Besides Wilson and Slac fermions a third improved fermion type will be presented. A first problem of improved lattice actions is seen to emerge by considering additional discrete symmetries of the continuum action. It will be argued that violations of these symmetries are minimal for Slac fermions. After comparing possible algorithms for dealing with the fermion determinant the hybrid Monte Carlo algorithm is revisited and improved in a significant way. The remainder of Sec. 4 is then devoted to the numerical analysis of the various lattice models. Sec. 5 summarizes the results and concludes with an outlook on further directions that may be pursued in future research.

The compilation of this thesis is solely due to the author. However, I fully appreciate the fruitful collaboration with my colleagues from the research group on quantum theory in Jena. The numerical results of Sec. 3.4.2 and Sec. 3.4.3 were obtained together with G. Bergner who contributed to the program codes and helped with the analysis of the twopoint functions. His collaboration on the implementation of the twisted Wilson model is also gratefully acknowledged. The research that eventually led to Sec. 4.5 was done together with C. Wozar. He contributed to the program code and accomplished the fine-tuning of the simulations. The numerical analysis of Sec. 4.7 is also partly due to him. As to the new analytical results of Sec. 3.2 and Sec. 4.2 I do not claim exclusive authorship. Instead, this has been the combined effort of our research group and it remains to emphasize the contributions from S. Uhlmann and A. Wipf.

2 Numerical methods in lattice field theories

This section outlines the basic concepts upon which the material of later section is built. It is self-evident that there are a number of excellent reviews and text books on lattice field theories. To name a few the standard reference is by Montvay & Münster [10], and an updated and readable account is due to Rothe [11]. A more recent reference is Smit [12] and a useful source for numerical aspects is DeGrand & DeTar [13]. All of them have been used in the compilation of this brief introduction and are not referenced any further in the following.

2.1 Lattice regulated field theories

For the sake of simplicity a field theory describing a real scalar field in a d -dimensional space-time will be considered. A short account regarding fermions is postponed to Sec.2.4, and fields with higher spin are not required for the purpose of this thesis. The action of this very simple model is given (in Minkowski space) by

$$S = \int d^d x \left(\frac{1}{2} (\eta^{\mu\nu} \partial_\mu \varphi \partial_\nu \varphi) - V(\varphi) \right) \quad (2.1.1)$$

and contains in addition to the kinetic part a potential $V(\varphi)$ describing self-interactions amongst the field. The dynamics of the quantum theory is encoded in the Green functions

$$G(x, y, \dots) = \langle \Omega | \mathcal{T} [\varphi(x) \varphi(y) \dots] | \Omega \rangle, \quad (2.1.2)$$

where $|\Omega\rangle$ denotes the (normalized) ground state of the interacting theory and the time-ordering operator \mathcal{T} sorts field operators in such a way that those with later time appear on the left of those with earlier time. A convenient way to represent the rhs. of (2.1.2) can be found with the help of the path integral

$$Z = \int \mathcal{D}\varphi e^{iS[\varphi]}. \quad (2.1.3)$$

It can be shown that $G(x, y, \dots)$ can be computed from (2.1.3) via insertions of classical fields into the functional integral,

$$\langle \Omega | \mathcal{T} \varphi(x_1) \dots \varphi(x_n) | \Omega \rangle = \frac{1}{Z} \int \mathcal{D}\varphi e^{iS} \varphi(x_1) \dots \varphi(x_n). \quad (2.1.4)$$

The problem with Eqs. (2.1.3) and (2.1.4) is of course, that the measure $\mathcal{D}\varphi$ is at most formally defined. Different strategies have been successfully applied to address this. Besides perturbation there are at least two intrinsically non-perturbative regularization schemes. One goes under the name of exact renormalization group equations [14] while another is the lattice approach to be described in the following. In essence, the lattice provides an UV cut-off to the theory by which divergences of the original quantum

theory are rendered finite.² In order to arrive at a lattice field theory for (2.1.1) two adjacent steps are needed. Firstly, the computation of the Green functions (2.1.2) is carried out at imaginary times, i.e. take $t \rightarrow -i\tau$ for every point x_1, x_2, \dots, x_n in (2.1.4). The corresponding path integral expression is then found from (2.1.1) and (2.1.4) by the formal replacements

$$t \rightarrow \tau = it, \quad dt \rightarrow id\tau, \quad \partial_0 \rightarrow -i\partial_0 \quad iS \rightarrow -S_E. \quad (2.1.5)$$

Thus the t dependence of the field is traded for a τ dependence and the action (2.1.3) gets replaced by what is called the Euclidean action. Using this, the Euclidean path integral becomes

$$Z_E = \int \mathcal{D}\varphi e^{-S_E}, \quad S_E = \int d_E^d x \left((\partial_\mu \varphi)^2 + V(\varphi) \right). \quad (2.1.6)$$

Analogously to (2.1.4) Euclidean or imaginary-time Green functions can now be computed from Z_E . Two features make (2.1.6) much better behaved than their real-time counterparts. Firstly whenever $V(\varphi)$ is bounded, the Euclidean action is bounded as well. Moreover the oscillatory phase e^{-iS} governing the integrand of Z has been replaced by a real positive weight factor e^{-S_E} . As will be explained in Sec. 2.5 it is this latter point which makes Monte-Carlo simulations so attractive for lattice field theories. Subsequently the continuous space-time is replaced with a hypercubic lattice $\Lambda \subset \mathbb{Z}^d$ filling the original space-time with neighboring sites being separated by some distance a (the lattice spacing). The field $\varphi(x)$ is reduced to a lattice field $\varphi_L(x_L)$ which is restricted to take its values only at the discrete set of points $x_L = an_L, n_L \in \Lambda$. As a dimensional quantity the inverse of a can be interpreted as the aforementioned UV cut-off since fluctuations in the original (continuum) field which are smaller than the lattice spacing cannot be resolved by the latter. For brevity the notation $\varphi_x \equiv \varphi_L(x_L)$ will be adopted from now on, and whenever a has been set to unity the subscript x will also denote the corresponding lattice point $x \equiv n \in \Lambda$. With these definitions it is now possible to give a precise meaning to the functional measure in (2.1.6), which becomes

$$\mathcal{D}\varphi = \prod_{x \in \Lambda} d\varphi_x. \quad (2.1.7)$$

Since φ was taken to be a real field the integral measures appearing on the rhs. are given by the usual Lebesgue measure on \mathbb{R} . With an as yet unknown lattice equivalent of $S_E[\varphi]$ one finally arrives at the desired path integral expression for the lattice field theory of (2.1.1)

$$Z_E = \int \prod_{x \in \Lambda} d\varphi_x e^{-S_E[\varphi_L]}, \quad (2.1.8)$$

²Although related to a hard momentum cut-off it should not be confused with that. Most obviously this can be seen from lattice perturbation theory where propagators and interactions look different, too.

where by an abuse of notation the symbol S_E was used again for the lattice action corresponding to (2.1.6). It is interesting to note that Z_E bears a striking resemblance with the well-known partition functions of statistical mechanics. It is by this close relationship that the highly developed machinery of statistical physics is made available to the study of quantum field theory.³

2.2 Symmetries in lattice field theories

So far nothing was said about the way the action S_E is taken from the continuum to the lattice and the problem how to guarantee that the latter will eventually lead to the original (Euclidean) quantum theory if the lattice spacing is taken to zero. To elucidate the subtleties involved some remarks on symmetries are appropriate. In the RG-flow picture of non-perturbative renormalization, field fluctuations are integrated out starting at a very high UV-scale down to some IR-scale. Along this flow operators different from those present in the original microscopic action will in general emerge and finally determine the degrees of freedom of the effective action at the lower energy scale. However, if the original action is invariant under certain symmetries the effective action has to be invariant, too. This forbids a wide class of operators and severely restricts the form of the effective action. If the lattice action which defines the lattice theory at its cut-off, i.e. the inverse of the lattice spacing respects those symmetries the physics living at the lower scale is supposed to yield the same results. Conversely if the lattice action is regarded as an effective action for the continuum action it should match the former symmetries as well. At least it is anticipated that they are broken in a controllable fashion. An example for the latter is Lorentz symmetry, which reduces to a discrete subgroup of $SO(N)$ in the lattice theory. If a formulation of the lattice action is found that yields the desired continuum limit

$$\lim_{a \rightarrow 0} S_E(\varphi_x, a) = S_E[\varphi] \quad (2.2.1)$$

and keeps all symmetries even at finite lattice spacing it is supposed to do so in particular in the above limit. In the seminal articles of Wegner [15] and Wilson [16] it was shown that this is possible for local gauge symmetries and it is fast to say that lattice gauge theories and especially lattice QCD owe their formidable success to this property. If some symmetry is not respected by the lattice action relevant operators may still be matched by counter-terms in order to be able to subtract them off in the renormalized theory. This however calls for the fine-tuning of the coefficients involved and is unfeasible in most situations.⁴

As to supersymmetry no satisfactory answers how to construct a supersymmetric

³One might think here of the many powerful theorems or the thoroughly worked out methodologies of weak and strong coupling expansions.

⁴E.g., this issue is specifically cumbersome in Super Yang-Mills theories with extended supersymmetry where a plethora of relevant operators can be formed from scalar fields alone. Nonetheless there is ongoing research in this field and it was claimed that for the $\mathcal{N} = 4$ SYM theory fine-tuning can be done [17].

lattice action have yet been found. A good review dealing with various approaches was compiled by Giedt [18]. As first pointed out by Dondi & Nicolai [19] the problem involved in the construction of a supersymmetric lattice action is due to the closure of the supersymmetry algebra on infinitesimal translations. For fields furnishing a representation of the algebra this amounts to the absence of the Leibniz rule on the lattice which obviates the possibility to find a discrete subgroup of the original supersymmetry group in the lattice theory.⁵ The supersymmetry algebra must therefore be deformed to become realizable on lattice fields. Most work in this regard has been done for models with extended supersymmetry, i.e. where the algebra admits several supercharges to form a multiplet under some internal symmetry group. By rearranging the original elements of this algebra it is possible to identify a certain nil-potent sub-algebra which does no longer need the Leibniz rule to close on the fields. For Super Yang-Mills theories this is achieved by twisting the original space-time symmetry with the internal symmetry [20–23]. Related to this are topological methods trying to formulate the lattice action as a Q -exact object. This usually amounts to the inclusion of auxiliary fields and was applied to Supersymmetric Quantum Mechanics [24], the two-dimensional $\mathcal{N} = (2, 2)$ Wess-Zumino model [25], the supersymmetric nonlinear sigma model [26, 27] and to Super Yang-Mills theories [28–32] as well.

The method to be described in more detail in this thesis utilizes yet another ansatz due to a special property of supersymmetric field theories, which was first described by Nicolai [33]. Its discussion however will be postponed to Sec. 3.2 and Sec. 4.1.2 respectively.

2.3 Physical properties from the lattice

Before dealing with the subject of how to compute correlation functions from the lattice path integral numerically, it should be recalled how the extraction of physical observables proceeds from that knowledge. Special attention is given to the first excited energy level of the Hamilton operator which is most readily accessible by MC simulations.

2.3.1 Determination of Masses

To extract information about the lowest lying energy level it is sufficient to study the twopoint correlator

$$C(\tau) = \langle \varphi(\tau)\varphi(0) \rangle. \quad (2.3.1)$$

In the operator formalism using the Heisenberg picture the operator $\varphi(\tau)$ is defined by $\varphi(\tau) = e^{-H\tau}\varphi(0)e^{H\tau}$, which when inserted into (2.3.1) together with a complete set of

⁵Strictly speaking, it is known that this is impossible for locally interacting theories. As will be shown later, free theories can be lattice-regularized such that supersymmetry is preserved.

eigenstates $|n\rangle$, yields

$$C(\tau) = \sum \langle \Omega | e^{-H\tau} \varphi(0) e^{H\tau} |n\rangle \langle n | \varphi(0) | \Omega \rangle = \sum e^{-\tau(E_n - E_0)} |\langle n | \varphi(0) | \Omega \rangle|^2, \quad (2.3.2)$$

provided that the ground state $|\Omega\rangle$ is unique. For large Euclidean times τ the exponential decay of $C(\tau)$ is governed by the contribution of the first excited state

$$C(\tau) = \underbrace{|\langle \Omega | \varphi(0) | \Omega \rangle|^2}_{=0} + e^{-\tau M} |\langle 1 | \varphi(0) | \Omega \rangle|^2 + \dots \quad (2.3.3)$$

For this to hold it is assumed that the ground state expectation value of $\langle \varphi \rangle$ vanishes⁶ and that the operator $\varphi(0)$ creates some overlap between the ground and first excited eigenstate of H . The value of $M = E_1 - E_0$ can be shown to be the one-particle pole of the propagator and is hence given the interpretation of the particle's mass. In this thesis this correlator will be studied for both the bosonic and fermionic fields. This way the masses of the particles that must be equal in supersymmetric theories can be compared to each other and conclusions from the dynamics of the quantum theory w.r.t. supersymmetry can be drawn.

2.3.2 Continuum limit & finite size effects

The most delicate question to ask is how any quantity computed in the lattice theory, be it analytically or numerically, can be related to the corresponding quantity in the continuum field theory. To this end the lattice-spacing has to be taken to zero, i.e. the regulator has to be removed and Green's functions previously computed have to be renormalized as well as the coupling constants therein. For instance in the simple case of a scalar field theory the bare mass lattice parameter is related to the physical mass as

$$m_{\text{phys}} = m_L \cdot a^{-1}. \quad (2.3.4)$$

To obtain a finite physical mass in the limit $a \rightarrow 0$ the bare quantity m_L must clearly go to zero. This is the same as to say that the typical correlation length $\xi = m_L^{-1}$ has to diverge.⁷ The latter behavior is typically found in statistical physics in the vicinity of a second order phase transition and hence relates the study of critical phenomena there to the study of lattice quantum field theories near the continuum limit [34].

The technical framework to actually perform the renormalization consists of different approaches each of which is quite involved. However, for the low-dimensional theories to be considered here not much from this theory is needed. The continuum limit can be obtained in obvious manner simply by tuning the bare lattice mass to zero.

Another related problem in actual numerical calculations arises from the finite size

⁶Otherwise it must be subtracted off.

⁷Heuristically this is expected. When the correlation length diverges lattice details such as the lattice spacing become irrelevant.

of the lattice. If the lattice spacing becomes smaller and smaller also the physical space-time volume covered by the lattice will shrink. If it becomes smaller than say the Compton wave-length of the particle the physics will be different from what would be found in the infinite volume limit.⁸ In essence two competing limits have to be dealt with: the continuum limit requiring a diverging correlation length and the thermodynamic limit requiring a sufficiently large space-time volume to be taken into account

$$a \ll \xi \ll L = Na. \quad (2.3.5)$$

This of course calls for large N which makes numerical simulations so challenging.

2.4 Fermions

For the study of supersymmetric field theories it is inevitable to deal with fermions as well. After all, supersymmetry relates bosons to fermions and many of the astonishing results found in these theories are immediate consequences thereof. Hence, in numerical lattice field theories they should be treated on equal footing with the bosons of the theory, i.e. dynamically. This poses numerous problems to cope with. For instance it is well known that if the kinetic operator for the fermions is taken to be the (anti-hermitean) symmetric difference operator the lattice theory includes more fermions than wanted.⁹ This phenomenon – known in the literature as species doubling – has been known for a long time and is related to such questions as chiral symmetry or the chiral anomaly.¹⁰ In the context of supersymmetry the presence of these unwanted doublers spoils the delicate balance between fermionic and bosonic degrees of freedom. Yet this balance is a key ingredient of supersymmetry and one should ensure it stays intact. More details will be discussed when the models themselves are introduced in later sections. In the following a short account on how fermions are introduced in the lattice path integral is given together with the basic definitions for the computation of fermionic correlation functions.

2.4.1 The fermion determinant

Since the path integral (unlike the operator formalism) deals with classical field configurations this notion has to be introduced for fermionic degrees of freedom as well. To this end fields with values in a Grassmann algebra are introduced, i.e. an algebra whose elements anti-commute with each other. In contrast to the bosonic case almost

⁸Yet another problem arises for theories with degenerate ground states which may happen due to some spontaneously broken discrete symmetry. From statistical mechanics it is known that in any finite volume no spontaneous symmetry breaking occurs and so this ground states will mix and eventually lead to finite-size corrections. In fact, the degeneracy is lifted due to instanton corrections (in the field-theoretical language) which disappear in the thermodynamic limit.

⁹More precisely, the momentum space propagator exhibits additional poles at the edge of the Brillouin zone. Since momentum is only conserved up to 2π these may interact with the 'physical pole' at the origin.

¹⁰In fact in one dimension there is one unwanted doubler, while in two dimensions already three and in four dimensions fifteen doublers are found.

all fermionic actions are quadratic in the fermionic fields.^{11,12} Hence it is possible to integrate them out analytically in the lattice path integral which for the fermionic part takes the form

$$Z_F = \int \mathcal{D}\bar{\psi} \mathcal{D}\psi e^{-\sum_{x,y} \bar{\psi}_x M_{xy} \psi_y}, \quad \text{with} \quad \mathcal{D}\bar{\psi} \mathcal{D}\psi = \prod_x d\bar{\psi}_x d\psi_x. \quad (2.4.1)$$

The linear operator M appearing in Z_F defines the fermionic (lattice) action and with the rules of Berezin integration [35] (2.4.1) can be worked out to yield

$$Z_F = \det M. \quad (2.4.2)$$

If interactions among bosons and fermions are turned on, e.g. some Yukawa-coupling to a scalar field, the fermion matrix M gets modified and the path integral over all fields becomes

$$Z = \int \mathcal{D}\varphi \mathcal{D}\bar{\psi} \mathcal{D}\psi e^{-S_B(\varphi) - \sum_{x,y} \bar{\psi}_x M(\varphi) \psi_y} = \int \mathcal{D}\varphi e^{-S_B(\varphi)} \det M(\varphi). \quad (2.4.3)$$

Hence numerical lattice computations have to calculate the determinant of M , whose dimensionality is at least the size of the lattice.¹³ The computation of this determinant exacerbates the numerical challenge to compute correlation functions from (2.4.3) dramatically and only within the last decade has it been possible to attack this problem successfully.

2.4.2 Fermionic correlation functions

Having introduced fermionic fields to the path integral one is of course interested in the computation of their correlation functions, too. In this thesis they will be needed on two occasions, namely for the determination of the mass of the fermionic particle and secondly for the evaluation of Ward identities (WIs) by which supersymmetry can be tested. For either task only the fermionic twopoint function is needed. From the fermionic path integral Z_F one finds

$$\langle \psi_x \bar{\psi}_y \rangle = \frac{1}{Z_F} \int \mathcal{D}\bar{\psi} \mathcal{D}\psi e^{-\bar{\psi} M \psi} \psi_x \bar{\psi}_y. \quad (2.4.4)$$

¹¹For this statement to make sense there are at least two different fields required. Usually these emerge as the components of a spinor that transforms under the Lorentz group of the space-time under consideration. In quantum mechanics two fields are still present, although they do not form one spinor any longer.

¹²Of course this is not true for the 4-Fermi theory of particle physics or the various supergravity models. Also in supersymmetric non-linear sigma models a 4-fermion vertex is present.

¹³Even worse, the dimensionality of M is multiplied with each internal degree of the fermion fields, e.g. spin or color.

As with Z_F itself this can be worked out analytically directly from the rules of Berezin integration to yield

$$\langle \psi_x \bar{\psi}_y \rangle = M_{x,y}^{-1}. \quad (2.4.5)$$

The numerical challenge to calculate the determinant of M is thus complemented with the computation of the inverse of M . Once more this illustrates why fermions are so hard to cope with on the lattice.

2.5 Monte Carlo simulation for lattice field theories

One of the most interesting features of lattice regulated functional integrals in the form of (2.1.8) is the possibility to evaluate them numerically. However, this task is challenging because every lattice site $x \in \Lambda$ contributes one integration variable. Lattice sizes used in this thesis are as large as $N = 200$ for the one-dimensional model and $V = 92 \times 64$ for the two-dimensional model.¹⁴ Such very high-dimensional integrals cannot be attacked with the standard tools of numerical integration such as the Simpson rule and its higher order successors. Instead of that randomized algorithms are used exclusively in this field. Amongst them the Monte Carlo (MC) importance sampling method is the most widely accepted. A very prominent algorithm within this class is known as the Hybrid Monte Carlo (HMC) algorithm and will be discussed after some basic facts of the general theory of importance sampling have been recalled.

2.5.1 Importance sampling and Markov chains

Due to the close relationship between Euclidean lattice field theory and statistical mechanics one may reinterpret the integral measure used to compute the expectation value of some Operator \mathcal{O} ,

$$\langle \mathcal{O} \rangle = \frac{1}{Z} \int \mathcal{D}\varphi e^{-S_E(\varphi)} \mathcal{O}(\varphi), \quad (2.5.1)$$

as a probability measure on configuration space¹⁵,

$$P(\varphi) = \frac{1}{Z} e^{-S(\varphi)}. \quad (2.5.2)$$

Although the configuration space is large, i.e. $\mathcal{C} = \mathbb{R}^V$, most configurations will not contribute to (2.5.1) since they are exponentially damped through the size of their (Euclidean) action. Moreover, for a localised ground state only fluctuations around this

¹⁴In four-dimensional lattice gauge theories achievable lattice sizes range from $V = 16^4$ to $V = 48^4$ or even larger, and in addition there are extra internal degrees of freedom in the single-site measure $d\mu$ which replaces the Lebesgue measure of (2.1.7) in these more complicated theories.

¹⁵At least this interpretation is correct as long as the Euclidean action is real and it is safe to assume $P(\varphi) > 0$.

state will contribute.¹⁶ Instead of integrating over all field configurations it is hence sufficient to only take these configurations into account. This is guaranteed if one can draw configurations a priori with the probability $P(\varphi)$ from the configuration space. The true expectation value (2.5.1) may then be approximated as

$$\langle \mathcal{O} \rangle = \frac{1}{M} \sum_{i=1}^M O(\varphi^{(i)}) + \mathcal{O}(\sqrt{M^{-1}}). \quad (2.5.3)$$

The more configurations are drawn, i.e. the bigger M becomes, the more precisely $\langle \mathcal{O} \rangle$ would be known. To proceed with the construction of such a method one introduces a Markov chain, which is given in terms of a transition matrix¹⁷

$$\mathcal{M}_{ij} \equiv \mathcal{M}(\varphi^{(i)} \rightarrow \varphi^{(j)}) \quad (2.5.4)$$

describing the probability to reach the configuration $\varphi^{(j)}$ from the configuration $\varphi^{(i)}$ by what is called an update step. For this to constitute a stochastic matrix it must obey

$$\mathcal{M}_{ij} \geq 0 \quad \forall i, j \quad \sum_j \mathcal{M}_{ij} = 1 \quad \forall i. \quad (2.5.5)$$

The Markov chain now consists of all configurations that are sequentially generated by a repeated application of the update step

$$\dots \rightarrow \varphi_k \xrightarrow{\text{update}} \varphi_{k+1} \xrightarrow{\text{update}} \varphi_{k+2} \rightarrow \dots \quad (2.5.6)$$

To relate this process with the equilibrium probability (2.5.2) two conditions must be fulfilled. The first requirement to be met reads

$$\forall i, j \quad \exists N : \mathcal{M}^{(N)}_{ij} = \sum_{\{i_k\}} \mathcal{M}_{ii_1} \mathcal{M}_{i_1 i_2} \dots \mathcal{M}_{i_{N-1} j} \neq 0 \quad (\text{ergodicity}). \quad (2.5.7a)$$

Then one can show that the limit $N \rightarrow \infty$ exists and leads to a unique probability distribution independent of the start configuration. This fixed-point distribution approaches the required distribution (2.5.2) if one further ensures¹⁸

$$P_i \mathcal{M}_{ij} = P_j \mathcal{M}_{ji} \quad (\text{detailed balance}). \quad (2.5.7b)$$

It is clear however, that it will take some time to drive the chain into the vicinity of the fixed-point. The number of updates it takes is called thermalization time and may be assessed by observing two chains with different start configurations converge. Eventually, given a probability $P(\varphi)$ the conditions (2.5.7) do not determine the update

¹⁶This assumption can be relaxed to some extent in case of multiple ground states if these are still localised.

¹⁷Without loss of generality a discrete set of states is assumed in the following.

¹⁸Indeed for a fixed-point to exist it suffices to demand $\sum_i P_i \mathcal{M}_{ij} = P_j$. However, this may leave room for non-trivial cycles [36] which are unwanted. Clearly from (2.5.7b) this weaker condition follows.

process completely. This freedom can thus be used to construct algorithms which are best suited for the specific problem.

2.5.2 The Hybrid Monte Carlo algorithm

For the numerical analysis of later sections the Hybrid Monte Carlo (HMC) algorithm due to Duane et al. [37] was employed. While for purely bosonic theories the Metropolis or the heat bath algorithm are more convenient it turns out that the HMC algorithm is much more efficient when dynamical fermions have to be included. Since later on some modifications are to be discussed the basic algorithm is given here in brief. In order to construct the Markov chain the HMC algorithm proceeds in two steps called the molecular dynamics step (MD) and the Metropolis accept/reject step. The first offers the opportunity to incorporate non-local objects of the action such as the fermion determinant in an efficient manner while the latter renders the algorithm exact.¹⁹ For the MD step fictitious momenta π_x conjugate to the bosonic field variables φ_x are introduced to form the Hamiltonian

$$H(\varphi, \pi) = \sum_x \frac{\pi_x^2}{2} + S_E(\varphi_x) \quad (2.5.8)$$

of a classical many-body system.²⁰ The partition function for this augmented system is then given by

$$Z' = \int \mathcal{D}\varphi \mathcal{D}\pi e^{-H(\varphi, \pi)}. \quad (2.5.9)$$

For expectation values containing the φ 's alone Z' gives the same result as the original path integral of Eq. (2.5.1) since the Gaussian integral over the momenta π is trivially done and contributes only an irrelevant pre-factor. According to the ergodic hypothesis of statistical physics the time average over a trajectory $\varphi(\tau)$ in MD time can be replaced with the ensemble average with probability $P(\varphi) \sim e^{-S_E(\varphi)}$ and vice versa. Of key importance for this is the property of H to be *time-reversible* and to preserve the phase-space volume element $\mathcal{D}\varphi \mathcal{D}\pi$. The latter is of course due to the fact that the flow generated by H is *symplectic*. The trajectory in phase space that belongs to a given start configuration is given by Hamilton's equations

$$\dot{\varphi}_x = \frac{\partial H}{\partial \pi_x} = \pi_x, \quad \dot{\pi}_x = -\frac{\partial H}{\partial \varphi_x} = -\frac{\partial S_E}{\partial \varphi_x}. \quad (2.5.10)$$

which however must be integrated numerically. It is possible to show, that the arising systematic errors can be eliminated by an extra accept/reject step that takes place after the integration was carried out for some interval length τ . This way the numerical

¹⁹In the MD method alone, a discrete time step $\delta\tau$ must be introduced which gives rise to a systematic error. This is removed with the help of the Metropolis accept/reject step provided the conditions that are mentioned in the text are met.

²⁰The term 'fictitious' refers to the fact that the time conjugate to H is neither the original real time nor the Euclidean time encountered in the lattice field theory. The Euclidean action serves only as a potential here.

integration can also be seen as providing a proposal for a Metropolis update step. The way this proposal is obtained is highly adapted to the problem at hand. To ensure detailed balance it is crucial that the two already mentioned properties of Hamiltonian dynamics are met, namely time-reversibility and symplecticity. Moreover, to improve on ergodicity and decorrelation the momenta π are updated from a heat-bath after each integration.²¹ This is possible simply because the weight factor for the momenta is Gaussian.

²¹This happens regardless of whether the end configuration of the trajectory was accepted or not.

3 Supersymmetric Quantum mechanics

Supersymmetric Quantum Mechanics [5] can be regarded as an ideal playground for many concepts and algorithms to come. As a one-dimensional field theory it is free of divergences and relatively easy to handle in Monte-Carlo simulations. At the same time, the model exhibits most of the relevant features which are of interest in higher-dimensional SUSY field theories. This section is organized as follows. At first the model is introduced and its various supersymmetries are discussed. Thereafter the model is discussed in the usual Hamiltonian formalism which allows for an easy interpretation of its supersymmetries. The remainder of the section is then entirely devoted to the discretisation and construction of the corresponding lattice models. In Section 3.2, a possible construction scheme to preserve half of the supersymmetry on the lattice is derived with the help of a so-called Nicolai map. Section 3.3 deals with various realizations of lattice fermions with regard to both conceptual and algorithmic aspects while in Section 3.4 results from numerical simulations are presented and discussed.

3.1 The Model and its symmetries in the continuum

3.1.1 Definition and terminology

In the continuum, the (Euclidean) action of the model to be considered here takes the form

$$S = \int d\tau L(\varphi, \bar{\psi}, \psi) = \int d\tau \left(\frac{1}{2} \dot{\varphi}^2 + \frac{1}{2} W'(\varphi)^2 + \bar{\psi} W''(\varphi) \psi + \bar{\psi} \dot{\psi} \right). \quad (3.1.1)$$

Besides the real scalar φ the model consists of two real anti-commuting variables $\bar{\psi}$ and ψ . Both the bosonic potential and the Yukawa interaction are derived from a so-called superpotential $W(\varphi)$.²² Under the variations

$$\delta^{(1)}\varphi = \bar{\varepsilon}\psi, \quad \delta^{(1)}\bar{\psi} = -\bar{\varepsilon}(\dot{\varphi} + W'), \quad \delta^{(1)}\psi = 0, \quad (3.1.2a)$$

$$\delta^{(2)}\varphi = \bar{\psi}\varepsilon, \quad \delta^{(2)}\bar{\psi} = 0, \quad \delta^{(2)}\psi = (\dot{\varphi} - W')\varepsilon, \quad (3.1.2b)$$

with infinitesimal anti-commuting parameters ε and $\bar{\varepsilon}$ ²³ the Lagrangian changes by a total derivative

$$\delta^{(1)}L = -\bar{\varepsilon} \frac{d}{dt} (W'\psi) \quad \text{and} \quad \delta^{(2)}L = \frac{d}{dt} (W'\bar{\psi}) \varepsilon, \quad (3.1.3)$$

respectively, so that the action (3.1.1) is invariant. Computing the commutator of both variations $\delta^{(1,2)}$ on φ for example, one finds

$$[\delta_{\varepsilon_2}^{(2)}, \delta_{\bar{\varepsilon}_1}^{(1)}]\varphi = \bar{\varepsilon}_1(\dot{\varphi} - W')\varepsilon_2 + \bar{\varepsilon}_1(\dot{\varphi} + W')\varepsilon_2 = 2\dot{\varphi}\bar{\varepsilon}_1\varepsilon_2, \quad (3.1.4)$$

²²Prime and double-primes in (3.1.1) denote usual differentiation with respect to the argument, i.e. φ .

²³That means that they anti-commute amongst each other and with ψ and $\bar{\psi}$.

which is up to a factor of two the action of an infinitesimal translation on φ as generated by the time translation or Hamiltonian operator H . Thus the variations (3.1.2) are a realization of the supersymmetry algebra

$$\{Q, \bar{Q}\} = 2H \quad (3.1.5)$$

and the model described by the action (3.1.1) possesses two supersymmetries. In the literature it is discussed as the one-dimensional Wess-Zumino model and this nomenclature will be adopted here from now on.

Demanding the action to have zero mass dimension and starting from the canonical mass dimension of the line element $d\tau$, one easily derives the following conditions on the mass dimensions of the various terms contributing to (3.1.1):

$$[d\tau] = -1, \quad [\varphi] = -\frac{1}{2}, \quad [\psi] = [\bar{\psi}] = 0, \quad [W'(\varphi)] = \frac{1}{2} \quad \text{and} \quad [W''(\varphi)] = 1. \quad (3.1.6)$$

The simplest superpotential to be considered below takes the form

$$W_2(\varphi) = \frac{1}{2}m\varphi^2, \quad W_2'(\varphi) = m\varphi, \quad W_2''(\varphi) = m \quad (3.1.7)$$

and will be referred to as the free theory. Its single coupling constant called m has dimension $[m] = 1$ and from either the resulting bosonic potential or fermionic interaction term it may be identified as a mass. As an example for a superpotential describing an interacting system the following superpotential will be discussed thoroughly in subsequent sections²⁴

$$W_4(\varphi) = \frac{1}{2}m\varphi^2 + \frac{g}{4}\varphi^4, \quad W_4'(\varphi) = m\varphi + g\varphi^3, \quad W_4''(\varphi) = m + 3g\varphi^2. \quad (3.1.8)$$

The dimension of the second parameter g is readily found from (3.1.6) to be $[g] = 2$ and the dimensionless ratio

$$\lambda = \frac{g}{m^2} \quad (3.1.9)$$

will be used to describe the interaction strength.

3.1.2 Hamiltonian formalism

It proves useful to investigate the model as a quantum-mechanical theory before switching back to the field-theoretical picture. The material within this section has been known for a long time and is discussed copiously in the literature. For the preparation of this section the lecture notes by Argyres [38] and Wipf [39] were used extensively.

The Hamilton operator for the model is found to act on a two-component Hilbert

²⁴From the definition of W_2 and W_4 it should be clear that the subscript refers to the highest monomial present in the superpotential. Thus the superpotential is always taken to be even. A reason will be given later in the text.

space describing a single particle with two internal (spin) states.²⁵ Borrowing from later interpretations the upper component will be called the 'bosonic' and the lower component the 'fermionic' sector. Introducing the operator $P = P^\dagger = i\frac{\partial}{\partial x}$ the Hamilton operator takes the explicit form

$$H = \frac{1}{2} \begin{pmatrix} H_B & 0 \\ 0 & H_F \end{pmatrix} = \frac{1}{2} \begin{pmatrix} P^2 + W'^2 - W'' & 0 \\ 0 & P^2 + W'^2 + W'' \end{pmatrix}. \quad (3.1.10)$$

The operators Q and \bar{Q} mentioned already in (3.1.5) are given by

$$Q = \begin{pmatrix} 0 & A \\ 0 & 0 \end{pmatrix} \quad \text{and} \quad \bar{Q} \equiv Q^\dagger = \begin{pmatrix} 0 & 0 \\ A^\dagger & 0 \end{pmatrix}, \quad (3.1.11)$$

where the operators A and A^\dagger take the form

$$A = P - iW' \quad \text{and} \quad A^\dagger = P + iW'. \quad (3.1.12)$$

It is not hard to show that $\{Q, \bar{Q}\} = 2H$ is fulfilled and furthermore $[Q, H] = [\bar{Q}, H] = 0$ holds. In particular one finds for the components

$$H_B = AA^\dagger, \quad H_F = A^\dagger A \quad (3.1.13)$$

which looks quite reminiscent of the algebra for the harmonic oscillator. For the free theory as described by $W(x) = \frac{1}{2}mx^2$ one finds

$$H = \frac{1}{2} \begin{pmatrix} -\partial_x^2 + m^2x^2 - m & 0 \\ 0 & -\partial_x^2 + m^2x^2 + m \end{pmatrix}, \quad (3.1.14)$$

i.e. H_B and H_F indeed describe harmonic oscillators with eigenstates $|k\rangle$. However their spectra are shifted by $\pm\frac{1}{2}m$ which is precisely the ground state energy of the usual harmonic oscillator. Hence the spectrum of H is given by

$$E_n = \{0, m, 2m, 3m, \dots\}. \quad (3.1.15)$$

and all eigenvalues save the first are doubly degenerate. Hence above the unique ground state

$$|\Psi_0\rangle = \begin{pmatrix} |0\rangle \\ 0 \end{pmatrix}, \quad H|\Psi_0\rangle = 0, \quad E_0 = 0 \quad (3.1.16)$$

²⁵For this identification to hold the field φ has to be interpreted as the position of the particle. Therefore in this section it is referred to simply as x .

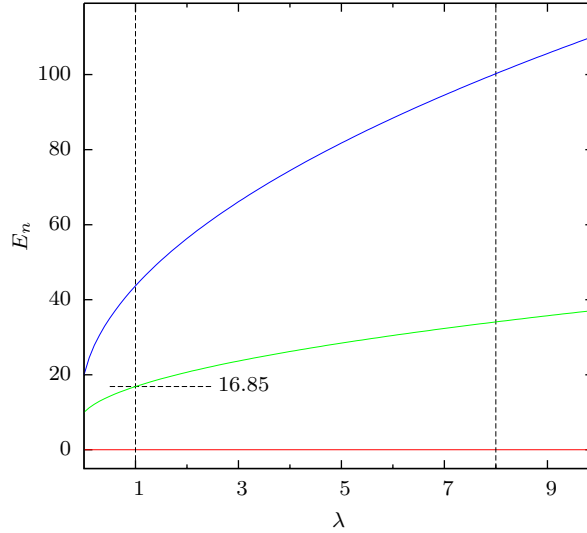
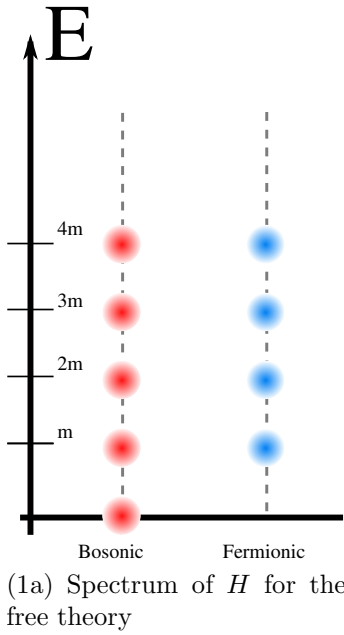


Figure 1: In Figure (1a) the spectrum of H for the free theory, i.e. using W_0 from (3.1.7) is depicted. All non-zero eigenvalues are double degenerate and the operators Q and \bar{Q} mediate between both sectors. In Figure (1b) the three lowest lying eigenvalues of H using the superpotential of (3.1.8) are shown as a function of λ . The dashed vertical lines refer to those values of λ where the Monte Carlo results of Section 3.4 are obtained.

the eigenstates form doublets

$$|\Psi_k\rangle = \alpha \begin{pmatrix} |k\rangle \\ 0 \end{pmatrix} + \beta \begin{pmatrix} 0 \\ |k-1\rangle \end{pmatrix}, \quad H|\Psi_k\rangle = E_k|\Psi_k\rangle, \quad E_k = m \cdot k, \quad (3.1.17)$$

which may be called 'bosonic' or 'fermionic' in obvious manner, cf. Fig. 1. Moreover $|\Psi_0\rangle$ is annihilated both from Q and \bar{Q} meaning that supersymmetry is unbroken²⁶. If interactions are turned on most of these structures remain. Given some excited fermionic eigenstate

$$|\Psi_{F,k}\rangle = \begin{pmatrix} 0 \\ |\psi_k\rangle \end{pmatrix} \quad (3.1.18)$$

with energy $E_k \neq 0$ it follows from $H_F|\psi_k\rangle = A^\dagger A|\psi_k\rangle$ that $A|\psi_k\rangle$ is an eigenstate of H_B to the same eigenvalue E_k ²⁷. Hence the action of Q

$$Q|\Psi_{F,k}\rangle = \begin{pmatrix} A|\psi_k\rangle \\ 0 \end{pmatrix} \quad (3.1.19)$$

turns a fermionic eigenstate into the corresponding bosonic one. Along the same reasoning Q^\dagger maps the bosonic eigenstate back to its fermionic counterpart. If either Q or Q^\dagger is applied twice to any state it is annihilated reflecting their anti-commuting nature,

²⁶ Q operates trivially on $|\Psi_0\rangle$ while from $H_B|0\rangle = AA^\dagger|0\rangle = 0$ one has $|A^\dagger|0\rangle|^2 = 0$ and hence $\bar{Q} = Q^\dagger|\Psi_0\rangle = 0$ follows.

²⁷With (3.1.13) one has $H_B A|\psi_k\rangle = AA^\dagger A|\psi_k\rangle = AH_F|\psi_k\rangle = E_k \cdot A|\psi_k\rangle$.

i.e. $\{Q, Q\} = \{Q^\dagger, Q^\dagger\} = 0$. Furthermore whether supersymmetry remains unbroken or not can still be judged from the spectrum of H since the necessary conditions

$$Q|\Psi_0\rangle = \bar{Q}|\Psi_0\rangle = 0 \quad (3.1.20)$$

are only met iff

$$\langle\Psi_0|2H|\Psi_0\rangle = \langle\Psi_0|\{Q, \bar{Q}\}|\Psi_0\rangle = |Q|\Psi_0\rangle|^2 + |\bar{Q}|\Psi_0\rangle|^2 = 0. \quad (3.1.21)$$

The existence of such a normalizable state with zero energy can be read off from the asymptotic behavior of the superpotential. Candidates for possible ground states are expected to be localised around $W'(\varphi) = 0$, i.e. around the extremal points of $W(\varphi)$. If there are no such points, i.e. if the superpotential takes the form $W(\varphi) = a\varphi^3 + b\varphi$ with $a, b > 0$ supersymmetry is inevitably broken. Indeed it is possible to show that for any unbounded superpotential²⁸ there is no such ground state. Conversely, if the leading power in the superpotential is even it is bounded from either below or above and will exhibit extremal points, i.e. locations where the classical bosonic potential vanishes. For this case too, it is possible to show that in supersymmetric quantum mechanics all states localized around these points save one are lifted by quantum corrections. Thus a single zero-energy ground state remains and supersymmetry is unbroken. In particular supersymmetry is unbroken in the quantum theory of the superpotential W_4 defined in (3.1.8).

Another useful feature of the quantum mechanical system described by (3.1.10) is the possibility to study its spectra for arbitrary superpotentials $W(\varphi)$ numerically by diagonalizing the Hamiltonian operator in position space: $H_{xy} = \langle x|H|y\rangle$. The continuum value²⁹ of the energy of the first excited states is thus known to very high precision. In Fig. (1b) it is plotted together with the ground state (red) and the second excited energy level (blue) as a function of λ for the interacting superpotential W_4 using $m = 10$. In Section 3.4.2 this will be compared to the continuum extrapolation of the same quantity as extracted from the two point functions computed from MC simulations. This way it is possible to estimate the impact of discretisation artifacts in the latter approach.

3.1.3 Ward identities

Starting from the classical action (3.1.1) the quantum theory is equivalently described with the help of the path integral, an alternative to the operator formalism of the previous section. The path integral takes the form

$$Z = \int \mathcal{D}\varphi \mathcal{D}\psi \mathcal{D}\bar{\psi} e^{-S[\varphi, \psi, \bar{\psi}]} \quad (3.1.22)$$

²⁸Equivalently one can speak of odd superpotentials referring to the leading (necessarily) odd power in φ .

²⁹Within this approach the discretisation can be made sufficiently small at least much smaller than what Monte Carlo simulations allow for.

and physical observables have to be extracted from correlation functions calculated with the help of corresponding insertions into (3.1.22), e.g. the two point correlator can be computed from

$$\langle \mathcal{T} [\varphi(\tau_1)\varphi(\tau_2)] \rangle = \frac{1}{Z} \int \mathcal{D}\varphi \mathcal{D}\psi \mathcal{D}\bar{\psi} e^{-S[\varphi, \psi, \bar{\psi}]} \varphi(\tau_1)\varphi(\tau_2). \quad (3.1.23)$$

Within the path integral formalism symmetries of the classical theory manifest themselves in the form of Ward identities, i.e. relations among specific correlation functions. They are most conveniently found by introducing external sources to the path integral³⁰

$$Z[j, \theta, \bar{\theta}] = \int \mathcal{D}\varphi \mathcal{D}\psi \mathcal{D}\bar{\psi} e^{-S[\varphi, \psi, \bar{\psi}] + j \cdot \varphi + \bar{\theta} \cdot \psi + \bar{\psi} \cdot \theta}. \quad (3.1.24)$$

For any continuous symmetry of the action implemented as an infinitesimal variation δ on the fields, i.e. as given by (3.1.2), one finds

$$0 = \delta Z = \int \mathcal{D}\varphi \mathcal{D}\psi \mathcal{D}\bar{\psi} e^{-S[\varphi, \psi, \bar{\psi}] + j \cdot \varphi + \bar{\theta} \cdot \psi + \bar{\psi} \cdot \theta} (j \cdot \delta\varphi + \delta\bar{\theta} \cdot \psi + \delta\bar{\psi} \cdot \theta) \quad (3.1.25)$$

provided that the functional integral measure is invariant as well³¹. Supersymmetric variations such as (3.1.2) mix bosonic and fermionic fields thus relating bosonic to fermionic correlation functions. Differentiating (3.1.25) once w.r.t. j and once w.r.t θ yields

$$\left. \frac{\delta^2}{\delta j(\tau_2)\delta\theta(\tau_1)} \right|_{j=\theta=0} \delta Z = \int \mathcal{D}\varphi \mathcal{D}\psi \mathcal{D}\bar{\psi} e^{-S[\varphi, \psi, \bar{\psi}]} (\bar{\psi}_{\tau_1} \delta\varphi_{\tau_2} + \delta\bar{\psi}_{\tau_1} \varphi_{\tau_2}). \quad (3.1.26)$$

Inserting finally (3.1.2a) into (3.1.26) one obtains

$$\langle \bar{\psi}_{\tau_1} \psi_{\tau_2} \rangle - \langle (\dot{\varphi}_{\tau_1} + W'_{\tau_1}) \varphi_{\tau_2} \rangle = 0. \quad (3.1.27)$$

Analogously a second Ward identity using (3.1.2b) may be found to take the form

$$\langle \psi_{\tau_1} \bar{\psi}_{\tau_2} \rangle + \langle (\dot{\varphi}_{\tau_1} - W'_{\tau_1}) \varphi_{\tau_2} \rangle = 0. \quad (3.1.28)$$

As illustrated above, Ward identities relate correlation functions to each other. Since the latter are directly computable from MC simulations, Ward identities might serve the purpose to measure the effect of supersymmetry breaking terms which are inevitably induced by lattice discretisation of the (supersymmetric) continuum action (3.1.1). A concrete numerical analysis involving (3.1.27) and (3.1.28) will be presented in Section

³⁰For better readability the notation $\alpha.\beta$ is introduced as a short-hand substitute for

$$\alpha.\beta \equiv \int d\tau \alpha(\tau)\beta(\tau).$$

³¹Otherwise the symmetry would be broken anomalously. This scenario does not apply here.

3.2 Construction of (improved) lattice models

To make MC simulations available as a tool for the study of supersymmetric quantum mechanics it is necessary to reformulate the theory on a one-dimensional lattice. However, as discussed below, supersymmetry is generically broken in the lattice theory. By a suitable choice for the difference operator and further amendments to the bosonic action, however some part of the original supersymmetry can be manifestly realized in the lattice theory. Much of the insights and results described below can be carried over to the two-dimensional $\mathcal{N} = (2, 2)$ Wess-Zumino model and provide the basis for the discussion found in Sec. 4.1.2. Peculiarities of the treatment of fermions on the lattice are postponed to the next subsection.

3.2.1 Free Theory

The discretization of the free theory which is described by W_2 , see (3.1.7), already leads to non-trivial conditions not met by the usual discretisation schemes for scalar fields. The action to be discretized here is obtained by plugging W_2 into (3.1.1),

$$S = \int d\tau \left(\frac{1}{2}(\partial_\tau \varphi)^2 + \frac{1}{2}m^2 \varphi^2 + \bar{\psi}(\partial_\tau + m)\psi \right). \quad (3.2.1)$$

With the help of a one-dimensional lattice whose sites will be labeled by x and which are separated by some lattice-spacing a the integral in (3.2.1) can be approximated with a Riemann sum. To end up with a theory entirely defined on the lattice the derivative operator ∂_τ is replaced by some difference operator ∂_{xy} ,

$$\hat{S} = a \sum_x \left(\frac{1}{2}(\partial \hat{\varphi})_x^2 + \frac{1}{2}\hat{m}^2 \hat{\varphi}_x^2 \right) + a \sum_{x,y} \hat{\psi}_x (\partial_{xy} + \hat{m} \delta_{xy}) \hat{\psi}_y. \quad (3.2.2)$$

Here, the hats denote dimensionless fields. The physical dimension is carried by the lattice spacing a alone. In the end the dimensions of the fields can be restored by multiplication with respective powers of a , which are given in (3.1.6), e.g. $\varphi = a^{-\frac{1}{2}}\hat{\varphi}$. Having mentioned this, they can be safely dropped again in the following. Also for convenience the lattice spacing is taken to be $a = 1$. On the lattice the variations (3.1.2) naively take the form

$$\delta^{(1)}\varphi_x = \bar{\varepsilon}\psi_x, \quad \delta^{(1)}\bar{\psi}_x = -\bar{\varepsilon}((\partial\varphi)_x + m\varphi_x), \quad \delta^{(1)}\psi_x = 0, \quad (3.2.3a)$$

$$\delta^{(2)}\varphi_x = \bar{\psi}_x\varepsilon, \quad \delta^{(2)}\bar{\psi}_x = 0, \quad \delta^{(2)}\psi_x = ((\partial\varphi)_x - m\varphi_x)\varepsilon. \quad (3.2.3b)$$

These variations are a symmetry of (3.2.1), if the difference operator ∂_{xy} is antisymmetric. This can be seen from the respective variations of the action. For instance, from

the application of $\delta^{(1)}$ one finds

$$\begin{aligned}\delta^{(1)}S &= \bar{\varepsilon} \left(\sum_x (\partial\varphi)_x (\partial\psi)_x + m^2 \varphi_x \psi_x - \sum_{x,y} ((\partial\varphi)_x + m\varphi_x) (\partial_{xy} + m\delta_{xy}) \psi_y \right) \\ &= -\bar{\varepsilon} m \sum_{x,y} \varphi_x \partial_{xy} \psi_y + \partial_{xy} \varphi_y \psi_x\end{aligned}\quad (3.2.4)$$

and hence $\partial_{xy} = -\partial_{yx}$ is required.³² In particular the left derivative ∂^L will not lead to a supersymmetric lattice action. The next choice is then the symmetric difference operator

$$\partial_{xy}^S = \frac{1}{2} (\delta_{x+1,y} - \delta_{x-1,y}) \quad (3.2.5)$$

which is still ultra-local. However, unwanted doublers in both the bosonic and fermionic spectrum are now present. To remove them Golterman and Patcher [40] and later Catterall and Gregory [24] introduced a Wilson term as part of the superpotential. In case of the free theory discussed here their choice amounts to using

$$\partial_{xy} = (\partial^S)_{xy}, \quad M_{xy} = m\delta_{xy} - \frac{r}{2} \Delta_{xy}. \quad (3.2.6)$$

Plugging ∂^S into (3.2.2) and replacing m with M yields

$$S = \sum_x \frac{1}{2} (\partial^S \varphi)_x^2 + \frac{1}{2} (M\varphi)_x^2 + \sum_{xy} \bar{\psi}_x (\partial^S + M)_{xy} \psi_y, \quad (3.2.7)$$

while all variations of the fields involving the superpotential are changed accordingly:

$$\delta^{(1)} \bar{\psi}_x = -\bar{\varepsilon} \left((\partial^S \varphi)_x + (M\varphi)_x \right), \quad (3.2.8a)$$

$$\delta^{(2)} \psi_x = \left((\partial^S \varphi)_x - (M\varphi)_x \right) \varepsilon. \quad (3.2.8b)$$

Besides the standard Wilson term in the fermionic bi-linear also the bosonic action becomes modified in (3.2.7) as to remove bosonic doublers as well. That both Wilson terms can be thought of as originating from the superpotential can be seen from (3.2.8) where they are included as well, cf. (3.1.2). This guarantees that supersymmetry remains unbroken. Recomputing $\delta^{(1)}S$ using (3.2.7) and (3.2.8a) leads to

$$\delta^{(1)}S = -\bar{\varepsilon} \sum_{x,y} \varphi_x M_{xy} \partial_{xy}^S \psi_y + \partial_{xy}^S \varphi_y M_{xy} \psi_x, \quad (3.2.9)$$

which still vanishes due to the symmetry of M_{xy} and the anti-symmetry of ∂_{xy}^S . Obviously the same arguments hold in any space-time dimension and thus it is found that the free Wess-Zumino model can be formulated on a space-time lattice in such a way that all

³²From the second set of transformations a similar result is found. The free lattice action hence preserves both supersymmetries if an antisymmetric difference operator is used.

its supersymmetries are preserved and unwanted doublers are absent. When different models are compared in Sec. 3.4 this particular solution will be referred to as the *Wilson model with shifted superpotential*.

3.2.2 Interacting Theory

If arbitrary superpotentials are considered the situation changes. A simple shift in the superpotential does no longer comply with the conditions that appear now. Nonetheless it is clear from the previous section that it suffices to consider solely antisymmetric difference operators from now on; this will always be assumed below. Let now W_x and W_{xy} be lattice operators that fulfill (in the naive sense)

$$\lim_{a \rightarrow 0} W_x = W'(\varphi(x)) \quad \text{and} \quad \lim_{a \rightarrow 0} W_{xy} = W''(\varphi(x)). \quad (3.2.10)$$

A lattice action of the interacting Wess-Zumino model (3.1.1) might then look like

$$S = \sum_x \left(\frac{1}{2} (\partial\varphi)_x^2 + \frac{1}{2} W_x^2 \right) + \sum_{x,y} \left(\bar{\psi}_x (\partial_{xy} + W_{xy}) \psi_y \right) \quad (3.2.11)$$

and the supersymmetry variations of the lattice fields take the form

$$\delta^{(1)}\varphi_x = \bar{\varepsilon}\psi_x, \quad \delta^{(1)}\bar{\psi}_x = -\bar{\varepsilon}((\partial\varphi)_x + W_x), \quad \delta^{(1)}\psi_x = 0, \quad (3.2.12a)$$

$$\delta^{(2)}\varphi_x = \bar{\psi}_x\varepsilon, \quad \delta^{(2)}\bar{\psi}_x = 0, \quad \delta^{(2)}\psi_x = ((\partial\varphi)_x - W_x)\varepsilon. \quad (3.2.12b)$$

The conditions already mentioned are again found from the requirement that the variation of the action under (3.2.12) should vanish:³³

$$\delta^{(1)}S = \bar{\varepsilon} \sum_{x,y} \left(W_x \frac{\partial W_x}{\partial \varphi_y} \psi_y - W_x W_{xy} \psi_y - W_x \partial_{xy} \psi_y - (\partial\varphi)_x W_{xy} \psi_y \right) \stackrel{!}{=} 0, \quad (3.2.13a)$$

$$\delta^{(2)}S = \sum_{x,y} \left(W_x \frac{\partial W_x}{\partial \varphi_y} \bar{\psi}_y - \bar{\psi}_x W_{xy} W_y + \bar{\psi}_x W_{xy} (\partial\varphi)_y - \bar{\psi}_x \partial_{xy} W_y \right) \varepsilon \stackrel{!}{=} 0. \quad (3.2.13b)$$

From their algebraic form it is clear that in both variations only the first and last two terms can be adjusted in such a way that they can cancel each other. For the first two terms in (3.2.13a) to vanish it suffices to demand

$$W_{xy} = \frac{\partial W_x}{\partial \varphi_y}. \quad (3.2.14a)$$

This also eliminates them from (3.2.13b) if furthermore

$$W_{xy} = W_{yx}. \quad (3.2.14b)$$

³³Terms that cancel without further manipulations or by the antisymmetry of ∂_{xy} are left out.

Both conditions are easily met by the choice

$$W_x = W'(\varphi_x), \quad W_{xy} = \delta_{xy}W''(\varphi_x), \quad (3.2.15)$$

which additionally is consistent with (3.2.10). Moreover, also the shifted superpotential solution agrees with (3.2.15). Explicitly, one has to choose

$$W_x = W'(\varphi_x) + \frac{r}{2}(\Delta\varphi)_x, \quad W_{xy} = \delta_{xy}W''(\varphi_x) + \frac{r}{2}\Delta_{xy}, \quad (3.2.16)$$

which reduces to (3.2.6) for the free theory, $W'(\varphi) = m\varphi$. Returning to the last two terms of (3.2.13) a third condition can be read off and takes the form³⁴

$$(\partial W)_x = \sum_y W_{xy}(\partial\varphi)_y. \quad (3.2.17)$$

Combining (3.2.14) with this last condition one realizes that for a supersymmetric theory with arbitrary superpotential a Leibniz rule for the lattice difference operator ∂_{xy} is needed [19]. However this requirement cannot be met by any difference operator, e.g. for the symmetric difference derivative it holds only up to terms of $\mathcal{O}(a)$. By consequence supersymmetries of the interacting continuum model cannot be preserved on the lattice. From another point of view, the supersymmetry algebra closes on infinitesimal translations which are represented by partial derivatives on fields over a continuous space-time. Yet this notion does not carry over to a lattice with finite lattice spacing. Recent research aiming at circumventing the lack of the Leibniz rule [41, 42] went not without criticism [43, 44] and could hitherto not present a consistent lattice action which would be suitable for Monte Carlo simulations.

3.2.3 The Nicolai map

Having identified the required properties of ∂_{xy} and W_{xy} and yet not succeeded in constructing a supersymmetric lattice theory one may still try to find additional terms to the lattice action (3.2.11) whose variation cancel exactly the remaining terms of (3.2.13) and at the same do not alter its (naive) continuum limit. This idea has been scrutinized, e.g. in [24, 26, 45, 46]. For Wilson fermions the method described below is also explained in [25].

Construction of the lattice action. A particular property of supersymmetric theories is the existence of a special mapping [33] which takes the functional integral of the interacting theory (after the fermions have been integrated out) into a functional integral for a free bosonic field. This characteristic is nowadays called by most authors *Nicolai-map*. Unfortunately, despite its existence, no statement can be made about its properties. For chiral models of extended supersymmetry it is at least known that the

³⁴Recall that ∂_{xy} is assumed to be antisymmetric.

mapping is local [47]. Until today an explicit local form is only known for a few special models including the Wess-Zumino model in one and the $\mathcal{N} = (2, 2)$ Wess-Zumino model in two dimensions. In the following it will be shown how part of the supersymmetry is preserved with the help of the Nicolai map. To begin with, consider the Gaussian functional integral over a real field ξ_x ,

$$Z = \int \mathcal{D}\xi e^{-\frac{1}{2} \sum_x \xi_x^2}. \quad (3.2.18)$$

Through the variable substitution $\xi_x = (\partial\varphi)_x + W_x$ the functional integral changes according to

$$Z = \int \mathcal{D}\varphi |\det \mathcal{J}_{xy}| e^{-\frac{1}{2} \sum_x ((\partial\varphi)_x + W_x)^2}, \quad \mathcal{J}_{xy} = \left(\frac{\partial \xi_x}{\partial \varphi_y} \right) = \partial_{xy} + \frac{\partial W_x}{\partial \varphi_y}. \quad (3.2.19)$$

Under the assumption that the Jacobian \mathcal{J}_{xy} is positive and that (3.2.14) holds, the determinant can be rewritten as a Berezin integral over two real fermionic fields

$$Z = \int \mathcal{D}\varphi \mathcal{D}\psi \mathcal{D}\bar{\psi} e^{-\frac{1}{2} \sum_x (\partial\varphi)_x + W_x)^2 - \sum_{x,y} \bar{\psi}_x (\partial_{xy} + W_{xy}) \psi_y}. \quad (3.2.20)$$

Thus the functional integral of an interacting theory is recovered. Its action may be directly read off from the equation above,

$$S = \frac{1}{2} \sum_x ((\partial\varphi)_x + W_x)^2 + \sum_{x,y} \bar{\psi}_x (\partial_{xy} + W_{xy}) \psi_y. \quad (3.2.21)$$

In terms of the original coordinates, this is

$$S = \frac{1}{2} \sum_x \xi_x^2 - \sum_{x,y} \bar{\psi}_x \frac{\partial \xi_x}{\partial \varphi_y} \psi_y. \quad (3.2.22)$$

The invariance under the variation

$$\delta\varphi_x = \bar{\varepsilon} \psi_x, \quad \delta\bar{\psi}_x = \bar{\varepsilon} \xi_x = \bar{\varepsilon} ((\partial\varphi)_x + W_x) \quad (3.2.23)$$

readily follows.³⁵ This variation is identical to (3.1.2a) and therefore one of the two supersymmetries is preserved. $\delta S = 0$ due to the algebraic structure of S , and no Leibniz rule is needed. In other approaches (mentioned at the beginning of this section) this feature was explained by the fact that S of Eq. (3.2.21) can likewise be obtained from $S = Q\Lambda$, where Q denotes the nil-potent Noether supercharge associated with (3.2.23) and Λ is some Grassmann valued object yet to be determined.³⁶ The statement

³⁵With $\xi_x = \xi_x(\varphi_y)$ the variation of ξ_x is given by

$$\delta\xi_x = \bar{\varepsilon} \sum_y \frac{\partial \xi_x}{\partial \varphi_y} \psi_y.$$

³⁶As in the BRST-formalism this is sometimes also called the gauge fermion.

$\delta S = QS = Q^2\Lambda = 0$ then follows from the aforementioned nil-potency of Q and, in particular, is algebraic again.

Comparing the naive discretisation of the previous section (3.2.11) with the improved expression found in (3.2.21) the difference is

$$\Delta S = \sum_x ((\partial\varphi)_x W_x), \quad (3.2.24)$$

while its variation under $\delta^{(1)}$ of (3.2.12) is given by

$$\delta^{(1)}(\Delta S) = \bar{\varepsilon} \sum_x ((\partial\psi)_x W_x) + \bar{\varepsilon} \sum_{x,y} (\partial\varphi)_x W_{xy} \psi_y. \quad (3.2.25)$$

These are exactly the terms needed to cancel the remaining terms of (3.2.13). Taking the naive continuum limit of ΔS ,

$$\lim_{a \rightarrow 0} \Delta S = \int d\tau \dot{\varphi} W'(\varphi) \quad (3.2.26)$$

reveals that it has turned into a surface term that will vanish upon choosing suitable boundary conditions. In this sense the continuum limits of the lattice actions (3.2.11) and (3.2.21) coincide as required. Now the variation of (3.2.24) with respect to $\delta^{(2)}$ yields

$$\delta^{(2)}(\Delta S) = \sum_x ((\partial\bar{\psi})_x W_x) \varepsilon + \sum_{x,y} (\partial\varphi)_x W_{xy} \bar{\psi}_y \varepsilon. \quad (3.2.27)$$

This time the variation is added to the same terms already present in (3.2.13) which shows that the improved action (3.2.21) does not respect both supersymmetries. Otherwise this would have meant that both operators Q and \bar{Q} would have generated symmetries of the lattice theory. Thus the full algebra would have been realized, which contradicts its closing on infinitesimal translations. On the other hand it is clear that the whole argument may also work for $\delta^{(2)}$ instead of $\delta^{(1)}$. It is not hard to find the Nicolai map to be used in this case. The result is given by $\tilde{\xi}_x = -(\partial\varphi)_x + W_x$, and the improved action takes the form

$$\tilde{S} = \frac{1}{2} \sum_x \tilde{\xi}_x^2 + \sum_{x,y} \bar{\psi}_x \frac{\partial \tilde{\xi}_y}{\partial \varphi_x} \psi_y = \frac{1}{2} \sum_x ((\partial\varphi)_x - W_x)^2 + \sum_{x,y} \bar{\psi}_x (\partial_{xy} + W_{xy}) \psi_y. \quad (3.2.28)$$

This shows that $\Delta\tilde{S} = -\Delta S$ holds and that the action \tilde{S} is invariant under, cf. (3.2.12b),

$$\delta\varphi_x = \bar{\psi}_x \varepsilon, \quad \delta\psi_x = -\tilde{\xi}_x \varepsilon = ((\partial\varphi)_x - W_x) \varepsilon. \quad (3.2.29)$$

For the free theory ($W_x = m\varphi_x$) the antisymmetry of ∂_{xy} implies that $\Delta S = \tilde{\Delta}S = 0$.³⁷ In this case (3.2.21) and (3.2.28) reduce to (3.2.2), and both supersymmetries are

³⁷This is still true after a Wilson term is introduced, since the additional term in W_x is also linear in φ and does not change the symmetry property of W_{xy}

preserved. So the improvement terms ΔS or $\tilde{\Delta} S$ are non-zero in interacting theories only and are expected to make all the more a difference the bigger the couplings become.

Ito & Stratonovich prescription. Another point to be mentioned here concerns the derivation of W_x and W_{xy} from the corresponding continuum expression. Recalling the inclusion of a Wilson term to the superpotential which is necessary to remove any doublers³⁸ (see end of Sec. 3.2.2),

$$W_x = (m\varphi_x + g\varphi_x^3) - \frac{1}{2}(\Delta\varphi)_x \equiv W'(\varphi_x) - \frac{1}{2}(\Delta\varphi)_x, \quad (3.2.15)$$

it is obvious that W_x becomes $W'(\varphi(x))$ if a is taken to zero because the second term becomes irrelevant due to its mass dimension. Instead of using (3.2.24) to compute ΔS one may alternatively combine the kinetic operators into

$$\partial^B = \partial^S - \frac{1}{2}\Delta, \quad (3.2.30)$$

to arrive at the standard choice for the scalar field.³⁹ The Nicolai map is then $\xi_x = (\partial^B\varphi)_x + W'(\varphi_x)$, and the difference to the usual sum of squares equals

$$\Delta S = \sum_x (\partial^S\varphi)_x W_x = \sum_x W'(\varphi_x)(\varphi_x - \varphi_{x-1}). \quad (3.2.31)$$

This prescription is the well-known Ito prescription. An alternative approximation for the evaluation of the surface term (3.2.31) would be the Stratonovich scheme [48]. It turns out that this possesses somewhat better properties as will be seen in Sec. 3.4.2. Introducing $\sigma_x = \frac{1}{2}(\varphi_x + \varphi_{x-1})$, one can construct the bosonic action from a slightly modified Nicolai map

$$\xi_x = (\partial^B\varphi)_x + W'(\sigma_x), \quad (3.2.32)$$

so that

$$S_{\text{Strat.}} = \frac{1}{2} \sum_x ((\partial^B\varphi)_x + W'(\sigma_x))^2. \quad (3.2.33)$$

The supersymmetry derived from the Nicolai variable is manifest while the other is broken again. The operators W_x and W_{xy} are easily worked out to take the form

$$W_x = -\frac{1}{2}(\Delta\varphi)_x + W'(\sigma_x), \quad W_{xy} = -\frac{1}{2}\Delta_{xy} + \frac{\partial W'(\sigma_x)}{\partial\varphi_y}. \quad (3.2.34)$$

The requirements (3.2.10) readily follow. The Stratonovich prescription indeed improves the behavior of the lattice theory with regard to the continuum limit as may be seen

³⁸Sect. 3.3 will deal with this issue in more detail.

³⁹The introduction of the Wilson term is thus less transparent compared to the formerly given treatment where it was included into the superpotential.

from several arguments. Together with Bergner et al. the author has shown in [9] that the normalized fermion determinant behaves much smoother and converges exactly to the desired normalized continuum expression. Moreover, for physical masses extracted at finite lattice spacing, the lattice artifacts are found to be much smaller compared to those obtained from the Ito prescription as will be discussed more thoroughly in Sec. 3.4.2. However there are some apparent drawbacks, too. Firstly the symmetry property $W_{xy} = W_{yx}$ is lost which was originally demanded for the second supersymmetry to be realised. Of course this is irrelevant here since a second supersymmetry is not expected anyway.⁴⁰ More discomfoting is the fact that the construction cannot straightforwardly be generalised to higher dimensions and remains a peculiarity for the discretization of the one-dimensional theory.

A baby Ward identity. From the existence of the Nicolai map a simple identity may be derived. The functional integral in the form of (3.2.18) can be used to compute the expectation value

$$\left\langle \frac{1}{2} \sum_x \xi_x^2 \right\rangle = \frac{\int \mathcal{D}\xi e^{-\frac{1}{2} \sum_x \xi_x^2} \left(\frac{1}{2} \sum_x \xi_x^2 \right)}{\int \mathcal{D}\xi e^{-\frac{1}{2} \sum_x \xi_x^2}} = \frac{N}{2}. \quad (3.2.35)$$

Since the exponent is quadratic in the fields the expectation value merely counts the number of lattice points N . Rewritten in the form of (3.2.21) the above expression is turned into an identity for the bosonic action, namely

$$\left\langle \frac{1}{2} \sum_x \xi_x^2 \right\rangle = \left\langle \frac{1}{2} \sum_x ((\partial\varphi)_x + W_x)^2 \right\rangle = \frac{N}{2}. \quad (3.2.36)$$

In particular, the expectation value of the bosonic action must not depend on any coupling constants entering the superpotential W . Making use of the fact that the expectation value of the fermionic action is also constant⁴¹ one arrives at the conclusion, that the expectation value of the action $\langle S \rangle$ is constant, too. The same result was found in [49] although using a different argument.⁴² In Sec. 4.6 the observation (3.2.35) will be subject to a detailed numerical analysis that offers interesting insights for the two-dimensional case. In the present context of the one-dimensional model it was mainly used to check the proper implementation of the various improved models to be discussed below.

⁴⁰An improved action using the Stratonovich prescription and preserving only the second supersymmetry is still possible. It suffices to take $\sigma_x = \frac{1}{2}(\varphi_x + \varphi_{x+1})$ and use the forward difference operator ∂^F instead of ∂^B .

⁴¹The fermionic contribution to S is bi-linear in $\bar{\psi}$ and ψ and evaluates by the rules of Berezin integration to

$$\left\langle \sum_{x,y} \bar{\psi}_x M_{xy} \psi_y \right\rangle_{Z_F} = \sum_{x,y} M_{xy} \langle \bar{\psi}_x \psi_y \rangle_{Z_F} = \text{tr} (MM^{-1}) = N,$$

for any bosonic configuration. Hence the expectation value taken over all fields is again N .

⁴²The expectation value of the total action can be written as $\langle S \rangle = \langle Q\Lambda \rangle = Q\langle \Lambda \rangle$. Hence this is referred to as a Ward identity.

Although it is not possible to realize all supersymmetries in a lattice theory a possible construction scheme has been presented by which at least half of the supersymmetry can be made manifest on the lattice. Since an antisymmetric difference operator is always required it was further shown that the improvement is compatible with the inclusion of additional terms into the superpotential, which might be needed to remove unwanted doublers arising from the usage of the symmetric difference operator ∂^S . However, this last step might be questionable for supersymmetric theories that do not allow for a superpotential, e.g. the supersymmetric non-linear sigma model. To this end it is useful to study possible alternative lattice fermions which are the subject of the next section.

3.3 Lattice fermions

For any MC simulations of the one or two-dimensional Wess-Zumino model it is vital to discuss the treatment of fermions on the lattice. Using a hermitean lattice derivative, e.g. the symmetric difference operator, inevitably leads to the inclusion of additional poles in the lattice propagator provided that locality is not sacrificed.⁴³ Since in supersymmetric theories a delicate balance of bosonic and fermionic degrees of freedom is needed⁴⁴ these doublers are clearly unwanted. In order to avoid doublers, two different approaches will be presented in the following. The first one will sacrifice chirality while in the second the requirement of locality is dropped. To make either approach readily applicable to MC simulations which are discussed in the next section, the superpotential is assumed to take on the concrete form

$$W_4(\varphi) = \frac{1}{2}m\varphi^2 + \frac{g}{4}\varphi^4, \quad W_4'(\varphi) = m\varphi + g\varphi^3, \quad W_4''(\varphi) = m + 3g\varphi^2. \quad (3.1.8)$$

Dealing with this issue in such great detail in a one-dimensional theory is motivated by several aspects. First of all the model is comparatively easy to handle. The fermion fields carry no spin which simplifies the resulting fermion matrix considerably and makes it fit into the memory of present day computers without difficulty. A variety of algorithms to handle the fermion determinant can thus be tested and compared with each other. The outcome of these observations may help in the design of algorithms for the higher dimensional analogues. Secondly, the computation of correlation functions and the extraction of physical observables is possible with a precision not achievable in higher dimensions.

⁴³This can be seen from the facts that firstly hermiticity implies a reality condition on the (inverse) propagator and secondly locality in position space amounts to analyticity in momentum space. In particular the inverse propagator for a massless fermion is a continuous function of the momentum and has therefore to vanish at least twice. So besides the physical pole at $p = 0$ an additional pole is found at the corner of the Brillouin zone at $p = \pi/a$. In a broader context this is, of course, known as the Nielsen-Ninomiya No-Go theorem [50], where it is more precisely stated that it is not possible to have a local (non-) interacting lattice theory of chiral fermions.

⁴⁴see also Sec. 3.1.2.

3.3.1 Wilson fermions

The first possibility to deal with the doublers (already mentioned in previous sections) goes under the name of Wilson fermions [10]. The operators W_x and W_{xy} given in (3.2.15) read with the help of (3.1.8)

$$W_x = (M\varphi)_x + g\varphi_x^3 \quad \text{and} \quad W_{xy} = M_{xy} + 3g\varphi_x\delta_{xy}. \quad (3.3.1)$$

Setting the Wilson parameter to $r = 1$ as usual the matrix M is defined by

$$M_{xy} = m\delta_{xy} - \frac{1}{2}(\delta_{x-1,y} + \delta_{x+1,y} - 2\delta_{xy}) \quad (3.3.2)$$

and fixes the fermionic part of the lattice action as

$$S_F = \sum_{x,y} \bar{\psi}_x (\partial_{xy}^S + M_{xy} + 3g\varphi_x\delta_{xy}) \psi_y \equiv \sum_{x,y} \bar{\psi}_x D_{xy} \psi_y. \quad (3.3.3)$$

The determinant of D_{xy} has to be computed during a MC simulation, a subject to be dealt with in a moment. For the bosonic sector three different actions are studied with the intent to compare the results from respective simulations. In detail they are defined as

$$S_{\text{unimpr}} = \sum_x \frac{1}{2}(\partial^L\varphi)_x^2 + \frac{1}{2}(m\varphi_x + 3g\varphi_x^3)^2, \quad (3.3.4)$$

$$S_{\text{shift.}} = \sum_x (\partial^S\varphi)_x^2 + W_x^2, \quad (3.3.5)$$

$$S_{\text{impr}} = \sum_x ((\partial^S\varphi)_x + W_x)^2. \quad (3.3.6)$$

The first corresponds to a naive discretization without bothering about supersymmetry at all. Since the difference operators used in the bosonic and fermionic sector differ from one another the model is even for the free theory not invariant under any supersymmetry transformation.

Numerical results are expected not to reach the correct continuum limit. The second choice is the same as in [24]. In the non-interacting case it is invariant under both supersymmetry transformations (3.2.3)⁴⁵. Hence both supersymmetries are preserved but will be broken as soon as $g \neq 0$. In agreement with the results of [24], however, it will turn out that this construction suffices to obtain the desired supersymmetric continuum limit. The last choice is constructed with the help of the Nicolai map as outlined in Sec. 3.2.3. This time the action is always invariant under one supersymmetry and reduces to the second variant for $g = 0$. Numerically this will manifest itself in the vanishing of the corresponding Ward identity even at finite lattice spacing and finite g which is discussed in Sec. 3.4.3.

The numerical simulation is carried out using a variant of the well-known hybrid

⁴⁵Provided that the required substitutions of (3.2.8) have been applied, of course.

Monte Carlo algorithm (HMC) [37]. Since for the models at hand a closed expression for the fermion determinant is known the fermionic contribution can be calculated considerably fast by utilizing this explicit expression. This closed form of the determinant follows easily from the fact that D_{xy} is almost lower triangular⁴⁶:

$$D_{xy} = \begin{pmatrix} 1 + m + 3g\varphi_1^2 & 0 & \dots & -1 \\ -1 & 1 + m + 3g\varphi_2^2 & 0 & \dots & 0 \\ 0 & -1 & \ddots & \ddots & \vdots \\ \vdots & & & & \\ 0 & \dots & & -1 & 1 + m + 3g\varphi_N^2 \end{pmatrix}. \quad (3.3.7)$$

If the determinant is expanded along the first row one finds

$$\det D_{xy} = (1 + m + 3g\varphi_1^2) \prod_{x=2}^N (1 + m + 3g\varphi_x^2) + (-1)^{N-1}(-1) \det(\tilde{D}). \quad (3.3.8)$$

The $(N-1) \times (N-1)$ -matrix \tilde{D} is upper triangular and so its determinant is given by the diagonal elements, hence

$$\det D_{xy} = \prod_x (1 + m + 3g\varphi_x^2) - 1. \quad (3.3.9)$$

This also shows that the fermion determinant is positive for $m > 0, g \geq 0$ and hence the determinant can be rewritten as an effective fermionic action

$$\det D_{xy} = e^{\ln \det D_{xy}} \equiv e^{-S_{\text{eff}}}. \quad (3.3.10)$$

With the help of (3.3.9) the contributions to the equations of motion can be readily computed. The common stochastic approximation of the determinant (based on the so-called pseudofermions) is completely avoided. For the Stratonovich prescription the computation of the fermion determinant can be carried out analogously, and using $\sigma_x = \frac{1}{2}(\varphi_x + \varphi_{x-1})$ once more yields

$$\det D_{xy} = \prod_x \left(1 + \frac{1}{2} (m + 3g\sigma_x^2) \right) - \prod_x \left(1 - \frac{1}{2} (m + 3g\sigma_x^2) \right). \quad (3.3.11)$$

Again, the determinant is found to be positive and so (3.3.10) remains valid. In conclusion it is worthwhile to mention that the formulas (3.3.9) and (3.3.11) can be easily generalized to arbitrary superpotentials [9].

⁴⁶This special shape is owed to the lack of spinor indices in one dimension. Unfortunately because of this it cannot be generalized to higher dimensions.

3.3.2 SLAC fermions

Stimulated by recent studies of the same model within the Hamiltonian formalism on a spatial lattice [51] an alternative choice of lattice fermions seems very promising. There it was shown for the Wess-Zumino model in one or two dimensions, that SLAC fermions [52, 53] are superior to Wilson fermions when extrapolating lattice results towards the continuum limit. For instance, large $\mathcal{O}(a)$ artifacts originating from the Wilson term are absent simply due to the fact that no doublers are encountered in the first place.

The matrix elements of the SLAC derivative for an odd number of lattice points are given by⁴⁷

$$\partial_{x \neq y} = (-1)^{x-y} \frac{\pi/N}{\sin(\pi(x-y)/N)} \quad \text{and} \quad \partial_{xx} = 0. \quad (3.3.12)$$

Apart from the fact that the SLAC derivative is anti-symmetric like the symmetric difference operator it has neither doublers in its spectrum nor is it local. Especially the latter point has led to its rejection in the context of four-dimensional lattice gauge theories a long time ago [54]. On the other hand recent calculations in lattice perturbation theory to one-loop order employing the SLAC derivative have shown that for the Wess-Zumino models in one and two dimensions no problems arise therefrom [9]. What remains nonetheless is the greater numerical effort which will be readdressed later on.

As with Wilson fermions different bosonic lattice actions can be considered:

$$S_{\text{unimpr}} = \sum_x \frac{1}{2} (\partial^{\text{slac}} \varphi)_x^2 + W_x^2, \quad (3.3.13)$$

$$S_{\text{impr}} = \frac{1}{2} \sum_x ((\partial^{\text{slac}} \varphi)_x + W_x)^2. \quad (3.3.14)$$

According to the lattice supersymmetry transformations (3.2.12) they behave exactly as their Wilsonian counterparts but differ of course from (3.3.6) both in the concrete form of the kinetic term and in their lack of a Wilson term in the lattice operators W_x and W_{xy} derived from the superpotential:

$$W_x = m\varphi_x + g\varphi_x^3, \quad W_{xy} = (m + 3g\varphi_x^2)\delta_{xy}. \quad (3.3.15)$$

Unfortunately, there is no longer a simple expression for the fermion determinant D_{xy} as the associated matrix is no longer sparse. Nonetheless the determinant is still positive. To see this first note that since D_{xy} is a real matrix all complex eigenvalues have to come in c.c. pairs from which no negative sign can arise. Real eigenvalues λ on the other hand

⁴⁷The reason for an odd number of lattice sites stems from the requirement to have all matrix elements of D_{xy} to be real.

Nr.	Model name	Equation	Supersymmetries		Superpotential modified
			$g = 0$	$g \neq 0$	
(1)	Wilson unimproved	(3.3.4)	none	none	yes
(2)	Wilson improved	(3.3.6)	both	one	yes
(3)	Wilson shifted superpot.	(3.3.5)	both	none	yes
(4)	Wilson Stratonovich	(3.2.33)	one	one	yes
(5)	Slac unimproved	(3.3.13)	both	none	no
(6)	Slac improved	(3.3.14)	both	one	no

Table 1: Overview of the various lattice models which are compared to each other. Besides the reference for their definition also the number of supersymmetries that are preserved is listed for the free and interacting case. The last columns shows whether the superpotential has to be supplemented with a Wilson term in order to avoid species doubling.

can be assigned to real, normalized eigenvectors v_x . Thus they take the form⁴⁸

$$\lambda = \sum_{x,y} v_x (\partial_{xy}^{\text{slac}} + W_{xy}) v_y = \sum_x W_{xx} v_x^2. \quad (3.3.16)$$

In other words $\lambda > 0$ holds for W_{xy} positive definite. This follows readily from (3.3.15) and proves the claim. The fermion determinant is again rewritten as

$$\det D_{xy} = e^{\ln \det D_{xy}} = e^{\text{tr} \ln D_{xy}} \equiv e^{-S_{\text{eff}}}. \quad (3.3.17)$$

and the contribution to the equations of motion are now computed from

$$\frac{\partial S_{\text{eff}}}{\partial \varphi_z} = \text{tr} \left(D^{-1} \frac{\partial D}{\partial \varphi_z} \right) = (D^{-1})_{zz} (m + 6g\varphi_z). \quad (3.3.18)$$

The last equation reveals that the inverse of D_{xy} has to be computed once for each time step in the integration. This increases the numerical effort considerably. However, even for large lattices of say a hundred lattice points it is nevertheless possible to treat the fermion matrix in this way, and stochastic and inevitably noisy estimates are still avoided.

3.4 Numerical analysis

Up to now the construction of six different lattice actions has been described as summarized in Table 1. The aim of this section is to present recent results about the dynamics of the respective lattice quantum theories. While the free theory can be solved exactly the interacting case is best analyzed by means of MC simulations. In particular this method can be easily generalized to higher dimensions where the Hamiltonian techniques of Sec. 3.1.2 become inapplicable.⁴⁹ In the following correlation functions for both the bosonic and fermionic fields are studied. From the twopoint functions the energy gap of

⁴⁸Recall that $(Dv)_x = \lambda v_x$ and $\sum_{x,y} v_x v_y = \delta_{xy}$ by assumption and $\sum_{x,y} v_x \partial_{xy}^{\text{slac}} v_y = 0$ because of the anti-symmetry of ∂^{slac} .

⁴⁹Having the latter as an alternative available here is fortunate and allows for a cross-check of the numerical results.

the first excited state is extracted in both channels to check whether they are degenerate at finite lattice spacing or become so at least in the continuum limit. Since from a field theoretical point of view the first excitation of the Hamiltonian in higher dimensions is usually referred to as the particle's mass this language will be adopted here, too. To set the scale it suffices to fix the space-time volume, i.e. length of the interval to equal unity in physical dimensions.⁵⁰ For a lattice of size N the lattice spacing is hence evaluated as $a = 1/N$. Together with the physical extension of the interval also the mass of the particle is held fixed at $m_{\text{phys}} = 10$.⁵¹ The bare lattice parameters m and g are then found from (3.1.6) and take the form

$$m = m_{\text{phys}} \cdot a = \frac{m_{\text{phys}}}{N}, \quad g = g_{\text{phys}} \cdot a^2 = \frac{m_{\text{phys}}}{N^2}. \quad (3.4.1)$$

For simplicity the coupling strength is from now on measured in terms of the dimensionless ratio λ , cf. (3.1.9). For the results presented below it was taken to be $\lambda = 1$ and $\lambda = 8$, i.e. the system was analyzed at strong and very strong coupling.

3.4.1 Free theory

For the free theory ($W'(\varphi) = m\varphi$) the action is quadratic in both the bosonic and fermionic fields:

$$S_{g=0} = \sum_{x,y} (\varphi_x K_{xy} \varphi_y + \bar{\psi}_x D_{xy} \psi_y). \quad (3.4.2)$$

This property may be utilized to invert the respective kernels K_{xy} and D_{xy} to compute the twopoint functions,

$$\langle \varphi_x \varphi_y \rangle = K_{xy}^{-1}, \quad \langle \psi_x \bar{\psi}_y \rangle = D_{xy}^{-1} \quad (3.4.3)$$

from the lattice path integral exactly. Furthermore from Tab.1 the models (2) and (3) as well as (5) and (6) coincide in this limit.⁵² One finds for them the relation

$$K = D^T D, \quad (3.4.4)$$

which is also true for model (4), i.e. the Wilson model with Stratonovich prescription. Obviously, in the free theory fermions and bosons decouple leading to $\det D_{xy} = \text{const.}$ That means that MC simulations can be performed without the inclusion of the fermion determinant, i.e. quenched. Comparing the data of the two point functions generated this way with the exact results determined from (3.4.3) it is possible to assess the amount of configurations necessary to achieve a given precision.

⁵⁰After all this is still quantum mechanics.

⁵¹It can be checked that the ground state wave function fits neatly into the interval, i.e. the Compton wave-length of the particle is 10 times smaller than the volume. Hence finite size effects can be safely neglected.

⁵²Recall that for $g = 0$ it was shown that $\Delta S = 0$, cf. Eq. (3.2.24) and below.

3.4.2 Masses

The effective masses in the bosonic and fermionic sector, m_B and m_F , are extracted from corresponding twopoint functions given by

$$\tilde{C}_B(t) = \langle \varphi_0 \varphi_t \rangle \quad \text{and} \quad \tilde{C}_F(t) = \langle \bar{\psi}_0 \psi_t \rangle. \quad (3.4.5)$$

To improve on the signal to noise ratio translational invariance due to periodic boundary conditions was used to average (3.4.5) over all N lattice sites in the following way⁵³

$$C_B(t) = \frac{1}{N} \sum_{t'} \langle \varphi_{t'} \varphi_{t+t'} \rangle, \quad C_F(t) = \frac{1}{N} \sum_{t'} \langle \bar{\psi}_{t'} \psi_{t+t'} \rangle. \quad (3.4.6)$$

As explained in the introduction the mass gap, i.e. the energy difference between the first excited state and the ground state is projected out at large times,

$$\lim_{t \rightarrow \infty} C_{B,F}(t) \sim e^{-m_{B,F}|t|}. \quad (3.4.7)$$

In awareness of systematic errors (including the possible influence of higher excitations) the fit was done for each single correlator several times, varying the fit window,

$$I = [0 + t_A, N/2 - t_B] \cup [N/2 + t_B, N - t_A] \quad (3.4.8)$$

with respect to t_A and t_B . In practice it was sufficient to discard the first few points $t_A \geq 4$ from the twopoint function to get rid of the contributions stemming from higher excited states.⁵⁴ The second parameter t_B was adjusted in such a way that too noisy data was discarded. Periodic boundary conditions imply $C(-t) = C(N - t)$, and it follows that

$$C_{B,F}(t) \sim e^{-m_{B,F}t} + e^{-m_{B,F}(N-t)} \sim 2e^{-\frac{N}{2}m_{B,F}} \cosh \left(m_{B,F} \left(t - \frac{N}{2} \right) \right). \quad (3.4.9)$$

The function to which the twopoint correlator is finally fitted in the interval I is thus given by

$$C(t) = C_0 \cosh \left(m \left(t - \frac{N}{2} \right) \right). \quad (3.4.10)$$

The low dimensionality of the system makes it possible to use very fine lattices of up to $N = 203$ points which amounts to very small lattice spacings of about $a = 5.0 \times 10^{-3}$. Especially for the evaluation of the bosonic two point function very high statistics were required. Typically 250,000 independent configurations were necessary to achieve the desired accuracy. For each correlator the data set was binned into 100 bins from which the Jack Knife error estimates for the fit parameters were computed. Finally these

⁵³The presence of a possible disconnected part in the bosonic correlator is not anticipated since the bosonic potential $V(\varphi) = W'(\varphi)^2$ is symmetric and hence $\langle \varphi \rangle = 0$.

⁵⁴It can be learned from Fig. 1, for instance, that the separation between the energy levels increases for larger values of λ leading to an increasingly large suppression of higher order contributions.

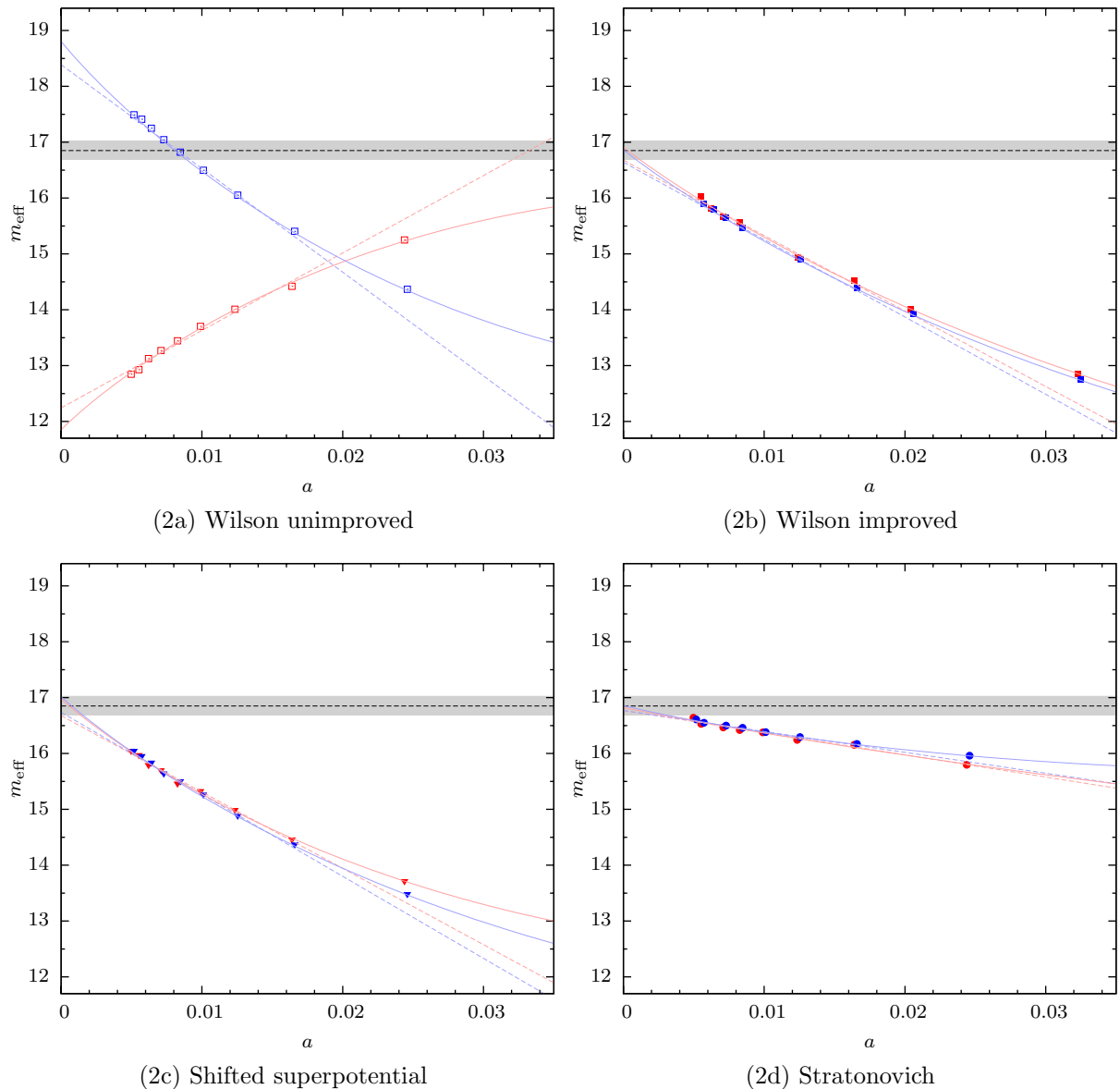


Figure 2: Continuum extrapolation of the effective mass (in physical units) for the models with Wilson fermions. Data for the fermions is set in blue, the bosonic data is set in red. All errors are smaller than the size of the symbols. For better visibility the blue points are shifted slightly to the right. The black dashed line denotes the continuum value as computed from the diagonalisation of the Hamiltonian, the gray area depicts the 1% interval. The colored dashed lines correspond to linear fits of the respective data while the solid curves correspond to the NLO-fit mentioned in the main text.

were combined with the analysis of the systematic error to yield the final error estimate for m_F and m_B . Due to the large statistics and the large number of lattice points available to the fit it was possible to reduce the uncertainty significantly below 1%. Since, however, the described procedure is quite involved the analysis was restricted to a single coupling strength, $\lambda = 1.0$. This is the same choice as in [24, 55], which makes a direct comparison possible. To extrapolate the lattice results to the continuum it was further required to repeat the analysis for various lattice sizes ranging from $N = 31$ to $N = 203$. The results are shown in Fig. 2 for the models with Wilson and in Fig. 3 for the two models with Slac fermions as a function of the lattice spacing. Given the available statistics and the chosen scale of the graphs errors could be made smaller than the symbols used to depict the data points. In case of Wilson fermions the large range

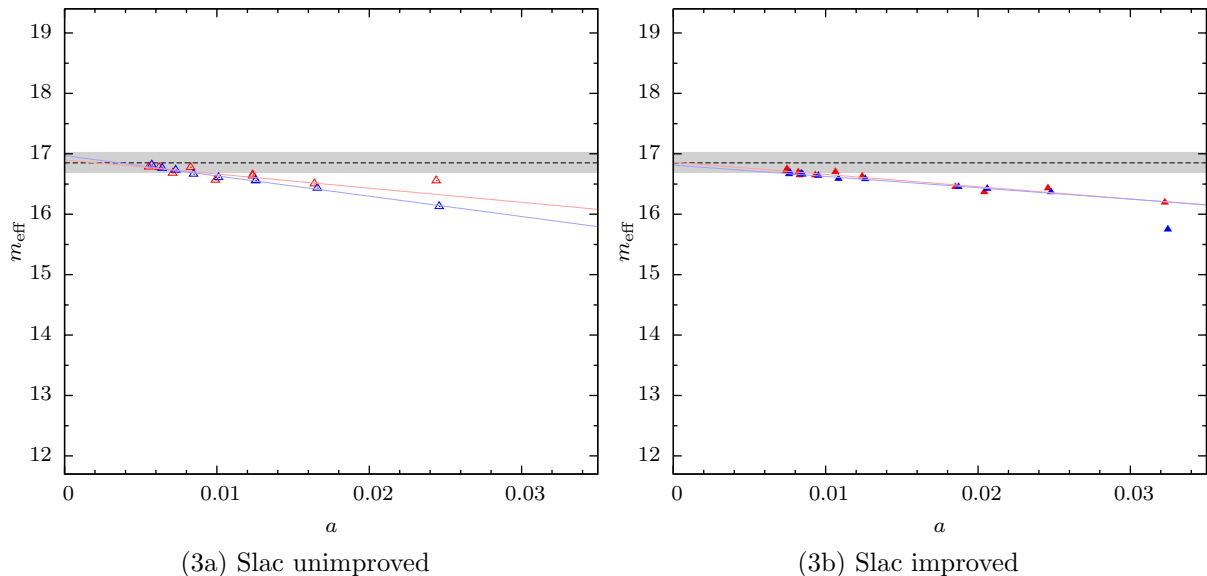


Figure 3: Continuum extrapolation of the effective mass (in physical units) as seen in the models with Slac fermions. Fermionic data is set in blue, bosonic data is set in red. Error bars could be omitted once more and the blue points are again slightly shifted to the right. Dashed black line and gray bar are the same as in Fig. 2.

of attainable lattice spacings made it possible to resolve next-to-leading order (NLO) corrections to the leading scaling behavior which is $\mathcal{O}(a)$ due to the Wilson term. For the extrapolation to the continuum all data was fitted twice using either

$$m(a) = m_{\text{eff}} + \beta \cdot a \quad (3.4.11)$$

or

$$m(a) = m_{\text{eff}} + \beta \cdot a + \gamma \cdot a^{3/2}. \quad (3.4.12)$$

The results for all six models are listed in Table 2. The exponent of the next to leading term in the second equation was found numerically by extrapolation the mass extracted from the exact free propagator from a much larger set of different lattice spacings. Upon the inclusion of the NLO term the extrapolation for the models (1) – (4) becomes much more reliable.⁵⁵ Comparing the various models the following can be said. As expected in the unimproved Wilson model (1) the two masses do not coincide at any finite lattice spacing. Moreover even in the continuum limit they are clearly separated. This discrepancy was also seen by Giedt et al. [55] who traced its origin to a special diagram belonging to the lattice fermion propagator. This contribution not being properly taken into account, the unimproved model fails to yield the correct (supersymmetric) continuum limit. For the other three models belonging to the class with Wilson fermions the

⁵⁵For completeness it has to be stated that the linear fit yields reliable figures only on a limited set of data points including only those with $a \leq 0.015$. The fit up to next-to-leading order matches the whole data set quite well. The second fit is also more stable w.r.t the removal of single points from either end. Omitted points match still very well afterwards. This is not the case for the linear fit and constrains the usable data points as mentioned before.

Model	m_B (linear fit)	m_B (NLO)	m_F (linear fit)	m_F (NLO)
Wilson naive	12.24(10)	11.85(12)	18.39(8)	18.81(4)
Wilson shifted superpot.	16.68(7)	16.98(10)	16.73(5)	17.02(5)
Wilson improved	16.68(10)	16.91(10)	16.64(5)	16.86(2)
Wilson improved (Strat.)	16.77(5)	16.82(9)	16.77(2)	16.86(2)
Slac unimproved	16.90(8)	–	16.97(4)	–
Slac improved	16.86(5)	–	16.81(3)	–

Table 2: Continuum extrapolations for the effective masses. For Slac fermions only a linear fit was applied. The continuum value to compare with is $m_{\text{eff}} = 16.865$.

situation is different. Bosonic and fermionic masses are in good agreement at any finite lattice spacing and reach the desired continuum result to high accuracy. Furthermore the models (2) and (3)⁵⁶ yield very similar masses. One may conclude from this, that the existence of both supersymmetries in the free theory is a sufficient condition to reach the supersymmetric continuum limit even at finite coupling. With respect to discretisation artifacts model (4) outperforms the former two clearly. At the same time the artifacts at finite lattice spacing are much smaller, the influence of the NLO-term in (3.4.12) is strongly reduced and the extrapolation is in still better agreement with the continuum result.

Comparing the Wilson models (1) – (4) to the Slac models (5), (6) lattice artifacts are once more drastically reduced. Discarding very coarse lattices no significant difference can be seen, and bosonic and fermionic masses are again in excellent agreement with each other. Employing the same reasoning this may once more be traced back to the fact that the unimproved model respects two supersymmetries at $\lambda = 0$. According to Tab. 2 the masses obtained from model (6) are closest to the correct value of $m_{\text{eff}} = 16.865$ despite the fact that the extraction of the NLO behavior was not possible so that only (3.4.11) could be reliably used.

3.4.3 Ward identities

Following the discussion of Section 3.1.3 the Ward identities (3.1.27) and (3.1.28) that is their lattice counterparts,

$$\mathcal{R}^{(1)}(t) \equiv \delta^{(1)} \langle \varphi_t \bar{\psi}_0 \rangle = \langle \psi_t \bar{\psi}_0 \rangle - \langle \varphi_t ((\partial\varphi)_0 + W_0) \rangle, \quad (3.4.13a)$$

$$\mathcal{R}^{(2)}(t) \equiv \delta^{(2)} \langle \psi_t \varphi_0 \rangle = \langle \psi_t \bar{\psi}_0 \rangle + \langle ((\partial\varphi)_t - W_t) \varphi_0 \rangle, \quad (3.4.13b)$$

were analysed by means of MC simulations for the models (2)–(6).^{57,58} At $\lambda = 0$ all of these preserve either one (model (4)) or both supersymmetries (models (2),(3),(5))

⁵⁶Model (3) is the same as analyzed in [24] and [55], their results being confirmed. The analysis of all other model is due to the research group in Jena to which the author belongs.

⁵⁷The unimproved Wilson model (1) is no longer considered because it does not yield the desired continuum limit, cf. Fig. 22a.

⁵⁸In both expressions the respective choice of the superpotential W_x for each distinct model is understood.

and (6)). This can be checked explicitly from $(\partial\varphi)_x + W_x = (D\varphi)_x$, (3.4.2) and (3.4.4), which leads to

$$\langle\psi_x\bar{\psi}_y\rangle - \langle\varphi_x D_{yz}\varphi_z\rangle = D^{-1}_{xy} - D_{yz}K^{-1}_{zx} = D^{-1}_{xy} - D_{yx}^{-T} = 0 \quad (3.4.14)$$

The first WI is thus reduced to a simple matrix identity and a similar calculation can also be carried out for the second WI.

For $\lambda \neq 0$ the models (2),(4) and (6) are still invariant under one supersymmetry and the corresponding WI (3.1.27) should also be found to hold numerically. However, the second supersymmetry is then inevitably broken and the aim is to measure the actual size by which it is violated. Since the action is no longer invariant the WI becomes in fact a Schwinger-Dyson equation and the non-vanishing variation of the action has to be taken into account. The result may be formally cast into

$$\langle(\delta A)B\rangle + \langle A(\delta B)\rangle = \langle AB(\delta S)\rangle. \quad (3.4.15)$$

Hence the rhs. of (3.4.13) is no longer expected to yield zero for the broken supersymmetry. To enhance the lattice artifacts a comparatively coarse lattice with $N = 21$ lattice points was used.⁵⁹ Since in both WIs fermionic twopoint functions are involved the WIs are expected to be suppressed exponentially for large t , too. To improve the signal to noise ratio translational invariance was used again to average both $\mathcal{R}_1(t)$ and $\mathcal{R}_2(t)$ over the lattice, cf. (3.4.6) and (3.4.7).

First of all the identity (3.4.14) was confirmed numerically from quenched ensembles. The results are shown in Fig. 4.⁶⁰ For each model four replicas, each consisting of 10^6 independent configurations, were sampled. This way the identities could be confirmed up to 1‰ for the models with Wilson fermions and up to 2‰ for the models with Slac fermions. The fact that for the latter the noise is larger by a factor of 20 may be traced back to the highly populated kinetic operator matrix and must be regarded as a genuine disadvantage. Also for model (4), i.e. Wilson fermions using the Stratonovich prescription both WIs are fulfilled to high accuracy. This may come as a surprise but can be understood analytically from the property of D being normal.⁶¹ As explained already these simulations were used to assess the resolution up to which possible deviations can be measured. The gray bars found in all figures of this section were determined as to include the above data together with its Jack Knife errors. They constitute the background upon which the WIs for the interacting theory will be judged.

To this end the WIs were once more computed at $\lambda = 8$. For the three types of Wilson fermions the results are given in Fig. 5. As expected the outcome is partly different.

⁵⁹This corresponds to a lattice spacing of roughly $a \approx 0.048$. Finer lattices were also studied but the effects to be discussed in the main text vanish rapidly for finer lattices and become indistinguishable from statistical noise very soon.

⁶⁰In all graphs in this section quantities are plotted in units of the lattice spacing. Hence t runs from 0 to 20 and not to 1.

⁶¹Normal matrices obey $DD^T = D^TD$, which follows from the fact that for the free theory D is (for every model) a circulant matrix and so is D^T . Circulant matrices, of course, commute.

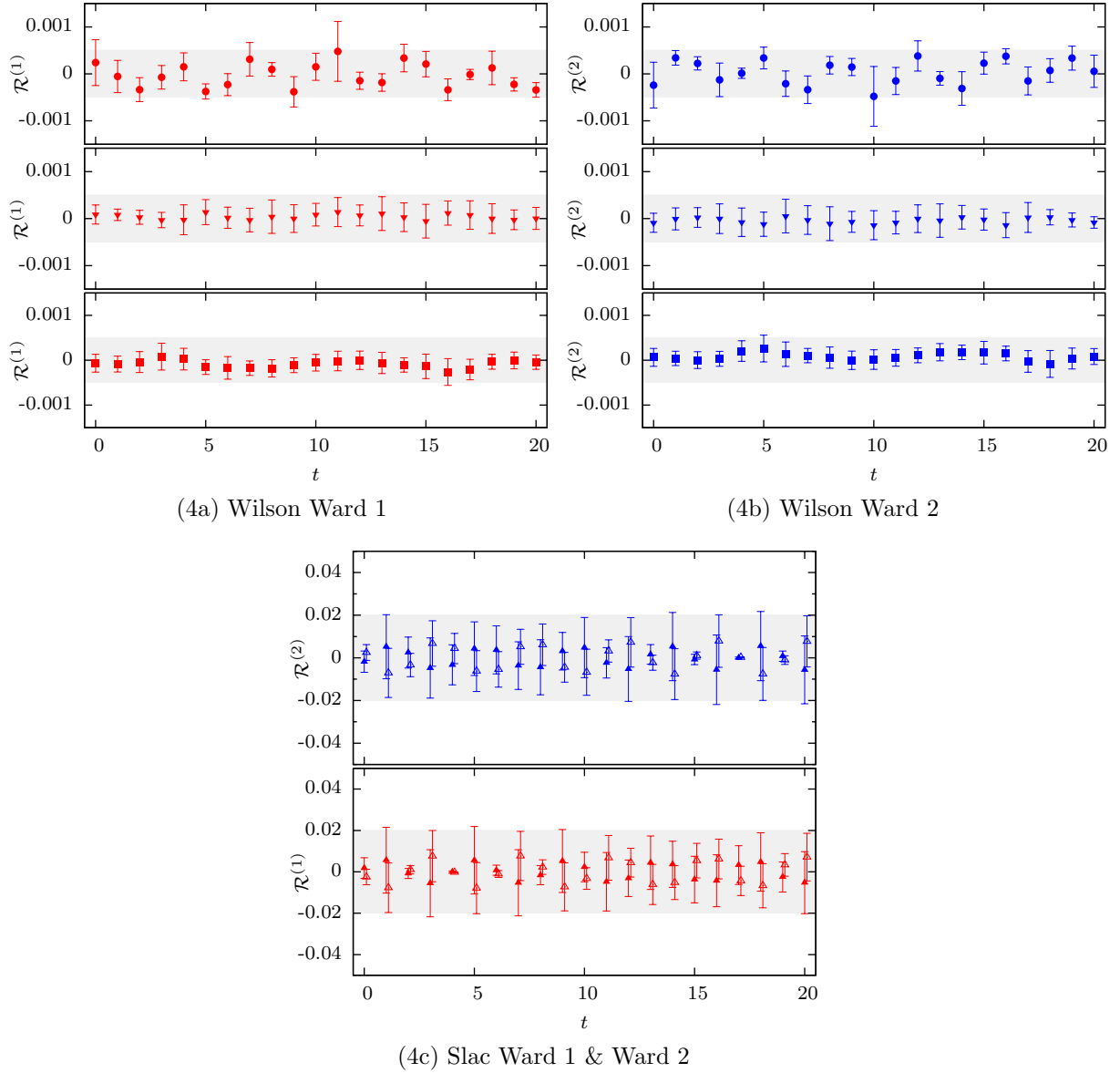


Figure 4: Ward identities $\mathcal{R}^{(1)}(t)$ (blue) and $\mathcal{R}^{(2)}(t)$ (red) for the free theory, i.e. at $\lambda = 0$. The data is obtained from (quenched) MC simulations to study the impact of statistical noise on the results. In Figs. (4a) and (4b) are shown from bottom-up models (2) \blacksquare , (3) \blacktriangledown and (4) \bullet . Fig. (4c) shows model (5) \triangle and model (6) \blacktriangle . The data points for model (5) are slightly shifted to the right for better visibility. The gray shaded areas include each time all data points and mark the given precision to distinguish the data from being zero. The interval bounds of the Wilson fermions is reused in Fig. 5 as well as in Fig. 6, see also the main text.

All improved models (2), (4) and (6) still respect the first WI (3.4.13a) depicted with blue symbols in all graphs while for model (3) the violation of both supersymmetries is now, cf. Fig (5b). For large times, i.e. $t \geq 4$ all deviations decrease and are found to be compatible with zero within the available statistics. Comparing the absolute sizes of the deviations the Stratonovich action is larger by a factor of about three when compared to the improved Wilson model. In Model (3) with shifted superpotential they are half the size than for model (2). This can be explained from the fact that the deviation couples directly to ΔS , cf. (3.4.15), which is – with regard to the second supersymmetry – twice the size for model (2) than for model (3) as was pointed out after (3.2.25).

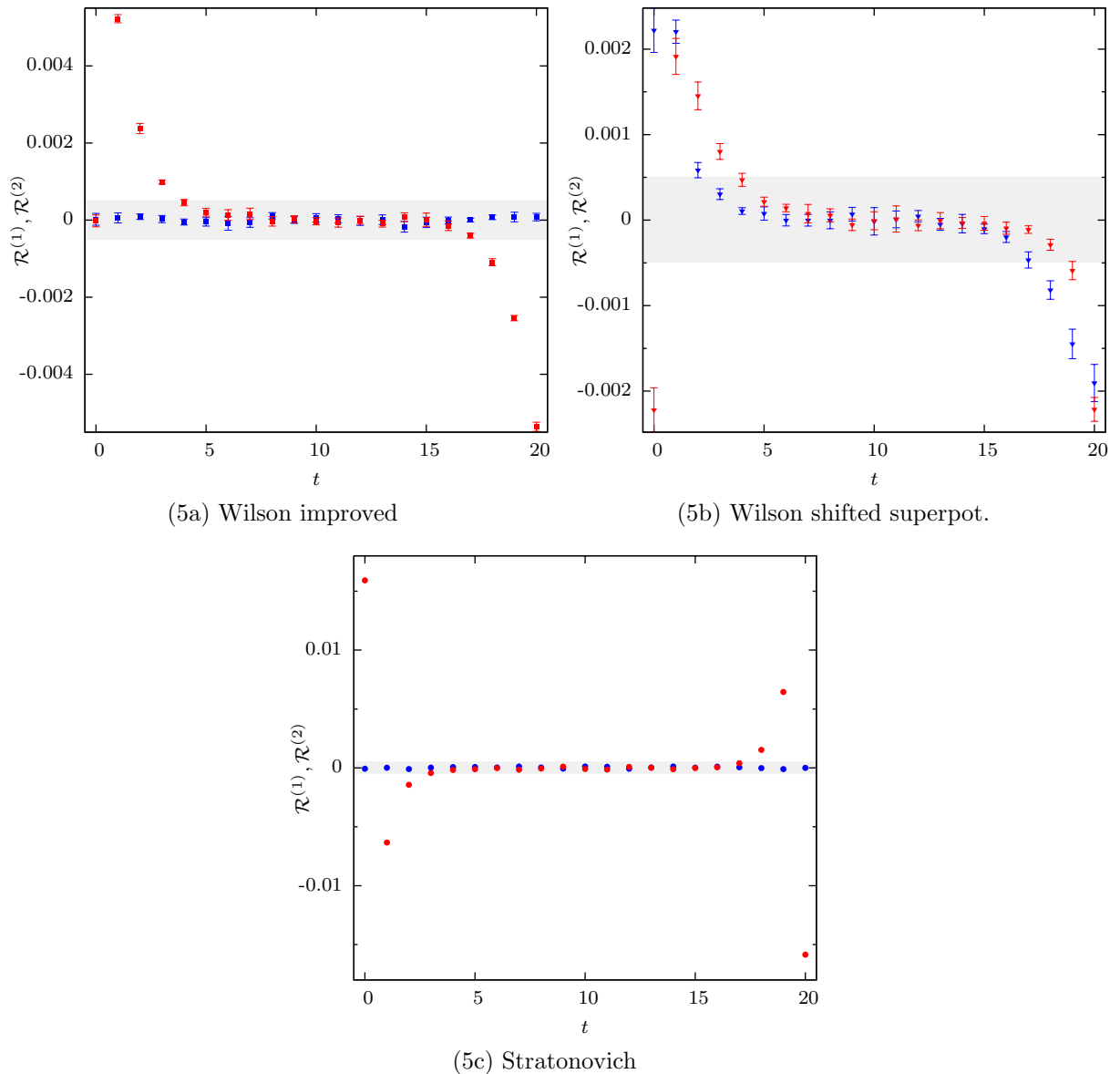


Figure 5: Ward identities $\mathcal{R}^{(1)}(t)$ (blue) and $\mathcal{R}^{(2)}(t)$ (red) for the interacting theory at $\lambda = 8$ using the Wilson models (2) $\blacksquare, \blacktriangledown$, (3) $\blacktriangledown, \blacktriangledown$ and (4) \bullet, \bullet . For the gray shaded areas see Fig. 4. In (5c) errors are smaller than the symbol size.

For Slac fermions the WIs again look quite different, cf. 6. In the improved model (6) the first WI is fulfilled to high precision. The fluctuations are now found to be of the same size than for the models with Wilson fermions which clearly differs from what was found for the free theory. The shaded area again corresponds to $I = [-5, 5] \times 10^{-4}$. A reason for this may be given heuristically by the observation that at $\lambda = 8$ corresponding to $m = 10$, $g = 800$, kinetic fluctuations are highly suppressed in favor of the very steep potential. Also the Dirac operator is now dominated by the interaction term, all off-diagonal matrix elements being comparatively irrelevant. At the contrary the second WI, i.e. $\mathcal{R}^{(2)} = 0$ is now violated for all t although an exponential decay remains visible. The oscillatory behavior typical for Slac fermions is directly related to the discontinuity of the momentum space Dirac operator at the edge of the Brillouin zone.⁶² For the

⁶²Applying suitably chosen filters to smoothen the discontinuity is possible and partly removes the oscillatory behavior. See also [9] for more details.

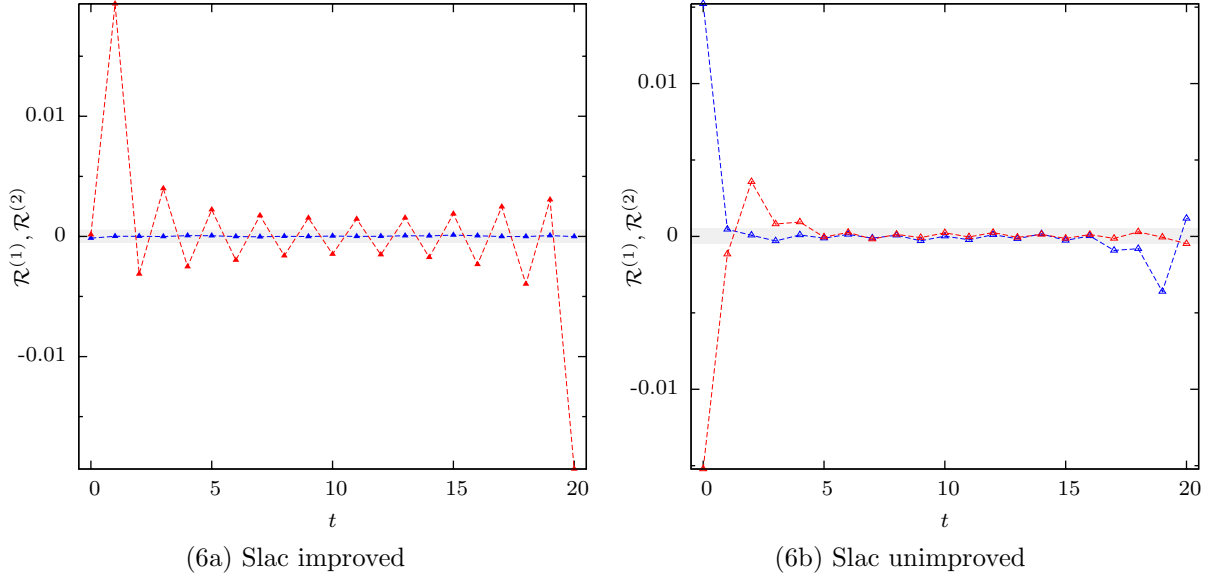


Figure 6: Ward identities $\mathcal{R}^{(1)}(t)$ (blue) and $\mathcal{R}^{(2)}(t)$ (red) for the interacting theory at $\lambda = 8$ using the Slac models (5) \triangle, \triangle and (6) $\blacktriangle, \blacktriangle$. For the gray shaded areas see Fig. 4. The dashed lines are drawn to guide the eyes.

unimproved model (5) both WIs are strongly violated for $t \leq 2$ but become compatible with zero afterwards. This could be taken again as an indicator that with the Slac derivative the continuum is much better approximated.

4 The $\mathcal{N} = (2, 2)$, $d = 2$ Wess-Zumino model

In this section the construction of supersymmetric lattice actions by means of a Nicolai-map is applied to the $\mathcal{N} = (2, 2)$ Wess-Zumino model⁶³ in two (Euclidean) dimensions. The organization of this section parallels those of the previous. However, more emphasis is put onto numerical issues since simulations become considerably more involved due to an increased effort in the computation of the fermion determinant. Firstly the continuum model is briefly recalled with intent to introduce the notation for the following. In Sec. 4.1.2 the improved lattice action is then constructed. Thereafter, different lattice fermions are once more discussed to establish the various lattice models for the numerical analysis. For a given specific superpotential, it turns out that the lattice models behave differently under some discrete symmetries specific to this choice. This is the subject of Sec. 4.3. Before the numerical results are presented two sections are devoted to performance issues of the MC simulations required. The first introduces distinct algorithms for the inclusion of the fermion determinant, while the second discusses two significant algorithmic improvements of the numerical integration which is part of the HMC algorithm. Finally, in Sec. 4.6 and 4.7 the numerical analysis is presented.

The $\mathcal{N} = (2, 2)$, $d = 2$ WZ-model has been thoroughly discussed in the literature . For a discussion of the underlying supersymmetry algebra and superspace construction see for instance the text book by West [56]. Numerical studies of this model may also be found in [48, 49, 57].

4.1 The continuum model

The $\mathcal{N} = (2, 2)$ Wess-Zumino model can be obtained from dimensional reduction of the $\mathcal{N} = 1$ Wess-Zumino model in four dimensions, the original model proposed by Wess and Zumino [2]. Alternatively, there is a powerful superspace-formalism in two dimensions from which the model can be constructed, too.

4.1.1 Definition and terminology

Motivated by the superspace formalism the model will be first described using complex coordinates in (Euclidean) space-time:

$$z = x_0 + ix_1, \quad \bar{z} = x_0 - ix_1, \quad \partial = \frac{1}{2}(\partial_0 - i\partial_1), \quad \bar{\partial} = \frac{1}{2}(\partial_0 + i\partial_1). \quad (4.1.1)$$

In this complex basis it is also more convenient to combine the real scalar and pseudo-scalar that made up the original field content of the (four-dimensional) WZ-model into

⁶³The notation $\mathcal{N} = (2, 2)$ will be explained below.

one complex scalar field⁶⁴

$$\varphi = \varphi_1 + i\varphi_2, \quad \bar{\varphi} = \varphi_1 - i\varphi_2. \quad (4.1.2)$$

To match the two (propagating) bosonic degrees of freedom the same number of fermionic degrees of freedom have to be introduced. In two dimensions these are provided by a two-dimensional Dirac spinor ψ . The action of the $\mathcal{N} = (2, 2)$, $d = 2$ WZ-model is then given by

$$S = \int d^2x \left(2(\bar{\partial}\bar{\varphi})(\partial\varphi) + \frac{1}{2}|W'(\varphi)|^2 + \bar{\psi}M\psi \right), \quad (4.1.3)$$

where

$$M = \gamma^\mu \partial_\mu + W''P_+ + \overline{W''}P_- = \begin{pmatrix} W'' & 2\bar{\partial} \\ 2\partial & \overline{W''} \end{pmatrix}, \quad P_\pm = \frac{1}{2}(1 \pm \gamma_*) . \quad (4.1.4)$$

Again bosonic potential and the Yukawa couplings are derived from a superpotential $W(\varphi)$. In contrast to the one-dimensional case the superpotential is now constrained to be a holomorphic function of its argument φ . The Dirac spinors can be decomposed according to

$$\psi = \begin{pmatrix} \psi_1 \\ \psi_2 \end{pmatrix}, \quad \bar{\psi} = (\bar{\psi}_1, \bar{\psi}_2), \quad (4.1.5)$$

and the Weyl basis is chosen for the gamma matrices,

$$\gamma_0 = \sigma_1, \quad \gamma_1 = -\sigma_2, \quad \gamma_* = \sigma_3. \quad (4.1.6)$$

In components the action (4.1.3) thus reads

$$S = \int d^2x \left(2(\bar{\partial}\bar{\varphi})(\partial\varphi) + \frac{1}{2}|W'(\varphi)|^2 + 2\bar{\psi}_1\bar{\partial}\psi_2 + 2\bar{\psi}_2\partial\psi_1 + \bar{\psi}_1W''\psi_1 + \bar{\psi}_2\overline{W''}\psi_2 \right). \quad (4.1.7)$$

From dimensional analysis the canonical mass dimensions of the various operators are

$$[\varphi] = 0, \quad [\psi] = [\bar{\psi}] = \frac{1}{2}, \quad [W(\varphi)] = [W'(\varphi)] = [W''(\varphi)] = 1. \quad (4.1.8)$$

It follows, that all coupling constants in $W(\varphi)$ have mass dimension one. The superpotential of the free theory is similar to the one-dimensional case and given by

$$W_2(\varphi) = \frac{1}{2}m\varphi^2, \quad W_2'(\varphi) = m\varphi, \quad W_2''(\varphi) = m. \quad (4.1.9)$$

⁶⁴Note that complex conjugation in the space-time and in the target space need not necessarily mean the same. This statement will be made more precise when classical symmetries are discussed in Sec.4.3

As an example for an interacting theory the superpotential

$$W_3(\varphi) = \frac{1}{2}m\varphi_2 + \frac{1}{3}g\varphi^3, \quad W_3'(\varphi) = m\varphi + g\varphi^2, \quad W_3''(\varphi) = m + 3g\varphi \quad (4.1.10)$$

will be considered later on and is the same as in [48, 49, 57]. It can be shown that supersymmetry is unbroken in the $\mathcal{N} = (2, 2)$ $d = 2$ WZ-model for any choice of the superpotential. In particular, for the superpotential $W_3(\varphi)$ the Witten index is $\text{tr}(-1)^F = n_B - n_F = 2$, which is a sufficient condition for unbroken supersymmetry [5]. As mentioned above all coupling constants have mass dimension one, so that the coupling strength for the superpotential $W_3(\varphi)$ will be measured by

$$\lambda = \frac{g}{m}, \quad (4.1.11)$$

which is hence dimensionless.

4.1.2 Supersymmetries and the Nicolai map

Given the following supersymmetry variations

$$\delta\phi = \bar{\psi}_1\varepsilon_1 + \bar{\varepsilon}_1\psi_1, \quad \delta\psi_1 = -\frac{1}{2}\overline{W'}\varepsilon_1 + \bar{\partial}\varphi\varepsilon_2, \quad \delta\bar{\psi}_1 = -\frac{1}{2}\overline{W'}\bar{\varepsilon}_1 - \partial\varphi\bar{\varepsilon}_2, \quad (4.1.12a)$$

$$\delta\bar{\phi} = \bar{\psi}_2\varepsilon_2 + \bar{\varepsilon}_2\psi_2, \quad \delta\psi_2 = \partial\bar{\varphi}\varepsilon_1 - \frac{1}{2}W'\varepsilon_2, \quad \delta\bar{\psi}_2 = -\bar{\partial}\bar{\varphi}\bar{\varepsilon}_1 - \frac{1}{2}W'\bar{\varepsilon}_2, \quad (4.1.12b)$$

the action (4.1.3) is invariant up to surface terms. This time there are four (real) anti-commuting parameters $\varepsilon_{1,2}$ and $\bar{\varepsilon}_{1,2}$ and hence four real supercharges which constitute the supersymmetry algebra. It can be shown, that this algebra can be decomposed into a chiral (or left-moving) and anti-chiral (or right-moving) sub-algebra, which points to the fact that the model is indeed invariant under an extended supersymmetry.⁶⁵ Moreover it is possible to read off the Nicolai variables from (4.1.12a) by forming suitable linear combinations of the infinitesimal parameters. E.g. with $\bar{\varepsilon}_1 = \bar{\varepsilon}_2 = \bar{\varepsilon}$ and $\varepsilon_1 = \varepsilon_2 = 0$ the variations (4.1.12a) become

$$\delta\phi = \bar{\varepsilon}\psi_1, \quad \delta\bar{\psi}_1 = \left(-\frac{1}{2}\overline{W'} - \partial\varphi\right)\bar{\varepsilon}, \quad \delta\psi_1 = 0, \quad (4.1.13a)$$

$$\delta\bar{\phi} = \bar{\varepsilon}\psi_2, \quad \delta\bar{\psi}_2 = \left(-\frac{1}{2}W' - \bar{\partial}\bar{\varphi}\right)\bar{\varepsilon}, \quad \delta\psi_2 = 0. \quad (4.1.13b)$$

Not surprisingly the Nicolai variable is taken to be a complex function as well,

$$\xi = \xi(\varphi, \bar{\varphi}), \quad \bar{\xi} = \xi(\varphi, \bar{\varphi}). \quad (4.1.14)$$

⁶⁵Finally this motivates the notation $\mathcal{N} = (2, 2)$.

	ε_1	ε_2	$\bar{\varepsilon}_1$	$\bar{\varepsilon}_2$	ξ
$\delta^{(1)}$	ε	ε	0	0	$-2\bar{\partial}\varphi + \bar{W}'$
$\delta^{(2)}$	ε	$-\varepsilon$	0	0	$2\bar{\partial}\varphi + \bar{W}'$
$\delta^{(3)}$	0	0	$\bar{\varepsilon}$	$\bar{\varepsilon}$	$2\bar{\partial}\bar{\varphi} + W'$
$\delta^{(4)}$	0	0	$\bar{\varepsilon}$	$-\bar{\varepsilon}$	$2\bar{\partial}\bar{\varphi} - W'$

Table 3: Linear combinations of infinitesimal generators and corresponding choice for the Nicolai variable. The lattice action will be constructed from $\delta^{(3)}$ in Sec. 4.1.2

Identifying $\delta\bar{\psi}_1 = -\frac{1}{2}\bar{\xi}\varepsilon$ and $\delta\bar{\psi}_2 = -\frac{1}{2}\xi\varepsilon$, the Nicolai map reads explicitly

$$\xi(\varphi, \bar{\varphi}) = 2\bar{\partial}\bar{\varphi} + W', \quad \bar{\xi}(\varphi, \bar{\varphi}) = 2\partial\varphi + \bar{W}'. \quad (4.1.15)$$

With this choice the Jacobian becomes

$$\mathcal{J} = \begin{pmatrix} \frac{\partial\xi}{\partial\varphi} & \frac{\partial\xi}{\partial\bar{\varphi}} \\ \frac{\partial\bar{\xi}}{\partial\varphi} & \frac{\partial\bar{\xi}}{\partial\bar{\varphi}} \end{pmatrix} = \begin{pmatrix} W'' & 2\bar{\partial} \\ 2\partial & \bar{W}'' \end{pmatrix} = M \quad (4.1.16)$$

and the resulting determinant can be written as a fermionic path integral

$$\int \mathcal{D}\xi\mathcal{D}\bar{\xi}e^{-\frac{1}{2}\int\xi\bar{\xi}} = \int \mathcal{D}\varphi\mathcal{D}\bar{\varphi}\mathcal{D}\psi\mathcal{D}\bar{\psi}e^{-\frac{1}{2}\int\bar{\xi}\xi + \int\bar{\psi}M\psi}. \quad (4.1.17)$$

The bosonic action in terms of ξ and $\bar{\xi}$ again differs by a surface term, which from

$$S^{\text{Nic.}} = \frac{1}{2} \int d^2x \bar{\xi}\xi = \frac{1}{2} \int d^2x (2\bar{\partial}\bar{\varphi} + W')(2\partial\varphi + \bar{W}') \quad (4.1.18)$$

may be inferred as

$$\Delta S = S^{\text{Nic.}} - S = W'\partial\varphi + c.c.. \quad (4.1.19)$$

This difference ΔS will be promoted to the lattice improvement term below to ensure that (4.1.13a) is preserved. Instead of the particular linear combination chosen above one may have used a different one to find a similar result. However, the identification of \mathcal{J} and M is most transparent for the choice adopted.⁶⁶ For convenience Table 3 lists all four possible choices.

⁶⁶Otherwise a unitary transformation in the spinor space is required. Of course the result is not affected by this [49].

4.2 Construction of the lattice actions

The construction of the supersymmetric lattice action can now proceed in close analogy to the discussion presented in Sec. 3.2.3. After the transcription of the complex continuum formalism has been achieved, the lattice model will be reformulated with real variables. The reason for this is to have a formalism at hand that is better suited for numerical simulations. Various possibilities for lattice fermions are discussed thereafter. All difference operators are once again assumed to be antisymmetric. This ensures that all four supersymmetries are preserved in the free theory.⁶⁷

4.2.1 Complex formalism

As in the one-dimensional model all lattice fields or operators are straightforwardly obtained from their respective continuum expressions, i.e.

$$\varphi(x), \psi(x) \rightarrow \varphi_x, \psi_x, \partial_0, \partial_1 \rightarrow (\partial_0)_{xy}, (\partial_1)_{xy}, \xi(x) \rightarrow \xi_x \equiv 2(\bar{\partial}\bar{\varphi})_x + W_x. \quad (4.2.1)$$

The construction of the Nicolai variable ξ_x is obviously based on the definition (4.1.15). The lattice action now takes the form

$$S = \frac{1}{2} \sum_x \bar{\xi}_x \xi_x + \sum_{xy} \bar{\psi}_x M_{xy} \psi_y, \quad (4.2.2)$$

with

$$M_{xy} = \begin{pmatrix} W_{xy} & 2\bar{\partial}_{xy} \\ 2\partial_{xy} & \bar{W}_{xy} \end{pmatrix} = \begin{pmatrix} \frac{\partial \xi_x}{\partial \varphi_y} & \frac{\partial \xi_x}{\partial \bar{\varphi}_y} \\ \frac{\partial \bar{\xi}_x}{\partial \varphi_y} & \frac{\partial \bar{\xi}_x}{\partial \bar{\varphi}_y} \end{pmatrix}. \quad (4.2.3)$$

It is assumed that the operators W_x and \bar{W}_x are subject to the same constraints as in the one-dimensional case which were given in Eq. (3.2.14). To see that (4.2.2) is indeed invariant under the lattice transcription of (4.1.13a),

$$\delta\varphi_x = \bar{\varepsilon}\psi_{1,x}, \quad \delta\bar{\psi}_{1,x} = -\frac{1}{2}\bar{\xi}_x\bar{\varepsilon}, \quad \delta\psi_{1,x} = 0, \quad (4.2.4a)$$

$$\delta\bar{\varphi}_x = \bar{\varepsilon}\psi_{2,x}, \quad \delta\bar{\psi}_{2,x} = -\frac{1}{2}\xi_x\bar{\varepsilon}, \quad \delta\psi_{2,x} = 0 \quad (4.2.4b)$$

is now easily worked out. Making use of the fact that M is a Jacobian, cf. (4.2.3), one finds⁶⁸

$$\delta\left(\frac{1}{2}\bar{\xi}_x\xi_x\right) = \frac{1}{2}\bar{\varepsilon}\left(\xi_x\frac{\partial\bar{\xi}_x}{\partial\varphi_y}\psi_{1,y} + \xi_x\frac{\partial\bar{\xi}_x}{\partial\bar{\varphi}_y}\psi_{2,y}\right) + \frac{1}{2}\bar{\varepsilon}\left(\bar{\xi}_x\frac{\partial\xi_x}{\partial\varphi_y}\psi_{1,y} + \bar{\xi}_x\frac{\partial\xi_x}{\partial\bar{\varphi}_y}\psi_{2,y}\right), \quad (4.2.5a)$$

⁶⁷An extra benefit is the possibility to switch smoothly between the complex and real formalism. If the complex kinetic term is expanded in terms of real fields mixed products of the form $\partial_0\varphi_1\partial_1\varphi_2$ appear. Given that ∂_{xy} is antisymmetric they vanish.

⁶⁸Summation over lattice points understood.

$$\delta(\bar{\psi}_x M_{xy} \psi_y) = -\frac{1}{2}\bar{\varepsilon} \left(\bar{\xi}_x \frac{\partial \xi_x}{\varphi_y} \psi_{1,y} + \bar{\xi}_x \frac{\partial \xi_x}{\bar{\varphi}_y} \psi_{2,y} \right) - \frac{1}{2}\bar{\varepsilon} \left(\xi_x \frac{\partial \bar{\xi}_x}{\varphi_y} \psi_{1,y} + \xi_x \frac{\partial \bar{\xi}_x}{\bar{\varphi}_y} \psi_{2,y} \right). \quad (4.2.5b)$$

Thus the variations cancel exactly against each other and no Leibniz rule is required. The same result would be found for any definition of Table 3. However, the Jacobian would equal the naive lattice prescription (4.1.3) of M only after some unitary transformation [49]. Written in full, (4.2.2) takes the form

$$S = \sum_x 2 \left((\bar{\partial}\bar{\varphi})_x (\partial\varphi)_x + \frac{1}{2} |W_x|^2 + W_x (\partial\varphi)_x + \overline{W_x} (\bar{\partial}\bar{\varphi})_x \right) + \sum_{x,y} (\bar{\psi}_{1,x}, \bar{\psi}_{2,x}) \begin{pmatrix} W_{xy} & 2\bar{\partial}_{xy} \\ 2\partial_{xy} & \overline{W_{xy}} \end{pmatrix} \begin{pmatrix} \psi_{1,y} \\ \psi_{2,y} \end{pmatrix}. \quad (4.2.6)$$

If the remaining three supersymmetry transformations (in their naive realizations) are applied one finds again that they lead to terms which would become surface terms in the continuum. Furthermore, the two terms missing from a straightforward discretization,

$$\Delta S = \sum_x \left(W_x (\partial\varphi)_x + \overline{W_x} (\bar{\partial}\bar{\varphi})_x \right) \quad (4.2.7)$$

not unexpectedly represent the lattice analogue of (4.1.19). For the free theory ($W_x = m\varphi_x$) it follows that $\Delta S = 0$ in direct analogy with Sec. 3.2.3. All lattice actions that are derived by this construction will be called *improved* in the following as to distinguish them from their *unimproved* counterparts which do not include ΔS .

4.2.2 Real formalism

As already mentioned real variables are better suited for numerical simulations. The reason for this is, that the fermion matrix M becomes a real matrix and hence the fermion determinant becomes manifestly real, too. This simplifies its treatment in several aspects, e.g. all numerical calculations can be done with real numbers. To arrive at this one adopts the Majorana basis for the gamma matrices,

$$\gamma_0 = \sigma_3, \quad \gamma_1 = \sigma_1, \quad \gamma_* = -\sigma_2. \quad (4.2.8)$$

From the real and imaginary part of φ a two-component vector $\vec{\varphi}_x = (\varphi_{1,x}, \varphi_{2,x})^T$ is formed, and the first and second holomorphic derivatives of the superpotential $W(\varphi)$ are decomposed likewise into real and imaginary parts⁶⁹

$$W_x = U_x(\varphi_1, \varphi_2) + iV_x(\varphi_1, \varphi_2), \quad W_{xy} = U_{xy}(\varphi_1, \varphi_2) + iV_{xy}(\varphi_1, \varphi_2). \quad (4.2.9)$$

⁶⁹The condition $W_{xy} = \frac{\partial W_x}{\partial \varphi_y}$ is of course translated into relations among the operators U_x, V_x and U_{xy}, V_{xy} given by the Cauchy-Riemann equations.

For the superpotential $W_3(\varphi)$ to be studied numerically later this leads to

$$U_x = m\varphi_{1,x} + g(\varphi_{1,x}^2 - \varphi_{2,x}^2), \quad V_x = m\varphi_{2,x} + 2g\varphi_{1,x}\varphi_{2,x}, \quad (4.2.10a)$$

$$U_{xy} = (m + g\varphi_{1,x})\delta_{xy}, \quad V_{xy} = (m\varphi_{2,x} + 2g\varphi_{2,x})\delta_{xy}. \quad (4.2.10b)$$

The Nicolai variable is then given by

$$\vec{\xi} = D\vec{\varphi} + g \begin{pmatrix} \varphi_1^2 - \varphi_2^2 \\ 2\varphi_1\varphi_2 \end{pmatrix}, \quad D = \begin{pmatrix} \partial_0 + m & \partial_1 \\ \partial_1 & -\partial_0 + m \end{pmatrix} \quad (4.2.11)$$

and the lattice action (4.1.14) reads⁷⁰

$$S = \sum_x \frac{1}{2} \left((D\vec{\varphi})_x + g(u_x, v_x)^T \right)^2 + \sum_{x,y} \bar{\psi}_x \begin{pmatrix} \partial_0 + m + 2g\varphi_1 & \partial_1 + 2g\varphi_2 \\ \partial_1 - 2g\varphi_2 & -\partial_0 + m + 2g\varphi_1 \end{pmatrix}_{xy} \psi_y. \quad (4.2.12)$$

The improvement term (4.2.7) translates into

$$\begin{aligned} \Delta S &= \sum_x \left[((\partial_0\varphi_1)_x + (\partial_1\varphi_2)_x)(m\varphi_{1,x} + g(\varphi_{1,x}^2 - \varphi_{2,x}^2)) \right. \\ &\quad \left. - ((\partial_0\varphi_2)_x - (\partial_1\varphi_1)_x)(m\varphi_{2,x} + g\varphi_{1,x}\varphi_{2,x}) \right] \\ &= g \sum_x \left[((\partial_0\varphi_1)_x + (\partial_1\varphi_2)_x)(\varphi_{1,x}^2 - \varphi_{2,x}^2) - ((\partial_0\varphi_2)_x - (\partial_1\varphi_1)_x)\varphi_{1,x}\varphi_{2,x} \right], \end{aligned} \quad (4.2.13)$$

and, as expected, it follows that $\Delta S = 0$ for $g = 0$.

4.2.3 Wilson Fermions

A convenient choice for an anti-symmetric local difference operator is given by $\partial_\mu = \partial_\mu^S$. The emerging doublers can be lifted once more by the inclusion of a Wilson term to the superpotential. This (standard) Wilson term is defined in terms of the lattice Laplacian,

$$\Delta_{xy} = \sum_\mu (\delta_{x,y+\hat{\mu}} + \delta_{x,y-\hat{\mu}}) - 4\delta_{x,y}, \quad (4.2.14)$$

which can be applied to either φ and $\bar{\varphi}$ or φ_1 and φ_2 and ψ_x or $\bar{\psi}_x$. Thinking of the Wilson term as a momentum dependent mass one is naturally lead to replace m in W_x by⁷¹

$$m \rightarrow m'_{xy} = m\delta_{xy} - \frac{r}{2}\Delta_{xy}. \quad (4.2.15)$$

⁷⁰Note that the fermion operator is $M = D + 2g\varphi_1 + 2g\gamma_*\varphi_2$. For $g = 0$ one finds for the kernels again the relation $K = M^T M = D^T D$, cf. (3.4.4).

⁷¹In all numerical simulations the Wilson parameter will be set to one as usual.

For the free theory the bosonic kernel hence is

$$K = D^T D = \begin{pmatrix} -\partial_0^2 - \partial_1^2 + \left(\frac{r}{2}\Delta\right)^2 + m^2 - rm\Delta & 0 \\ 0 & -\partial_0^2 - \partial_1^2 + \left(\frac{r}{2}\Delta\right)^2 + m^2 - rm\Delta \end{pmatrix}, \quad (4.2.16a)$$

while the fermionic kernel takes the form

$$M = D = \begin{pmatrix} \partial_0 + m - \frac{r}{2}\Delta & \partial_1 \\ \partial_1 & -\partial_0 + m - \frac{r}{2}\Delta \end{pmatrix}. \quad (4.2.16b)$$

Restoring the lattice spacing a the eigenvalues μ_p of $D^T D$ and λ_p^\pm of D are given by

$$\mu_p = \left(\frac{\sin(ap_\mu)}{a}\right)^2 + \left(m + \frac{2r}{a} \sin^2\left(\frac{ap_\mu}{2}\right)\right)^2, \quad (4.2.17)$$

$$\lambda_p^\pm = \pm i \left|\frac{\sin(ap_\mu)}{a}\right| + \left(m + \frac{2r}{a} \sin^2\left(\frac{ap_\mu}{2}\right)\right). \quad (4.2.18)$$

As expected it follows that $\mu_p = \lambda_p^+ \lambda_p^-$. An expansion of the eigenvalues in powers of the lattice spacing yields

$$\mu_p = p^2 + m^2 + amr p^2 + O(a^2), \quad \lambda_p^\pm = \pm i|p| + m + \frac{ar}{2} p^2 + O(a^2). \quad (4.2.19)$$

Hence discretization errors are of order a in both channels. The extraction of physical masses thus suffers from the presence of large lattice artifacts. Moreover, for the interacting model, there is no longer a closed expression for the determinant of M . Even worse, in general it is no longer true that the determinant is positive.

4.2.4 Twisted Wilson Fermions

In order to improve on the scaling behavior of Wilson fermions a second amendment to the superpotential is possible. Switching back to the complex formalism for the time being, (4.2.15) reads (for a general superpotential)

$$W_x = W'(\varphi_x) - \frac{ar}{2}(\Delta\varphi)_x. \quad (4.2.20)$$

Since it is only required that the superpotential be holomorphic, the expression

$$W_x = W'(\varphi_x) + \frac{i ar}{2}(\Delta\varphi)_x \quad (4.2.21)$$

is equally valid and compatible with supersymmetry. For the free theory one now has

$$W_x = m\varphi_{1,x} - \frac{ar}{2}(\Delta\varphi_2)_x + i \left(m\varphi_{2,x} + \frac{ar}{2}(\Delta\varphi_1)_x\right), \quad (4.2.22)$$

from which the respective kernels are easily read off:

$$M = D = \begin{pmatrix} \partial_0 + m & \partial_1 - \frac{ar}{2}\Delta \\ \partial_1 + \frac{ar}{2}\Delta & -\partial_0 + m \end{pmatrix}, \quad (4.2.23a)$$

$$K = D^T D = \begin{pmatrix} -\partial_0^2 - \partial_1^2 + m^2 + (\frac{ar}{2}\Delta)^2 & 0 \\ 0 & -\partial_0^2 - \partial_1^2 + m^2 + (\frac{ar}{2}\Delta)^2 \end{pmatrix}. \quad (4.2.23b)$$

The Wilson term now appears in the off-diagonal entries of (4.2.23a), thus the jargon of *twisted Wilson fermions*. In a more compact form M can be written as

$$M = \gamma^\mu \partial_\mu + m + \frac{iar}{2} \gamma_* \Delta. \quad (4.2.24)$$

It is important to note that this construction is not to be confused with the twisted mass formulation of lattice QCD.⁷² For the free theory the fermionic eigenvalues square once again to the bosonic ones:

$$\mu_p = \left(\frac{\sin(ap_\mu)}{a} \right)^2 + m^2 + \left(\frac{2r}{a} \sin^2 \left(\frac{ap_\mu}{2} \right) \right)^2 \quad (4.2.25a)$$

$$\lambda_p^\pm = m \pm i \sqrt{\left(\frac{\sin(ap_\mu)}{a} \right)^2 + \left(\frac{2r}{a} \sin^2 \left(\frac{ap_\mu}{2} \right) \right)^2}. \quad (4.2.25b)$$

In contrast to the standard Wilson fermions the expansion in powers of a now yields

$$\mu_p = p^2 + m^2 + \kappa a^2 + O(a^4), \quad \lambda_p^\pm = m \pm i \sqrt{p^2 + \kappa a^2} + O(a^4), \quad (4.2.26)$$

$$\kappa = -\frac{1}{3} \sum_\mu p_\mu^4 + \frac{r^2}{4} \left(\sum_\mu p_\mu^2 \right)^2. \quad (4.2.27)$$

Hence it follows that artifacts are $\mathcal{O}(a^2)$. Since the coefficient κ vanishes if $3r^2 = 4$ and if either $p_0 = 0$ or $p_1 = 0$, artifacts are absent up to $\mathcal{O}(a^4)$. However, this implies that reflection positivity is violated because $r > 1$ in that case. As will be discussed later, numerical simulations are not hindered by that, and a sensible extraction of physical properties or the extrapolation towards the continuum remains possible.

4.2.5 Slac Fermions

As a third choice Slac fermions are reconsidered here. Although the difference operator $\partial_\mu = \partial_\mu^{\text{Slac}}$ becomes non-local, the added benefit is the absence of additional terms from the superpotential. Moreover, lattice perturbation theory also suggests that this choice

⁷²In twisted mass QCD [58] twisting refers to a twist in the two-flavor space of the theory to improve the chiral properties of the lattice theory. Here only one flavor is present and twisting is done directly in the two-dimensional spinor space.

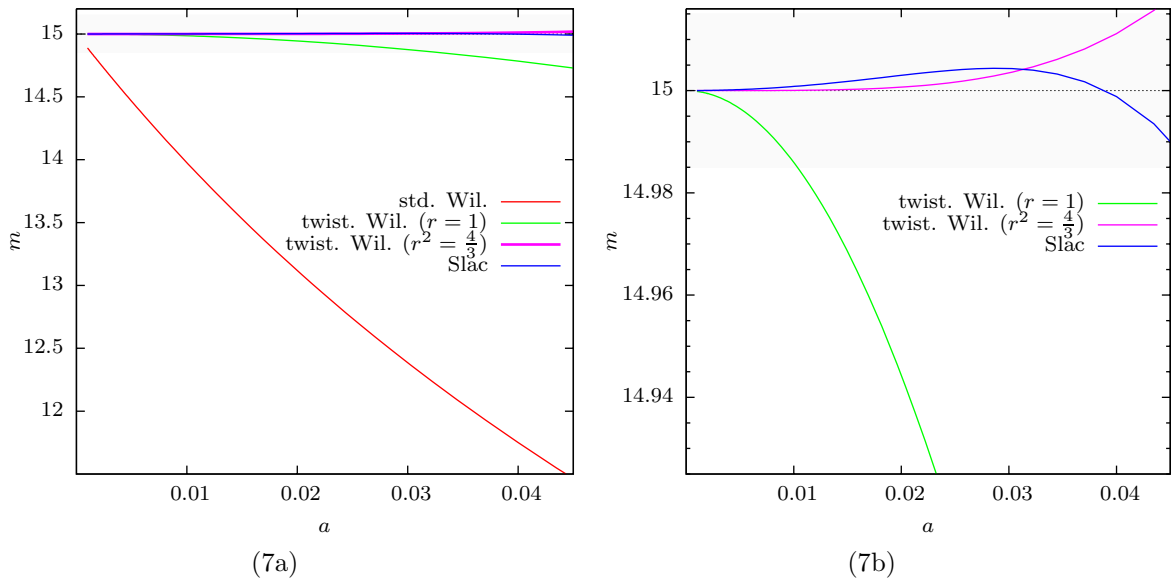


Figure 7: Comparison of different lattice fermions w.r.t the extracted mass. The data was generated by fitting the free propagator for several hundred lattice sizes. The gray shaded bar in Fig. (7a) depicts the 1% interval around the exact value of $m = 15$. In Fig. (7b) on the right the bar depicts the 0.1% interval.

is meaningful. At least at one-loop level the theory is renormalizable and does not spoil Lorentz symmetry as was pointed out in [9]. Also the larger numerical effort can be compensated to great extent. For instance, due to the tiny lattice artifacts masses are already close to the continuum values and only a few coarse lattices are required to extrapolate. For the free theory the fermionic kernel D is simply given by (4.2.11) while the bosonic kernel is again $K = D^T D$, and, as expected, all four supersymmetries are respected. However, as with the other two models the fermion determinant is no longer positive for arbitrary field configurations in the interacting theory.

To conclude with the subject of lattice artifacts all three lattice fermions are compared to each other in Fig. 7. The data was obtained for the free theory by fitting the bosonic twopoint function which can readily be computed from the inverse of $K = D^T D$. Of course the same mass would be found in the fermionic channel. It is expected that the scaling behavior does not change too much when the weakly coupled theory is analysed in Sec. 4.7. From Fig. (7a) it is also clear to see that for Wilson fermions the leading $O(a)$ behavior is superimposed by the NLO contribution as discussed in Sec. 3.4.2.

4.3 Discrete symmetries

The discrete symmetries of the classical action induced by the particular choice of $W_3(\varphi)$, cf. (4.1.10), are most transparently discussed in continuum language. It turns out besides the continuous supersymmetry transformations (4.1.12a), the action is also invariant under a finite abelian group corresponding to these extra discrete symmetries. A naively discretized lattice action respects this group as well. However, the improvement term breaks part of this symmetry down to some diagonal subgroup which in the case of Wilson and twisted Wilson fermions breaks down even further.

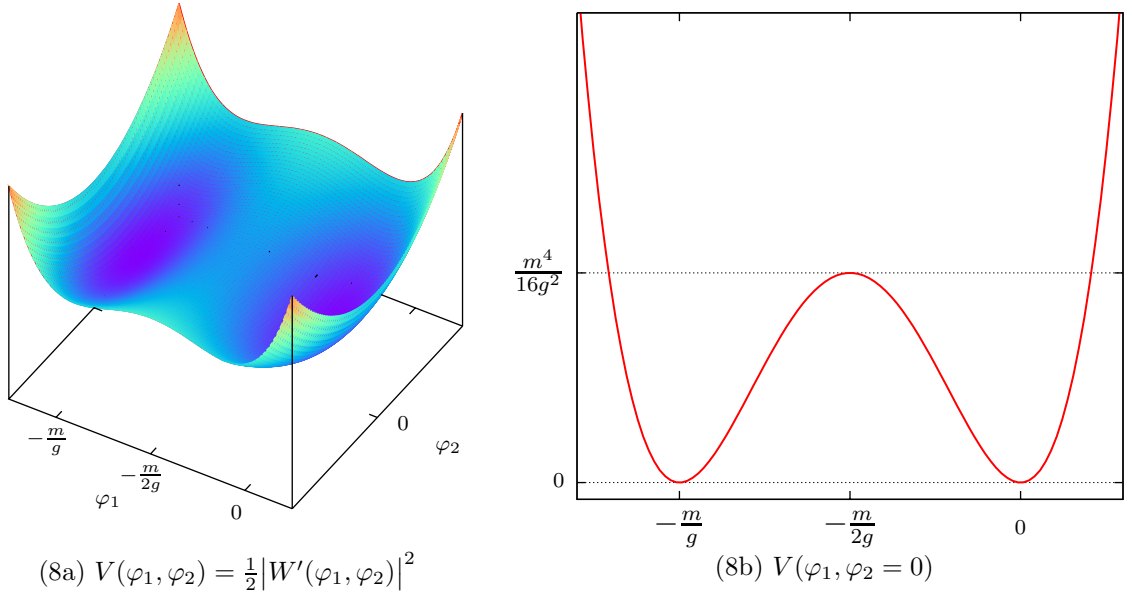


Figure 8: Classical potential for the superpotential $W_3(\varphi)$, cf. Eq. (4.1.10).

4.3.1 Continuum model

For m and g real and positive the classical potential⁷³ for the (complex) scalar field, $V(\varphi, \bar{\varphi}) = \frac{1}{2} |W'(\varphi)|^2$, has three local extrema located at

$$\varphi_0 = 0, \quad \varphi_1 = -\frac{m}{2g} \quad \text{and} \quad \varphi_2 = -\frac{m}{g}. \quad (4.3.1)$$

The points φ_0 and φ_2 correspond to minima of $V(\varphi)$ while at the point φ_1 the potential has as local maximum,

$$V(\varphi_0) = V(\varphi_2) = 0, \quad V(\varphi_1) = \frac{m^4}{16g^2}. \quad (4.3.2)$$

From (4.3.1) it is easy to see that in the free theory limit the second minimum is pushed to minus infinity. In the zero mass limit the three extremal points become degenerate while the barrier height separating the minima drops to zero.⁷⁴ In Fig. 8 the potential is plotted in two ways – above the complex φ -plane (Fig. (8a)) and as a function of φ_1 alone, setting $\varphi_2 = 0$ (Fig. (8b)). The graph of Fig. (8a) strongly suggests the presence of a four-fold symmetry. In fact it is not hard to work out that the mapping

$$\varphi \mapsto -\frac{m}{g} - \varphi \quad (4.3.3)$$

leaves $W'(\varphi)$ and hence $V(\varphi, \bar{\varphi})$ invariant, which can also be deduced from Fig (8b). The second \mathbb{Z}_2 factor is found from complex conjugation in the target space, i.e.

$$\varphi \mapsto \bar{\varphi}, \quad W'(\varphi) \mapsto \overline{W'(\bar{\varphi})}. \quad (4.3.4)$$

⁷³The superpotential $W(\varphi)$ of this section is always assumed to be $W_3(\varphi)$ of (4.1.10).

⁷⁴It can be argued that in this limit also \mathcal{R} symmetry gets restored [57].

Clearly this also leaves the bosonic action invariant. The second derivative of the superpotential, $W''(\varphi)$, on the other hand transforms as

$$\varphi \mapsto -\frac{m}{g} - \varphi \quad \Rightarrow \quad W''(\varphi) \mapsto -W''(\varphi), \quad (4.3.5a)$$

$$\varphi \mapsto \bar{\varphi} \quad \Rightarrow \quad W''(\varphi) \mapsto \overline{W''(\bar{\varphi})}. \quad (4.3.5b)$$

At first it may seem that also the fermionic part of the action is modified. However with a suitable unitary transformation of the spinors ψ and $\bar{\psi}$ this term can be made invariant, too. Alternatively it is possible to show that the fermion determinant does not change. The fermion matrix M and its adjoint M^\dagger read explicitly

$$M = \gamma^\mu \partial_\mu + m + 2g(\varphi_1 + i\gamma_*\varphi_2), \quad (4.3.6a)$$

$$M^\dagger = -\gamma^\mu \partial_\mu + m + 2g(\varphi_1 - i\gamma_*\varphi_2). \quad (4.3.6b)$$

Employing the auxiliary identity⁷⁵

$$\gamma_* M^\dagger \gamma_* = \gamma^\mu \partial_\mu + m + 2g(\varphi_1 - i\gamma_*\varphi_2) \quad (4.3.7)$$

one finds

$$\varphi \mapsto -\frac{m}{g} - \varphi \quad \Rightarrow \quad M \mapsto -\gamma_* M \gamma_*, \quad (4.3.8a)$$

$$\varphi \mapsto \bar{\varphi} \quad \Rightarrow \quad M \mapsto \gamma_* M^\dagger \gamma_* \quad (4.3.8b)$$

and hence the determinant is invariant.⁷⁶ Thus one indeed ends up with the claimed four-fold symmetry generated by the group $\mathbb{Z}_2 \times \mathbb{Z}_2$.

4.3.2 Lattice models

In order to translate the above discussion successfully onto the lattice an extra note on the discrete space-time symmetries is appropriate. Namely, the continuum model is not only invariant under proper Lorentz transformations but also under time reversal and parity transformations⁷⁷

$$T : (x_0, x_1) \mapsto (-x_0, x_1), \quad P : (x_0, x_1) \mapsto (x_0, -x_1). \quad (4.3.9)$$

⁷⁵ $(\gamma^\mu)^\dagger = \gamma^\mu$, $\gamma_*^\dagger = \gamma_*$, $(\gamma_*)^2 = 1$.

⁷⁶This is true at least up to an irrelevant phase in (4.3.8a). On the lattice the fermion matrix M always has an even number of rows and columns, hence this phase does not show up.

⁷⁷The identification of time and parity is somewhat formal here and simply refers to the zero- and one-directions on the lattice, respectively.

In the complex basis introduced in (4.1.1) this translates into

$$T : (z, \bar{z}) \mapsto (-\bar{z}, -z), \quad P : (z, \bar{z}) \mapsto (\bar{z}, z) \quad (4.3.10)$$

and obvious expressions follow for the partial derivatives ∂_μ , ∂ and $\bar{\partial}$. Both symmetries hold irrespectively of the concrete form of the superpotential and come in addition to the ones already discussed. However, it turns out, that the supersymmetrically improved lattice model is invariant only under the combined action of these symmetries. From Eq. (4.2.6) the (improved) bosonic action reads

$$S_B = \sum_x \left(2(\bar{\partial}\bar{\varphi})_x(\partial\varphi)_x + \frac{1}{2}|W'_x|^2 + W'_x(\partial\varphi)_x + \overline{W}'_x(\bar{\partial}\bar{\varphi})_x \right). \quad (4.3.11)$$

Under the transformation (4.3.3) the first two terms (corresponding to the naive transcription) are invariant according to the same reasoning as in the continuum model. By contrast, the last two terms pick up an extra sign

$$\varphi_x \mapsto -\frac{m}{g} - \varphi_x \quad \Rightarrow \quad W'_x(\partial\varphi)_x \mapsto -W'_x(\partial\varphi)_x, \quad \overline{W}'_x(\bar{\partial}\bar{\varphi})_x \mapsto -\overline{W}'_x(\bar{\partial}\bar{\varphi})_x. \quad (4.3.12)$$

Under the transformation (4.3.4) both these terms transform again

$$\varphi_x \mapsto \bar{\varphi}_x \quad \Rightarrow \quad W'_x(\partial\varphi)_x \mapsto W'_x(\partial\bar{\varphi})_x, \quad \overline{W}'_x(\bar{\partial}\bar{\varphi})_x \mapsto W'_x(\bar{\partial}\varphi)_x. \quad (4.3.13)$$

Only if together with (4.3.3) also time and space are reversed, i.e. $\partial \mapsto -\partial$ and $\bar{\partial} \mapsto -\bar{\partial}$ the improvement terms in (4.3.12) become invariant, too. Likewise if only parity is reversed, i.e. $\partial \mapsto \bar{\partial}$, the improvement terms in (4.3.13) are invariant. In conclusion the $\mathbb{Z}_2 \times \mathbb{Z}_2$ symmetry is only maintained if combined with the space-time symmetries T and P . Effectively, the group of all discrete symmetry transformations is thus reduced according to the pattern

$$\underbrace{\mathbb{Z}_2}_T \times \underbrace{\mathbb{Z}_2}_P \times \underbrace{\mathbb{Z}_2}_{\varphi \rightarrow -\varphi - \frac{m}{g}} \times \underbrace{\mathbb{Z}_2}_{\varphi \rightarrow \bar{\varphi}} \Rightarrow \underbrace{\mathbb{Z}_2}_{TP, \varphi \rightarrow -\varphi - \frac{m}{g}} \times \underbrace{\mathbb{Z}_2}_{P, \varphi \rightarrow \bar{\varphi}}. \quad (4.3.14)$$

This confirms the claim that the improvement term must have a vanishing expectation value in the original ensemble before improvement. In Sec. 4.6 this will be confirmed numerically to large precision. Without further manipulations of the superpotential it follows that also the improved lattice action will possess the aforementioned symmetries of the classical continuum action. Since only the improvement terms transform an unimproved lattice action will respect the complete lhs. of (4.3.14). This is certainly true for Slac fermions. For Wilson and twisted Wilson fermions it will be argued below that the residual $\mathbb{Z}_2 \times \mathbb{Z}_2$, i.e. the rhs. of (4.3.14), is broken further down for the respective improved lattice actions.

4.3.3 Wilson and Twisted Wilson fermions

It was argued that in case of Wilson fermions unwanted doublers can be removed without supersymmetric violations if the superpotential is augmented appropriately. Thus the Wilson term also enters the bosonic action,

$$S_B = \frac{1}{2} \sum_x ((\bar{\partial}\bar{\varphi})_x + W'_x - \frac{r}{2}(\Delta\varphi)_x)((\partial\varphi)_x + \overline{W}'_x - \frac{r}{2}(\Delta\bar{\varphi})_x). \quad (4.3.15)$$

With respect to the second \mathbb{Z}_2 factor in (4.3.14) nothing is changed that way,⁷⁸ but the Wilson term changes sign under the action of the first factor. Thus one \mathbb{Z}_2 is lost due to the Wilson term. Although this symmetry is nonetheless expected to be restored in the continuum limit (the symmetry breaking term couples to a higher-order operator [25,57]) at finite lattice spacing this will certainly affect MC simulations. As for the unimproved model with Wilson fermions this particular \mathbb{Z}_2 remains broken although T and P become independent symmetries again. Besides the scaling with the lattice spacing it is possible to show that the symmetry breaking terms are also proportional to g . Their relevance for numerical simulations grows hence for larger couplings λ .

For twisted Wilson fermions the situation is slightly different w.r.t. the two \mathbb{Z}_2 factors of (4.3.14). The bosonic action reads now

$$S_B = \frac{1}{2} \sum_x ((\bar{\partial}\bar{\varphi})_x + W'_x + \frac{ir}{2}(\Delta\varphi)_x)((\partial\varphi)_x + \overline{W}'_x - \frac{ir}{2}(\Delta\bar{\varphi})_x). \quad (4.3.16)$$

and is found to be invariant under $\varphi \rightarrow -\frac{m}{g} - \bar{\varphi}$ combined with T , i.e. $\partial \rightarrow -\bar{\partial}$ alone. Note that this is not exactly the second \mathbb{Z}_2 of (4.3.14).⁷⁹ Again, this would not change for an unimproved action although the latter would restore T and P invariance again. Concerning the continuum limit the same arguments as for Wilson fermions apply, and effects due to the symmetry breaking are again expected to be proportional to $g \mathcal{O}(a)$.

4.3.4 Comparison and Summary

It was shown that for the construction of a supersymmetric action some of the discrete symmetries have to be sacrificed. The introduction of a (twisted) Wilson term to the superpotential reduces the residual symmetries by another \mathbb{Z}_2 factor. It is difficult to assess how the dynamics of the theory is influenced by this. To answer this question one has to resort to MC simulations. To this end five different models (summarized in Tab. 4) will be analysed numerically. From the discussion above Slac fermions are surely exceptional, since they preserve most of the symmetries discussed above.

⁷⁸The Laplace operator is invariant under either T or P .

⁷⁹Instead of the complex basis chosen here one could have used a real basis in both space-time and the target space. Then one would conclude that twisted Wilson fermions respect the transformation $\varphi_1 \mapsto -\frac{m}{g} - \varphi_1$, $\varphi_2 \mapsto \varphi_2$, $\partial_0 \mapsto -\partial_0$, $\partial_1 \mapsto \partial_1$.

	(1)	(2)	(3)	(4)	(5)
	Wilson impr.	Wilson unimpr.	Twisted Wilson ^a	Slac impr.	Slac unimpr.
lattice derivative	local	local	local	non-local	non-local
lattice artifacts modifications	$O(a)$	$O(a)$	$O(a)^b$	'perfect'	'perfect' ^c
to superpot. discrete symmetries	yes	yes	yes	no	no
super-symmetries	$\mathbb{Z}_{2,P}$	P, T, \mathbb{Z}_2	$\mathbb{Z}_{2,T}$	$\mathbb{Z}_{2,PT} \times \mathbb{Z}_{2,P}$	$P, T, \mathbb{Z}_2 \times \mathbb{Z}_2$
super-symmetries	one	none	one	one	none

Table 4: Comparison of various lattice models w.r.t their symmetries. All statements refer to the interacting theory, i.e. $g \neq 0$. The notion $\mathbb{Z}_{2,P}$ denotes the combined action of a field and parity transformation as discussed in the text.

^aOnly improved considered

^bIn the interacting case the good scaling properties are lost. However the overall size of lattice artifacts is still much smaller when compared to Wilson fermions.

^cThe dispersion relation is up to the cut-off the same as in the continuum.

4.4 Taming the fermion determinant

To formulate an efficient and (hopefully) stable algorithm to deal with dynamical fermions is an important stage for the preparation of lattice Monte Carlo simulations. Nowadays lattice QCD simulations with dynamical quarks show, that this is most critical in terms of resources. The purpose of this section is to better understand and discuss this in relation to the theories considered here.

Recall from Sec. 2.4.1 that in order to account for fermionic contributions to the dynamics of the quantum theory one has to compute repeatedly the fermion determinant in⁸⁰

$$Z = \int \mathcal{D}\varphi e^{-S_B(\varphi)} \det M(\varphi). \quad (2.4.3)$$

For the importance sampling scheme of MC simulations this means that the determinant has to be included into the probability measure of the Markov process. Although the Yukawa interactions of the models relevant to this thesis take a very simple form, i.e. a single site variable $\varphi_{1,x}$ appears only in a single matrix element⁸¹, the determinant of M remains a highly non-local function of the matrix elements. Thus a small change to $\varphi_{1,x}$ cannot be easily mapped to a small change of $\det M$. This impedes (as already mentioned) the usage of the standard Metropolis or the Heat bath algorithm. With the HMC algorithm that was discussed in Sec. 2.5.2 this task can be tackled more successfully, although it remains challenging. In the following three different approaches are investigated and compared to each other. Beginning from the simplest in terms of

⁸⁰For brevity, by $\mathcal{D}\varphi$ the functional integral measure over both components φ_1 and φ_2 is to be understood in the following.

⁸¹See also Eq. (4.2.12)

implementation complexity each successive step will prove itself likewise technically more involved and more admissible. By this procedure it is guaranteed that each constituent of the final algorithm to be used for the numerical analysis of later sections is by all means necessary and not free to be omitted.

4.4.1 The Reweighting algorithm

Motivated by the fact that quenched ensembles can be generated at almost no cost it is tantalizing to hope (at least in the weakly coupled regime, i.e. $\lambda \ll 1$) for small fluctuations in the fermion determinant. If so, the so-called Reweighting algorithm would become applicable. Being long known in statistical physics this method has also been applied widely in the context of lattice field theory. In brief, the expectation value of an observable

$$\langle \mathcal{O} \rangle = \frac{\int \mathcal{D} \varphi e^{-S_B(\varphi)} \det(M(\varphi)) \mathcal{O}(\varphi)}{\int \mathcal{D} \varphi e^{-S_B(\varphi)} \det(M(\varphi))}, \quad (4.4.1)$$

is reinterpreted as the quotient of two related expectation values according to a different ensemble. Namely, one rewrites $\langle \mathcal{O}(\varphi) \rangle$ as

$$\langle \mathcal{O} \rangle = \frac{\langle \det(M(\varphi)) \mathcal{O}(\varphi) \rangle_0}{\langle \det M(\varphi) \rangle_0}, \quad (4.4.2)$$

where the subscript '0' denotes the average w.r.t. $e^{-S_B(\varphi)}$ alone, i.e.

$$\langle \mathcal{O} \rangle_0 = \frac{\int \mathcal{D} \varphi e^{-S_B(\varphi)} \mathcal{O}(\varphi)}{\int \mathcal{D} \varphi e^{-S_B(\varphi)}}. \quad (4.4.3)$$

This is just the average over the quenched ensemble, i.e. where $\det M(\varphi)$ has been artificially set to one. The effect of the fermion determinant is thus neglected during the generation of the configurations and only afterwards taken into account, i.e. when actual observables are evaluated. An added benefit is, that in order to account for correlations amongst subsequently generated configurations an appropriate spacing of the configurations whereupon observables are evaluated can be accomplished at almost no further cost. It suffices to compute the fermion determinant only for the latter instead of all (and hence correlated) configurations. This becomes all the more important the closer the critical point is approached and autocorrelation effects become large.

Conversely, there are also several difficulties with this method. Firstly it is not guaranteed that the fluctuations of $\det M$ computed on the quenched field configurations are small. After all it is excluded explicitly from what defines the a priori measure of the importance sampling scheme. In the end, this would lead to a drastic reduction of relevant configurations since only configurations with the largest encountered values for the determinant contribute. Further below an attempt will be made to discuss this

L	g	$\langle S_B \rangle_0$	$\langle S_B \rangle$
11	0.2	121.00(5)	120.99(8)
11	0.5	121.02(5)	120.97(8)
11	1.0	121.32(5)	121.09(10)
11	2.0	122.30(5)	121.39(30)
15	0.2	224.99(8)	225.00(10)
15	0.5	225.03(8)	225.02(10)
15	1.0	225.41(8)	225.13(13)
15	2.0	226.84(8)	225.25(45)

(a) Slac

L	g	$\langle S_B \rangle_0$	$\langle S_B \rangle$
12	0.2	144.09(6)	144.03(7)
12	0.5	144.39(6)	144.07(9)
12	1.0	145.49(6)	144.18(23)
12	2.0	150.92(6)	146.4(1.4)
16	0.2	255.92(8)	255.84(9)
16	0.5	256.48(8)	255.91(141)
16	1.0	258.53(8)	255.5(4)
16	2.0	269.10(8)	263(4)

(b) twisted Wilson

Table 5: Expectation value of the bosonic action. Although the lack of dynamical fermion contributions is traceable it cannot be judged whether the reweighed result is really different from the quenched one due to the large errors on the former. The results found for Wilson fermions are similar to those with twisted Wilson fermions. Errors were found from a Jack Knife analysis.

more quantitatively. From the concrete form of M ,⁸²

$$M = \gamma^\mu \partial_\mu + m + 2g(\varphi_1 + \gamma_* \varphi_2) \quad (4.3.6a)$$

it is clear that for $g = 0$ the determinant is constant

$$\det M \Big|_{g=0} \equiv \det M_0 = C_0. \quad (4.4.4)$$

For $\lambda \ll 1$ the size of the fluctuations in $\det(M)$ should then be normalized w.r.t. to C_0 , motivating the obvious definition⁸³

$$\mathcal{R}(\varphi) = \frac{\det(M(\varphi))}{\det(M_0)} = \frac{1}{C_0} \det(M(\varphi)). \quad (4.4.5)$$

It follows at once that $\mathcal{R} = 1$ for $g = 0$, while $\mathcal{R} \simeq 1$ would indicate that reweighing will work properly. A useful test observable may be found in the bosonic action. In Sec. 3.2.3 it was shown, that its expectation value is known exactly for the improved models. For the two-dimensional model discussed here this leads to $\langle S_B \rangle = N$, where N denotes the number of lattice sites.⁸⁴ Given the large statistics attainable with quenched ensembles it is possible to resolve a significant deviation from this value. Tab. 5 lists the results for the models with Slac and twisted Wilson fermions (results for Wilson fermions are very similar to the reported twisted Wilson data). A very clean signal is found for $g = 1.0$ ($\lambda = 0.1$) and may be seen as a proof of principle for this method to work. Deviations for the quenched theory are large enough to be detectable while the reweighed data restores compatibility with the predicted value in a distinguishable manner. However, if g is increased further the achievable precision drops significantly.⁸⁵

⁸²Wilson terms are omitted since they play no crucial role here.

⁸³Obviously it is safe to replace $\det M([\Phi])$ with $\mathcal{R}[\Phi]$ in (4.4.2).

⁸⁴Recall, that for the one-dimensional model $\langle S_B \rangle = \frac{1}{2}N$ was found.

⁸⁵It is interesting that SLAC fermions are not as much affected as (twisted) Wilson fermions are. This will be confirmed below.

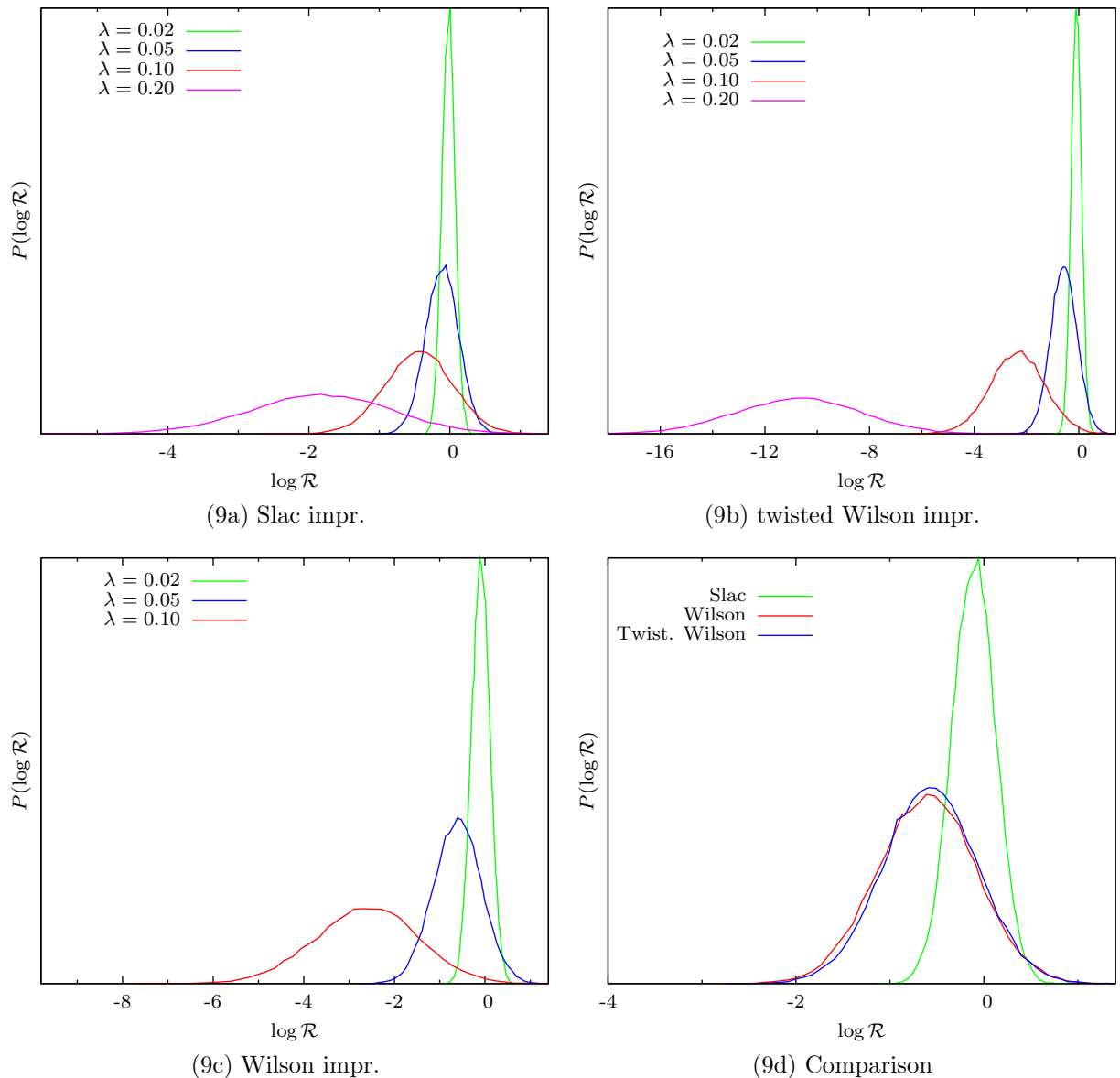


Figure 9: Histograms for the logarithm of the Reweigh factor. The data for Fig. (9a) was obtained from the same ensembles than in Fig. 10. For the data with Wilson and twisted Wilson fermions 50,000 configurations from a 16×16 lattice with $m = 10$ were analysed. The broadening of the histogram is more pronounced for Wilson and twisted Wilson than for SLAC fermions. Also the shift in the mean is lesser. While for SLAC and twisted Wilson fermions the determinant can still be evaluated at $\lambda = 0.2$ the simulation using Wilson fermions yields no sensible data therefore.

The growing errors are closely related to the fluctuations in \mathcal{R} becoming larger. Since these fluctuations are found to spread over several orders of magnitude it is more convenient to consider the histogram of $\log \mathcal{R}$. The results of this analysis are shown in Fig. 9. Irrespective of the concrete fermion type the distribution broadens if λ is increased. Incidentally, also the mean of the distributions shifts by two (SLAC) respectively as much as ten ((twisted) Wilson) orders of magnitude at $\lambda = 0.2$. This indicates that quenched and dynamical ensembles will eventually dissociate completely.⁸⁶ For Wilson fermions it is already impossible to compute the determinant reliably at this value of λ .

Another method to obtain information about the applicability of the reweighing

⁸⁶Strictly speaking this could also be due to an improper normalization. However, dynamical simulations clearly show that the determinant becomes larger in the interacting case.

method will be discussed now. On any fixed ensemble with M configurations labeled from $i = 1$ to M the estimate $\overline{\mathcal{R}}$ is given by

$$\overline{\mathcal{R}} = \frac{1}{M} \sum_{i=1}^M \mathcal{R}_i = \sum_{i=1}^M p_i \mathcal{R}_i. \quad (4.4.6)$$

Obviously, $p_i = \frac{1}{M}$ may be interpreted as an a priori measure on the reduced configuration space given by the ensemble itself. For any observable evaluated from (4.4.2) however, the a priori measure is given by⁸⁷

$$\tilde{p}_i = \frac{p_i \mathcal{R}_i}{\overline{\mathcal{R}}}. \quad (4.4.7)$$

With the help of these definitions Reweighting will cease to work when the \tilde{p}_i 's strongly deviate from the uniform distribution of the p_i 's. It is instructive to consider the cumulative distribution functions

$$P(i) = \sum_{j=1}^i p_j, \quad \tilde{P}(i) = \sum_{j=1}^i \tilde{p}_j. \quad (4.4.8)$$

It follows readily that $P(M) = \tilde{P}(M) = 1$. While $P(i)$ is of course a straight line with slope $1/M$ when plotted against the configuration number i , $\tilde{P}(i)$ is expected to deviate and may even exhibit distinctive jumps. This happens whenever a configuration with a value of \mathcal{R}_i very large is added. To allow for a better visualization the \tilde{p}_i 's may be sorted first and be accumulated afterwards

$$P_S(i) = \sum_{j=1}^i \tilde{p}_{s,j}, \quad p_{s,1} \leq p_{s,2} \leq \dots \leq p_{s,M} \quad (4.4.9)$$

In Fig. 10 both quantities are shown for the improved model with SLAC fermions. As already anticipated from the discussion above they show, that the Reweighting method will break down for $\lambda \geq 0.2$. Already at $\lambda = 0.5$ the measure is concentrated on a few configurations as seen by the distinct jumps (blue graph in Fig.(10a)). To conclude, reweighting is unfortunately inappropriate for the problem at hand. Working in principle for very small coupling constants λ , the method cannot be applied at larger couplings and especially not for the study of the non-perturbative regime of the theory.

4.4.2 The Naive Inversion algorithm

It was seen, that to be able to study the theory at larger couplings, it becomes necessary to fully incorporate fermionic contributions into the probability measure. The simplest and surely most naive way to accomplish this, was already applied to the quantum

⁸⁷In the following it is assumed the observable, that is considered is not correlated to \mathcal{R}^{-1} . Such observables would of course not suffer from the effects described below. The bosonic action for instance is of the type this discussion has in mind.

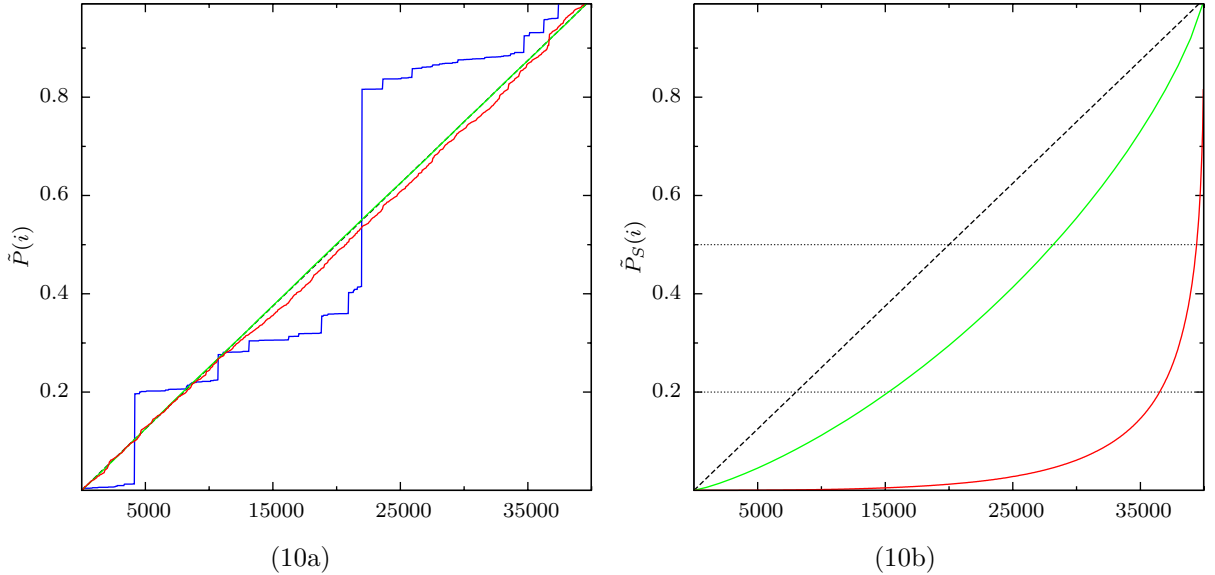


Figure 10: Analysis of cumulative distribution functions from a quenched ensemble using SLAC fermions and improved action on a 15×15 lattice at $m = 10$ and $\lambda = 0.05$ (green), $\lambda = 0.2$ (red), $\lambda = 0.5$ (blue). Each ensemble consisted of 50,000 configurations. For the blue graph in Fig. 10(a) distinct jumps are clearly visible indicating a very strong localization of the measure. The corresponding graph for $\tilde{P}_S(i)$ is omitted from Fig. (10b) since it cannot be displayed properly above the chosen scale. Therefore the deformation at weaker couplings are more apparent there than on the left. The thick dotted line denotes a uniform distribution.

mechanical systems, see e.g. Sec. 3.3.2 and is now adopted to the two-dimensional case.

Although it was argued that $\det(M)$ is still real, the positivity $\det(M) > 0$ can no longer be proven to hold. In fact, configurations that lead to $\det(M) < 0$ are easily found numerically.⁸⁸ A possible way out, is to bring the functional integral into the form

$$Z = \int \mathcal{D}\varphi e^{-S_B(\varphi)} \det(M(\varphi)) = \int \mathcal{D}\varphi e^{-S_B(\varphi)} |\det(M(\varphi))| \operatorname{sgn}(M(\varphi)), \quad (4.4.10)$$

where for brevity $\operatorname{sgn}(M(\varphi)) \equiv \operatorname{sgn}(\det(M(\varphi)))$. The modulus can now be rewritten as

$$|\det(M(\varphi))| = \sqrt{\det(M(\varphi)M^T(\varphi))}, \quad (4.4.11)$$

since $\det(MM^T) \geq 0$. The above expression can now be promoted to the exponent of (4.4.10) to yield the effective action

$$S_{\text{eff}}(\varphi) = S_B(\varphi) - \frac{1}{2} \operatorname{tr} \ln(M(\varphi)M^T(\varphi)). \quad (4.4.12)$$

The remaining sign of (4.4.10) may be finally taken into account by reweighing.⁸⁹ The contributions to the equations of motion for the fields φ_1 and φ_2 get additional contri-

⁸⁸Whether these configurations will contribute significantly in simulations is however a complete different issue.

⁸⁹This would be done quite similar to what was described in the previous section.

λ	Wilson		Twist. Wilson		SLAC	
	$\langle S_B \rangle$	$\#\det M < 0$	$\langle S_B \rangle$	$\#\det M < 0$	$\langle S_B \rangle$	$\#\det M < 0$
0.2	143.89(34)	0	144.15(40)	0	120.89(28)	0
0.5	143.81(31)	0	143.76(34)	0	120.83(18)	0
1.0	143.73(28)	816 ($\approx 3\%$)	143.57(91)	1733 ($\approx 8\%$)	120.90(33)	287 ($\leq 1\%$)
1.5	144.36(22)	488 ($\approx 2\%$)	144.37(72)	486 ($\approx 2\%$)	121.03(54)	917 ($\approx 2\%$)
2.0	143.79(22)	483 ($\approx 2\%$)	143.68(35)	264 ($\approx 1\%$)	121.06(25)	124 ($\leq 1\%$)

Table 6: Expectation value of the bosonic action. The data for Wilson and twisted Wilson fermions was obtained from a 12×12 lattice with $m = 5$ ($m_L = 0.4$) and 25,000 configurations for each λ . The SLAC data was obtained from 45,000 configurations each on a 11×11 lattice with the mass set to $m = 5$. Where necessary reweighing with the sign of the determinant was applied.

butions which read ⁹⁰

$$\frac{\partial S_{\text{eff}}}{\partial \varphi_{1,z}} = \frac{\partial S_B}{\partial \varphi_{1,z}} - \text{tr} \left(M^{-1} \frac{\partial M}{\partial \varphi_{1,z}} \right), \quad \frac{\partial S_{\text{eff}}}{\partial \varphi_{2,z}} = \frac{\partial S_B}{\partial \varphi_{2,z}} - \text{tr} \left(M^{-1} \frac{\partial M}{\partial \varphi_{2,z}} \right). \quad (4.4.13)$$

From the shape of the fermion matrix⁹¹

$$M_{xy}^{\alpha\beta} = (\gamma^\mu)^{\alpha\beta} \partial_{\mu,xy} + \delta^{\alpha\beta} \delta_{xy} m + 2g \delta_{xy} (\delta^{\alpha\beta} \varphi_{1,x} + \gamma_*^{\alpha\beta} \varphi_{2,x}) \quad (4.4.14)$$

one computes readily

$$\frac{\partial M_{xy}^{\alpha\beta}}{\partial \varphi_{1,z}} = 2g \delta_{xz} \delta_{yz} \delta^{\alpha\beta}, \quad \frac{\partial M_{xy}^{\alpha\beta}}{\partial \varphi_{2,z}} = 2g \delta_{xz} \delta_{yz} \gamma_*^{\alpha\beta}, \quad (4.4.15)$$

and the trace in (4.4.13) reduces to the sum of two matrix elements times a factor of $2g$. Unfortunately, this does not save much since the main computational cost is of course still the computation of the inverse of M . It is well known that the cost for the inversion of a matrix of size $N \times N$ grows like N^3 , so that only small lattices will be feasible with this algorithm. However, such simulations can play a valuable role in the development and validation of other algorithms, one such being presented in the next section.

Complying with this constraint for the time being, simulations can be performed at much larger values of λ than before. Again the bosonic action was used for testing, the results being presented in Tab. 6. All three models investigated yield the expected result of $\langle S_B \rangle = N$, and from the quoted figures for the number of configurations with a determinant smaller than zero it is also clear, that up to $\lambda \approx 2$ this problem is not severe. Nonetheless, care has to be taken. The naive inversion algorithm splits the determinant into its modulus and sign. Assuming that the determinant is a continuous function of the scalar fields it has hence to vanish for the sign to change. This may not necessarily happen numerically, however, the inversion of M near such a transition becomes delicate and the numerical integration may break down anyhow. Despite of

⁹⁰To arrive at the form given in (4.4.13) the cyclic property of the trace together with $\text{tr}(A + A^T) = 2\text{tr} A$ has been used.

⁹¹The (Twisted-)Wilson term is omitted here since it does not contribute to the derivatives computed below. It must be included however in the computation of M^{-1} in (4.4.13).

this, the complete algorithm remains exact because of the Metropolis accept/reject step. Interpreting the results of Tab. 6 one may infer that the determinant is mostly positive, and even when a transition into the sector with $\det M < 0$ has taken place the system will prefer to return to the sector with $\det M > 0$ soon after.

4.4.3 The Pseudo Fermion algorithm

To escape the problem that the inversion cost grows with $(2N)^3$ alternative algorithms are needed⁹². In this section one such method, called the pseudofermion algorithm [59] will be adapted to the Wess-Zumino model. This algorithm replaces the exact computation of the fermion determinant with a stochastic estimate thereof. For any invertible matrix Q one has

$$\det(Q) = \frac{1}{\det(Q^{-1})}. \quad (4.4.16)$$

Provided $Q = Q^\dagger$, the rhs. of (4.4.16) can be rewritten as a Gaussian functional integral over a complex scalar field χ ,

$$\int \mathcal{D}\chi \mathcal{D}\chi^\dagger e^{-\chi^\dagger Q^{-1} \chi} = \frac{C}{\det(Q^{-1})} = C \det Q, \quad (4.4.17)$$

with C some irrelevant normalization constant. The fermion matrix M for the WZ model is not self-adjoint but can be used to form the self-adjoint matrix $Q = MM^T$.⁹³ The use of a complex pseudofermion field doubles the number of fermion flavors from one to two. Yet this must be avoided, since it would unbalance the bosonic and fermionic degrees of freedom. Alternatively, one may take χ to be a real scalar field. Since M and Q are real, the resulting pseudofermion action remains real by this modification, but the integration over χ yields now

$$\frac{1}{C'} \int \mathcal{D}\chi e^{-\chi^T Q^{-1} \chi} = \sqrt{\det Q} = |\det(M(\varphi))|, \quad (4.4.18)$$

implying, that reweighing against a possible negative sign of the determinant is still required. The so-called pseudofermion action

$$S_{\text{pf}}(\chi, \varphi) = \chi^T M^{-T}(\varphi) M^{-1}(\varphi) \chi = \sum_{\substack{x,y \\ \alpha,\beta}} \chi_{\alpha,x} \left(M(\varphi) M^T(\varphi) \right)_{\alpha,x;\beta,y}^{-1} \chi_{\beta,y} \quad (4.4.19)$$

replaces the fermion determinant $\det(M)$ in the functional integral

$$Z = \int \mathcal{D}\varphi \mathcal{D}\chi e^{-S_B(\varphi) - S_{\text{pf}}(\varphi, \chi)}, \quad (4.4.20)$$

⁹²The additional factor of two accounts for the dimensionality of the spinor space.

⁹³Recall that M is a real matrix in the Majorana basis.

which becomes by this an integral over the complex scalar field φ and the real scalar field χ . A particular advantage of (4.4.19) is the fact that it can be rewritten as⁹⁴

$$S_{\text{pf}} = \eta^T \eta, \quad \eta = M_\varphi^{-1} \chi. \quad (4.4.21)$$

The field η is normally distributed and can hence be sampled from a heat bath, and a properly distributed χ is then found from $\chi = M_\varphi \eta$. In the HMC algorithm this is performed at the beginning of a new trajectory, i.e. at the same time when the momenta conjugate to φ are refreshed. For the numerical integration the pseudofermion is held fixed, i.e. there is no need to introduce conjugate momenta for the pseudofermion. The contributions to the equations of motion for the bosonic field φ are furthermore found from⁹⁵

$$\delta S_{\text{pf}} = \chi^T \delta (M_\varphi^{-T} M_\varphi^{-1}) \chi = -2\eta^T \delta M_\varphi^T \eta', \quad (4.4.22)$$

where η and η' are solutions of

$$M_\varphi \eta = \chi, \quad (MM^T)_\varphi \eta' = \chi. \quad (4.4.23)$$

The inversion of M in the naive inversion algorithm is so reduced to the problem of solving two linear systems. Considering the computation of the inverse of M as solving a linear system for each column of M^{-1} this drops one factor of N in the total cost. However, the price to pay comes in the form of additional noise entering the simulation through stochastic nature of the pseudofermions. Observations on small lattices have indeed shown, that the numerical integration is more unstable than with the naive inversion algorithm. To better understand the reason for this, it is useful to consider

$$Q^{-1} = \sum_\lambda |\lambda\rangle \frac{1}{\lambda} \langle \lambda|, \quad (4.4.24)$$

where $|\lambda\rangle$ denotes the set of eigenstates of Q . Since it may happen in this model that some eigenvalues can become very small, the fermionic force contributions can become very large if a particular pseudo fermion configuration has a large overlap with the corresponding eigenstate. Possible algorithmic improvements that could cope with this include the Polynomial HMC (PHMC) [60] and the Rational Hybrid Monte Carlo (RHMC) [61] algorithm. While in the PHMC small eigenvalues are treated separately [62, 63], the RHMC can be adopted to use multiple pseudo-fermion fields as to smear out effects due to the stochastic nature of the pseudo-fermions [64]. Hitherto, it is an open yet very interesting question whether these algorithms – originally invented for lattice QCD – will also contribute significant improvements to the models discussed here.

⁹⁴For brevity $M_\varphi \equiv M(\varphi)$

⁹⁵The calculation is straightforward if one makes use of the matrix identity $\delta M^{-1} = -M^{-1} \delta M M^{-1}$.

To solve (4.4.23) it is straightforward to utilize the LU-decomposition of M .⁹⁶ At moderate lattice sizes the fermion matrix M fits comfortably into the memory of modern computers and very efficient numerical libraries such as LAPACK [65] can be used. A further advantage of the LU-decomposition is, that $\det(M)$ can be computed from the product of the diagonal elements of U ⁹⁷, i.e. $\det(M) = \prod_i U_{ii}$. As already mentioned the sign of the determinant is still required and hence given for free. But also the fermion determinant is an interesting observable in its own right as will be seen in Sec. 4.6.

The second option to solve (4.4.23) is to use an iterative algorithm.⁹⁸ Perhaps most popular is the so-called conjugate gradient algorithm (CG) [66] which can be applied to hermitean positive definite matrices such as Q . To solve for η' the CG algorithm can hence straightforwardly be applied. Afterwards the solution for η is found from $\eta = M^T \eta'$. The most significant improvement is, that only the action of the matrix M on a vector ρ must be computed. For (twisted) Wilson fermions the cost of this operation grows only with N , since both derivatives are ultra-local. For a dense matrix one must of course expect to have a cost that goes like N^2 .⁹⁹ Without rounding errors the CG algorithm will always converge and yield the correct solution after at most N iterations. Far better than this, in most practical situations the convergence is much faster and sufficient convergence is found after a comparatively small number of iterations.

For the models discussed here, the pseudofermion algorithm with this CG solver step was found to be the only algorithm to allow for simulations on lattices with more than 32×32 lattice sites. With available computing resources about 4,000 configurations per hour can then be generated for lattices of with 64×64 lattice points and even for lattices with 128×128 lattice points the performance is still 300 configurations per hour. To be honest, these figures are only valid for coupling constants of $\lambda \leq 1$ and reduce by roughly 20 – 30% for coupling constants $1 \leq \lambda \leq 2$.

4.5 Tuning the simulations

In this sections two modifications to the standard integration scheme of the molecular dynamics step inside the hybrid Monte Carlo algorithm are presented. Higher order integrators to be discussed first allow for much larger finite time-step sizes which becomes important for larger lattice sizes or larger coupling constants where otherwise the time-step size needs to be drastically reduced. The second modification, Fourier acceleration, was originally proposed for systems using Langevin dynamics [67] and only

⁹⁶Note that no second decomposition is needed here. The solution of η' is found from $M^T \eta' = \eta$ using the fact that the solution of $A^T x = b$ can be obtained from the LU-decomposition of A .

⁹⁷Most algorithms compute instead of $M = LU$ the numerically more stable expression $M = PLU$, where P is the permutation or pivoting matrix. Obviously, any signs from transpositions due to P have to be considered properly in the computation of $\det(M)$.

⁹⁸This is also done in lattice QCD simulations since save for the smallest lattice sizes the fermion matrix of four-dimensional lattice QCD does not fit into computer memory as a whole, not to mention that a LU-decomposition would be far too slow.

⁹⁹Fortunately, even for the non-sparse Slac fermions the actual cost is much cheaper than this. Since the Slac derivative is diagonal in momentum space it is best to apply M in momentum space to the Fast Fourier Transform of ρ . This increases the cost to be of size $N \log(N)$ but is still very efficient.

later extended to the HMC algorithm by Toral et al. [68]. The idea was first applied to the simulation of supersymmetric lattice field theories by Catterall et al. [24, 69] and later also utilized by Giedt [57]. However, the method remains problematic in terms of admissible time-step sizes. The suggested combination of both methods to be finally discussed will be seen to overcome this issue while maintaining the superior decorrelation capabilities of Fourier acceleration near the critical point of the (lattice) theory.

4.5.1 Symplectic integrators of higher order

As already outlined in Sec. 2.5 of key importance to the HMC algorithm is the use of a symplectic integration scheme inside the MD step. For the already introduced leap frog (LF) integration the final error made in H after one trajectory length is

$$\Delta H \equiv H|_{\tau=1} - H|_{\tau=0} \sim \delta\tau^2. \quad (4.5.1)$$

Since the accept/reject probability P_{acc} in the Metropolis step is controlled by this, it should obviously not become larger than some threshold to achieve an effective sampling of the configuration space. For instance this means that $\delta\tau$ must be chosen smaller in order to keep ΔH at a fixed value if the number of lattice points is increased.¹⁰⁰ Moreover, it will in general also depend on the coupling constants of the action.

Higher order symplectic integrators may reduce this problem and help to keep up the efficiency of the whole algorithm. One such integrator of fourth order was described by Omelyan et al. [70] and was also tested in the context of lattice QCD in [71]. As will be shown below, this integrator improves significantly on the behavior of ΔH . In order to discuss briefly how this integrator emerges, it is useful to simplify the notation. Let therefore q and p denote canonical variables on phase space. The classical Hamiltonian

$$H(p, q) = \frac{1}{2}p^2 + S(q) \quad (4.5.2)$$

generates the time evolution of any function on phase space via the Poisson bracket, i.e.

$$\dot{q} = \{q, H\} \quad \dot{p} = \{p, H\}. \quad (4.5.3)$$

This can equivalently be expressed with the help of a linear operator $L(H)$ acting on phase space functions by

$$\dot{f} = L(H)f \equiv \{f, H\}, \quad (4.5.4)$$

and a formal solution of Hamilton's equations of motion can then be expressed by

$$f(t + \delta t) = e^{\delta t L(H)} f(t). \quad (4.5.5)$$

¹⁰⁰This is a direct consequence of the fact that H is an extensive quantity and hence ΔH is also proportional to the number of degrees of freedom.

An exact solution for the time evolution operator $e^{\delta t L(H)}$ is in general not known. Instead, one tries to approximate this operator from simpler and analytically solvable ones up to a given order in δt . To this end $L(H)$ is decomposed into

$$L(H) = L\left(\frac{1}{2}p^2\right) + L(S(q)) = T + V, \quad (4.5.6)$$

since the action of T and V on $q(t)$ and $p(t)$ can be integrated in closed form, i.e.

$$e^{\delta t T} \begin{pmatrix} q(t) \\ p(t) \end{pmatrix} = \begin{pmatrix} q(t) + \delta t p(t) \\ p(t) \end{pmatrix}, \quad e^{\delta t V} \begin{pmatrix} q(t) \\ p(t) \end{pmatrix} = \begin{pmatrix} q(t) \\ p(t) - \delta t \frac{\partial S(q)}{\partial q} \end{pmatrix}. \quad (4.5.7)$$

Because the linear maps defined by (4.5.7) have unit determinant,¹⁰¹ both maps are symplectic and so is their composition. The time evolution operator $e^{\delta t(T+V)}$ can now be written as

$$e^{\delta t(T+V) + \mathcal{O}(\delta t^{n+1})} = \prod_{i=1}^k e^{c_i \delta t T} e^{d_i \delta t V}, \quad \mathcal{O}(\delta t^{n+1}) = \mathcal{O}_1 \delta \tau + \dots + \mathcal{O}_{n+1} \delta \tau^{n+1} + \dots \quad (4.5.8)$$

The c_i and d_i are real constants which can be tuned in such a way, that the \mathcal{O}_i vanish up to a given order. E.g. for $\mathcal{O}_1 = 0$ to hold they are restricted by $\sum c_i = \sum d_i = 1$. Time reversibility is likewise translated into a constraint, which from

$$1 \stackrel{!}{=} \prod_{i=1}^n e^{c_i \delta t T} e^{d_i \delta t V} \cdot \prod_{j=1}^n e^{-c_j \delta t T} e^{-d_j \delta t V} \quad (4.5.9)$$

reads either $d_n = 0$, $c_j = c_{n+1-j}$, $d_j = d_{n-j}$ or $c_1 = 0$, $c_j = c_{n+2-j}$, $d_j = d_{n+1-j}$. It can be shown that time reversibility already implies, that all \mathcal{O}_i with i even vanish [70]. Now with $n = 2$ and $k = 2$ in (4.5.8) this leads to

$$I_2(\delta t) = e^{\frac{\delta t}{2} T} e^{\delta t V} e^{\frac{\delta t}{2} T}, \quad (4.5.10)$$

which is recognized as the Leap Frog integrator. By the above constraints all constants in this example (c_1, c_2, d_1, d_2) are completely fixed, so that the solution is unique¹⁰². At higher stages k additional freedoms appear and can be used to zero out more error-terms \mathcal{O}_i . In particular at $k = 5$ the constraints from $\mathcal{O}_1 = 0$ and time-reversibility (which

¹⁰¹This follows directly from their matrix representations

$$e^{\delta t T} \equiv \begin{pmatrix} 1 & \delta t \\ 0 & 1 \end{pmatrix}, \quad e^{\delta t V} \equiv \begin{pmatrix} 1 & 0 \\ -\frac{\delta t}{q} \frac{\partial S(q)}{\partial q} & 1 \end{pmatrix}.$$

¹⁰²More precisely, there exists also the solution I'_2 with V and T interchanged. Nonetheless the constants remain completely fixed.

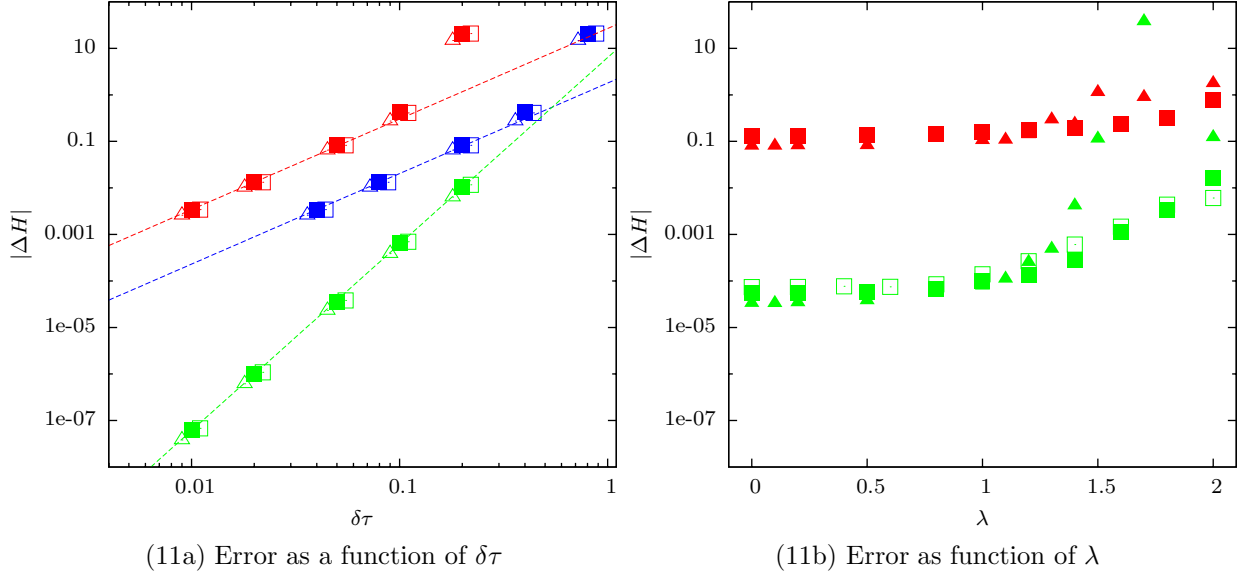


Figure 11: Comparison of LF and Omelyan integrator. Symbols in (11a) denote different fermions, i.e. Wilson unimproved (squares), Wilson improved (filled boxes) and Slac unimproved (triangles). LF data is plotted in red, data for for the Omelyan integrator in green. The effective error for the LF integrator is shown in blue, cf. the main text. In (11b) only data for improved Wilson fermions is shown. Different symbols denote here different lattice sizes, i.e. 15×15 (triangle), 25×25 (filled boxes), 48×48 (squares).

induces $\mathcal{O}_2 = 0$) are given by

$$c_1 = c_5 = \rho, \quad c_2 = c_4 = \theta, \quad c_3 = 1 - 2(\theta + \rho), \quad d_1 = d_4 = \lambda, \quad d_2 = d_3 = \frac{1}{2}(1 - 2\lambda). \quad (4.5.11)$$

The additional conditions for \mathcal{O}_3 to vanish take the form

$$0 = \frac{1}{12} - \frac{\rho}{2}(1 - \rho) - \theta \left(\frac{1}{2} - \lambda - \rho + 2\rho\lambda \right) + \theta^2 \left(\frac{1}{2} - \lambda \right), \quad (4.5.12a)$$

$$0 = \frac{1}{24} - \frac{\rho}{4} - \theta \left(\frac{1}{4} - \lambda + \lambda^2 \right) \quad (4.5.12b)$$

and allow still for a parametric set of solutions. This can be utilized to minimize \mathcal{O}_5 in some metric, that needs to be specified. Omelyan et al. obtained [70]

$$\rho = 0.1781178958448091, \quad (4.5.13a)$$

$$\theta = -0.06626458266981843, \quad (4.5.13b)$$

$$\lambda = 0.7123418310626056, \quad (4.5.13c)$$

which for their choice of metric represents the optimal solution amongst the class of all fourth order integrators. It will be used exclusively in the following. That this integrator is indeed of fourth order becomes apparent in Fig. (11a), where ΔH is plotted against $\delta\tau$.¹⁰³ Linear fits – depicted with dashed lines – yield for the slope of the LF

¹⁰³The data was computed on a 15×15 lattice from 1,000 configurations in thermal equilibrium using the pseudofermion algorithm. The parameters were $m = 10$ and $\lambda = 0.5$.

integrator $s_{\text{LF}} = 1.95$ and for the 4th order integrator $s_{4\text{th}} = 4.01$ both being in very good agreement with the theoretical prediction. However, since the Omelyan integrator requires four force computations in a single integration step it is also four times more expensive than the leap frog. Hence the latter could use a time-step four times smaller for the same computational cost. The blue graph shown in Fig. (11a) corrects the LF data for this and brings both integrators somewhat closer together. Yet the qualitative picture is not changed and the Omelyan integrator remains the better choice. Furthermore, it is worthwhile to mention that almost no differences between Wilson and Slac fermions are found.

In Fig (11b) the error is studied for Wilson fermions using the improved action as a function of λ for different lattice sizes at fixed time-step $\delta\tau = 0.05$ and fixed $m = 10$. For $\lambda < 1$ both integrators depend at most marginally on either λ or the lattice size. While the first may have been expected for the weak coupling regime the pretended independence from the lattice size deserves probably some explanation. At the beginning it was stated, that the error is expected to grow with the number of lattice points which would clearly contradict the observations. However, in these simulations the larger lattice size was used to shrink the lattice spacing. Along with this, the bare parameters of the lattice action are also scaled and become smaller. Thus it seems very likely, that these effects work in opposite direction and happen to cancel each other in the observed parameter range.¹⁰⁴ At larger couplings a faint dependence on λ becomes visible, albeit the Omelyan integrator remains the superior choice.¹⁰⁵

4.5.2 Fourier acceleration

Another problem that arises in MC simulations is due to correlations amongst adjacently generated configurations. This can be measured in terms of the autocorrelation time, which for a given operator \mathcal{O} is defined as¹⁰⁶

$$C_{\mathcal{O}}(\tau) = \frac{\langle \mathcal{O}(\tau)\mathcal{O}(0) \rangle - \langle \mathcal{O}(\tau) \rangle \langle \mathcal{O}(0) \rangle}{\langle \mathcal{O}(0)^2 \rangle - \langle \mathcal{O}(0) \rangle^2}. \quad (4.5.14)$$

The argument τ refers to MC time, i.e. it labels subsequent configurations of the Markov chain. The function $C(\tau)$ decays exponentially for large τ from which the autocorrelation time can be defined as $C(\tau) \sim \exp(\tau/\tau_{\text{auto}})$. In general, the autocorrelation time depends on the operator \mathcal{O} . To avoid false predictions three different operators given by the bosonic action, the lattice average of φ_2 and the bosonic twopoint correlator¹⁰⁷ at a

¹⁰⁴Contrary, if the lattice size is increased without scaling the bare parameters as to cover a larger physical space-time volume, the error is indeed found to be proportional to the lattice size.

¹⁰⁵That the error grows extraordinarily on the smallest lattice (green triangles) is due to some other effect, which will be discussed at length in Sec. 4.6.

¹⁰⁶Precisely speaking, here the average refers to many ensembles, i.e. replicas. However, for practical purposes these many replicas are replaced by averaging over a single one for different starting times.

¹⁰⁷The reason why in \mathcal{O}_2 and \mathcal{O}_3 preference is given to φ_2 instead of φ_1 follows from the fact, that the effective potential has two separate minima for φ_1 which will mix for large λ within a single simulation. A straightforward computation of the autocorrelation time is so not possible. Since φ_2 fluctuates around a unique vacuum expectation value this difficulties are circumvented.

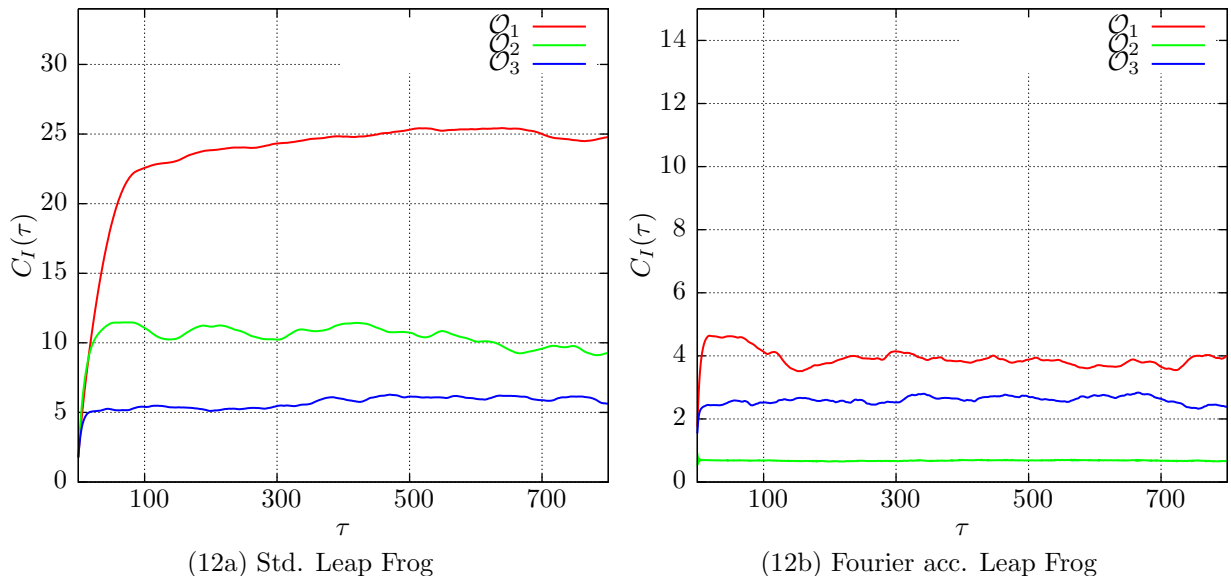


Figure 12: Integrated autocorrelation function $C_I(\tau)$ for std. LF and Four. acc. LF integrator. The corresponding autocorrelation times for three different operators $\mathcal{O}_{1,2,3}$ (defined in the text) are read off from these graphs, e.g. from (12a) $\tau_{\text{int},1} \approx 25$, $\tau_{\text{int},2} \approx 10$ and $\tau_{\text{int},3} \approx 5$. It is clearly seen that τ_{int} depends on the operator. The efficiency of Fourier acceleration is likewise different for different observables although always superior to std. LF integration. (Wilson unimproved, $N = 20 \times 20$, $\lambda = 0.5$, $m_L = 0.5$)

fixed time, i.e.

$$\mathcal{O}_1 = S_B, \quad \mathcal{O}_2 = \frac{1}{V} \sum_x \varphi_{2,x}, \quad \mathcal{O}_3 = C_{B,22}(t)|_{t=5} = \sum_{x,x',t'} \varphi_2(t'+5, x) \varphi_2(t', x'). \quad (4.5.15)$$

were investigated since they will be needed in the numerical analysis of later sections. To estimate the autocorrelation time numerically, it is more convenient to consider the integrated autocorrelation time instead:

$$C_{I,\mathcal{O}}(\tau) = \sum_{\tau'=0}^{\tau} C_{\mathcal{O}}(\tau'). \quad (4.5.16)$$

From the exponential decay of $C(\tau)$ the above function will form a plateau at late times, $C_I(\tau) = \tau_{\text{int}}$, which yields a good approximation for the autocorrelation time, i.e. $\tau_{\text{auto}} \approx \tau_{\text{int}}$. Assuming this, the following discussion will exclusively refer to the integrated autocorrelation time. In Fig. 12 the function $C_I(\tau)$ is shown for a specific run. It is well-known that the error on expectation values grows as $\sqrt{\tau_{\text{int}}}$ and hence the numerical effort to achieve a given precision grows if τ_{int} becomes large which from statistical mechanics is furthermore known to happen in the vicinity of a second order phase transition. Namely, the autocorrelation time grows like $\tau \sim \xi^z$, where ξ is a typical correlation length of the system and z is called the dynamical critical exponent [72]. Since ξ is supposed to diverge when the critical point is approached so is the autocorrelation time. Here, the critical point is reached for $m_L \rightarrow 0$ for which τ_{int} is expected to grow as demonstrated in Fig. 13 (blank symbols). This phenomenon (called critical slowing down (CSD)) considerably hampers MC simulations of lattice field theories near the continuum limit.

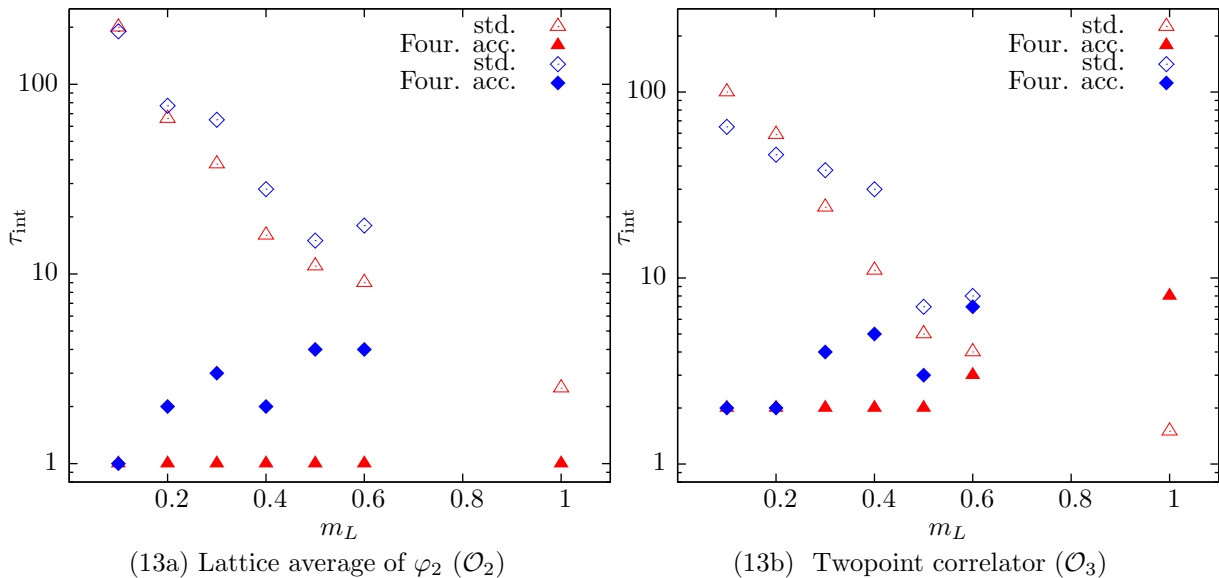


Figure 13: Integrated autocorrelation time for the three operators defined in the text and two different coupling constants ($\lambda = 0.5$ in red, $\lambda = 1.0$ in blue). Full symbols depict Fourier acc. LF, blank depict std. LF. (Wilson unimproved, $N = 20 \times 20$)

To escape CSD several approaches have been discussed in the literature. A particular technique, called Fourier acceleration [67], will turn out to be very useful in the present context as may also be seen from Fig. 13. Obviously, for the std. LF algorithm τ_{int} increases by orders of magnitude while a roughly constant value is maintained with Fourier acceleration. In brief Four. acc. amounts to propagate the long-range (or slow) modes of the dynamical fields φ_1 and φ_2 with much larger time-step sizes than their short-range (or fast) modes inside the MD step. A preliminary (and to some extent heuristic) justification may be found from Fig. 14 where the impact on the sampling behavior of the spatial lattice average of φ_1 , i.e. the slowest mode of this field is depicted. At $\lambda = 0.5$, i.e. when the two ground states are far apart from each other, only the Four. acc. LF integrator can sample both of them due to the increased velocity of the slowest mode.¹⁰⁸ Albeit at $\lambda = 1.0$ tunneling is also observed with the std. LF integrator, the distinct tunneling events are far less frequent and the slowest mode still moves at a much faster pace.

More rigorously, the LF integration scheme, cf. (4.5.10) can be written as

$$q_x(\tau + \delta\tau) = q_x(\tau) + \delta\tau p_x(\tau) + \frac{\delta\tau^2}{2} F_x(\tau), \quad (4.5.17a)$$

$$p_x(\tau + \delta\tau) = p_x(\tau) + \frac{\delta\tau}{2} (F_x(\tau) + F_x(\tau + \delta\tau)), \quad (4.5.17b)$$

where $F_x \equiv -\frac{\partial S}{\partial q_x}$ and the subscript x refers to two-dimensional lattice coordinates.¹⁰⁹ Now the Hamiltonian $H(p, q)$ is also preserved, if the time evolution conforms to gener-

¹⁰⁸It should be stressed that to choose a uniform time-step size that large would break the numerical integration from the very beginning.

¹⁰⁹Notice that the original half steps reappear upon identifying (and suppressing higher order cor-

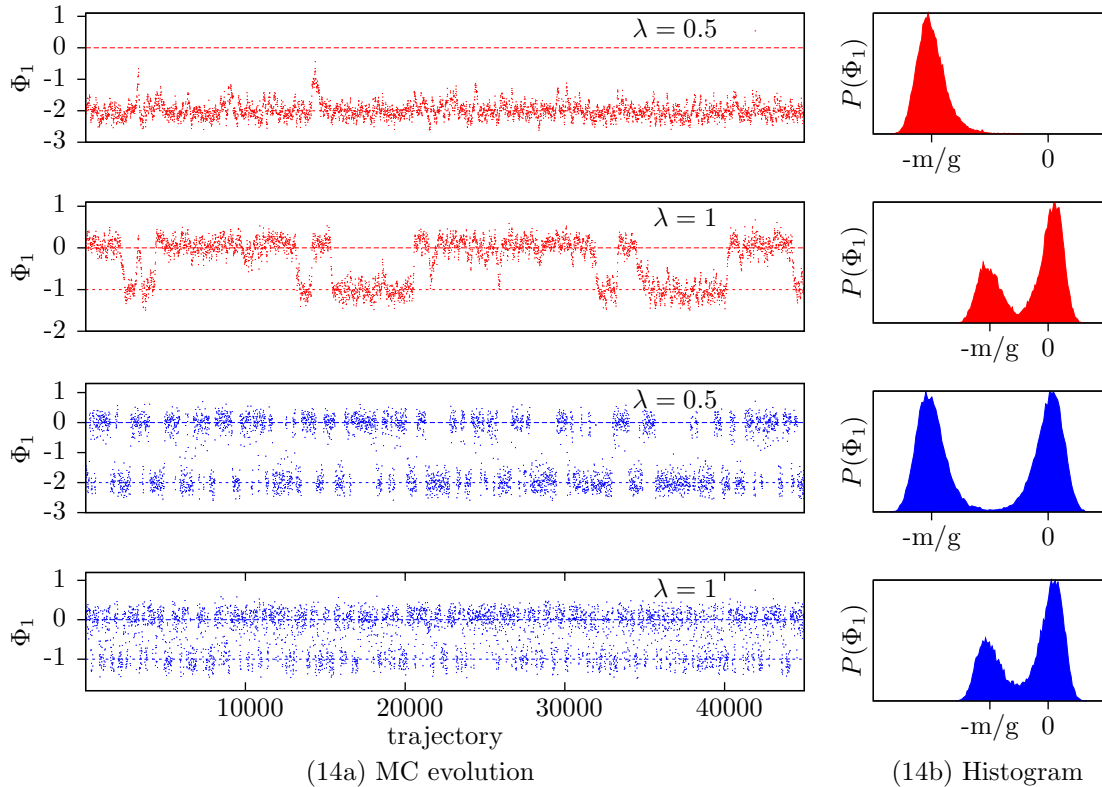


Figure 14: Comparison of the evolution of Φ_1 for std. (\bullet) and Four. acc. (\bullet) LF algorithm at $m_L = 0.2$. In (14a) the locations of the classical minima are denoted with dashed lines. The difference in the height of the peaks at $\lambda = 1.0$ is due to the Wilson term as discussed in Sec. 4.3 (Wilson unimproved, $N = 20 \times 20$)

alized equations of motion

$$q_x(\tau + \delta\tau) = q_x(\tau) + \delta\tau \sum_y A_{xy} p_y(\tau) + \frac{\delta\tau^2}{2} \sum_{y,z} A_{xy} A_{yz}^T F_z(\tau), \quad (4.5.18a)$$

$$p_x(\tau + \delta\tau) = p_x(\tau) + \frac{\delta\tau}{2} \sum_y A_{xy}^T (F_y(\tau) + F_y(\tau + \delta\tau)), \quad (4.5.18b)$$

with A_{xy} an arbitrary matrix connecting different lattice sites [68]. A particular choice for A is to take it to be diagonal in Fourier space. The Eqs. (4.5.18) should then better

rections)

$$p_x\left(\tau + \frac{\delta\tau}{2}\right) = p_x(\tau) + \frac{\delta\tau}{2} F_x(\tau), \quad F_x\left(\tau + \frac{\delta\tau}{2}\right) = \frac{1}{2}(F_x(\tau) + F_x(\tau + \delta\tau)).$$

be studied in momentum space as well, i.e.¹¹⁰

$$\tilde{q}_k(\tau + \delta\tau) = \tilde{q}_k(\tau) + \delta\tau \tilde{A}_k \tilde{p}_k(\tau) + \frac{\delta\tau^2}{2} \tilde{A}_k^2 \tilde{F}_k(\tau), \quad (4.5.19a)$$

$$\tilde{p}_k(\tau + \delta\tau) = \tilde{p}_k(\tau) + \frac{\delta\tau}{2} \tilde{A}_k (\tilde{F}_k(\tau) + \tilde{F}_k(\tau + \delta\tau)). \quad (4.5.19b)$$

Hence \tilde{A}_k may be interpreted as a multiplier for the uniform step size $\delta\tau$ to form the mode dependent step size $\delta\tau_k \equiv \tilde{A}_k \delta\tau$. To find suitable values for A_k the free theory may be analyzed and it is found, that the time step $\delta\tau_k$ should be proportional to the inverse of the size of the propagator for that mode. For the three different lattice fermions introduced earlier this amounts to three different time step formulas.

However, it was found numerically, that the inverse of the (truncated) continuum propagator is a sufficiently effective choice for all three models, i.e. in all models the time step may be taken to be

$$\delta\tau_k = \frac{\delta\tau \sqrt{\pi^2 + m_{\text{acc}}^2}}{\sqrt{p_0^2 + p_1^2 + m_{\text{acc}}^2}}, \quad p_i = \frac{\pi k_i}{L_i}. \quad (4.5.20)$$

The overall normalization is arbitrary and has been adjusted here in such a way, that the highest momentum modes propagate with almost the original step size $\delta\tau$ while all slower modes propagate with a larger time step. The parameter m_{acc} is initially set to the bare lattice mass parameter, and may be fine-tuned once interactions are turned on. The practical gain of Fourier acceleration was tested with Wilson fermions using the unimproved action on a 20×20 lattice. The critical point was approached by $m_L \rightarrow 0$, i.e. runs at $m_L = 1.0, 0.6, \dots, 0.2, 0.1$ were analyzed.¹¹¹ The

λ	m_L	\mathcal{O}_1		\mathcal{O}_2		\mathcal{O}_3		
		std.	acc.	std.	acc.	std.	acc.	
0	0.1	20	2	140	1	60	2	
	0.2	30	13	35	1	18	2	
	0.3	40	6	25	1	10	2	
	0.4	20	3	10	1	5	3	
	0.5	50	7	8	1	4	3	
	0.6	25	4	4	1	2	6	
	1.0	34	50	2	1	2	45	
0.5	0.1	10	2	200	1	100	2	
	0.2	7	3	66	1	59	2	
	0.3	10	3	38	1	24	2	
	0.4	12	4	16	1	11	2	
	*	0.5	25	4	10	1	5	2
	0.6	6	7	9	1	4	3	
	1.0	4	14	2.5	1	1.5	8	
1.0	0.1	8	2	190	1	65	2	
	0.2	4	3	77	2	46	2	
	0.3	7	4	65	3	38	4	
	0.4	10	4	28	2	30	5	
	0.5	22	10	15	4	7	3	
	0.6	6	13	18	4	8	7	

Table 7: Integrated autocorrelation times for the three operators defined in (4.5.15) for the free theory, i.e. at $\lambda = g/m = 0$, at $\lambda = 0.5$ and at $\lambda = 1.0$. The large value at $\lambda = 0$, $m_L = 1$ for the Four. acc. LF is due to a significant smaller acceptance rate for this run. (*) corresponds to Fig. 12.

¹¹⁰The (lattice) Fourier transform of the field q_x is defined by

$$\tilde{q}_k = \frac{1}{\sqrt{N^2}} \sum_x e^{-ik \cdot x} q_x, \quad k \cdot x = k_0 x_0 + k_1 x_1$$

and a similar expression follows for p_x .

¹¹¹The values $m_L = 0.3, \dots, 0.6$ are of special interest here since they will be reused for the extraction of masses in Sec. 4.7.

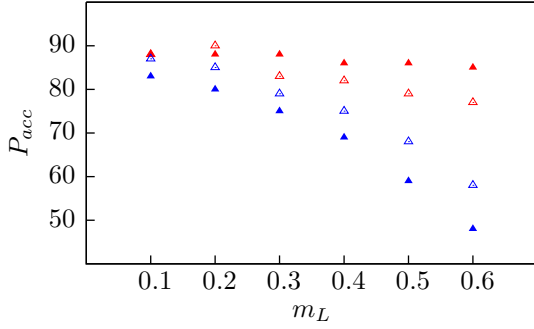


Figure 15: Acceptance rate as a function of m_L at $\lambda = 0.5$ ($\triangle, \blacktriangle$) and $\lambda = 1.0$ ($\triangle, \blacktriangle$). Empty symbols refer again to std. LF and filled to Fourier acc. LF.

m_L	$\lambda = 0.5$		$\lambda = 1$	
	std.	four.	std.	four.
0.1	0	5	0	96
0.2	0	2	2	127
0.3	0	3	3	244
0.4	0	0	20	426
0.5	0	0	124	1321
0.6	0	0	619	2057
1	1	3	15,976	42,699

Table 8: Number of broken integrations (in 50,000)

measured autocorrelation lengths are summarized in Tab. 7 and indicate a significant improvement as mentioned at the beginning which, most interestingly, can be maintained even at intermediate and strong coupling constants. The extensive analysis confirms earlier results in the one-dimensional WZ model [69] and shows that for the two-dimensional WZ model Fourier acceleration is useful again.

4.5.3 Higher order integration schemes and Fourier acceleration

One problem with Fourier acceleration being discussed so far, is the fact that it is based upon the 2nd order LF algorithm. As discussed in Sec. 4.5.1 a 4th order integrator would lead to far better results w.r.t. to the overall numerical stability and the acceptance rate in particular. Fig. 15 illustrates that the acceptance rate falls off for both methods in the range $0.3 \leq m_L \leq 0.6$ which is of most interest with regard to computations of correlation functions later on. This decay can be partly understood by an increased number of broken integrations, i.e. where numerical calculations in double precision fail to obtain a finite result. That this is more severe when using Fourier acceleration may be learnt from Tab. 8.

It is tempting then to combine Fourier acc. with the 4th order integrator introduced in Sec. 4.5.1 into a Four. acc. 4th order integrator. That this proposal is expected to work can be derived from (4.5.18) when regarded as an approximation (in order $\mathcal{O}(\delta\tau^3)$) of

$$\dot{q}_x = \sum_y A_{xy} p_y, \quad \dot{p}_x = \sum_y A_{xy}^T F_y. \quad (4.5.21)$$

It was already pointed out that albeit (4.5.21) does not derive from Hamilton's equations of motion the Hamiltonian $H(q, p)$ is still conserved. Hence using any time-reversible symplectic approximation of (4.5.21) will suffice for the HMC to work properly. In particular it is suggested that the 4th order integrator already introduced will do this job. In doing so however, an extra cost arises from the needed Fourier transforms. These must be carried out each time the force is computed – the latter being done most

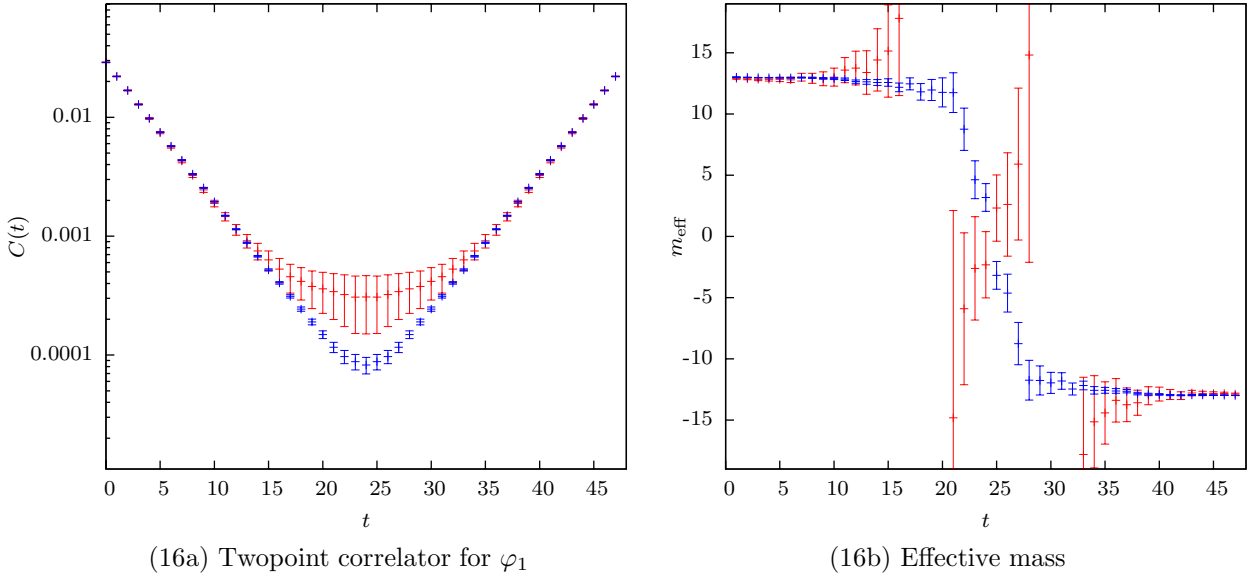


Figure 16

conveniently in position space. Fortunately, this does not count much for the overall cost when done via a Fast Fourier Transform.¹¹² The results are quite remarkable. While the algorithm inherits a superior small error ΔH at comparative large time-step sizes¹¹³ $\delta\tau$ from the std. 4th order integrator, the Fourier acceleration takes care that critical slowing down remains evaded. Finally, by carefully tuning $\delta\tau$, m_{acc} and the total trajectory length τ , autocorrelation times of $\tau_{\text{auto}} \approx 1$ can be realized for a bare mass parameter in the desired range on lattices as large as 64×64 . On even larger lattices the autocorrelation times are still found to be of order one.

The overall gain is illustrated best by comparing actual measurements. In Fig. (16a) the bosonic twopoint function using the improved model with Wilson fermions is shown. The data was obtained from a 48×48 lattice with $m = 15$ and $g = 3$ ($m_L \approx 0.3$, $\lambda = 0.2$). The red symbols depict the data using the std. 4th order integrator while the blue symbols depict the same as obtained from the Fourier accelerated 4th order integrator. For each correlator 10^6 configurations were evaluated. Even more clearly, Fig. (16b) shows the effective masses given by

$$m_{\text{eff}}(t) = \ln \frac{C(t)}{C(t+1)}, \quad (4.5.22)$$

for the two correlators on the left. From either figure it follows, that the Fourier accelerated integrator is superior and leads to a far better signal-to-noise ratio. Comparing wall-clock times the Fourier acc. ensemble took only half the time due to a shorter trajectory length that became possible and negligible costs for the FFT. Likewise the std. LF algorithm would have taken as much as twice the time due to the required smaller time-step size. Since this trend is further enhanced when the coupling constants become

¹¹²A very versatile and fast library publicly available is the FFTW library [73].

¹¹³In fact the time-step can be chosen as much as 10 times larger than with the 2nd order LF algorithm.

larger the Fourier acc. 4th-order integrator is found to perform better over the whole parameter space. For the $\mathcal{N} = (2, 2)$, $d = 2$ WZ-model this amounts to a numerical control that has not been achieved previously. It is only due to the combined effort of the presented algorithms that lattices as large as 64×64 or even larger can be sampled in almost arbitrarily large statistics. Moreover it is believed that this method applies to other Yukawa-like models – supersymmetric or not – equally well.

4.6 A closer look at the improvement term

In this section a detailed analysis concerning the improvement term which was introduced in Sec. 4.2 is presented. It will be argued that at small coupling only the improved actions preserve part of the supersymmetry by analyzing the expectation value of the bosonic action on both improved and unimproved ensembles and with and without dynamical fermions. In this comprehensiveness the analysis has hitherto not been carried out and the results therefrom are presented in the following for the first time. Moreover, if the coupling strength exceeds some threshold it is found, that the simulations become unstable and a new unphysical 'broken' phase appears. This too, has not been reported previously.

4.6.1 Presence of Supersymmetry

As discussed in Sec. 3.1.3 the expectation value of the (bosonic) action is for the supersymmetric model given by¹¹⁴

$$\langle S_B \rangle = N^2. \quad (4.6.1)$$

Whether this observable can be used to distinguish improved and unimproved actions remains nonetheless a dynamical question. Moreover it turns out, that (4.6.1) is found to be only fulfilled when dynamical fermions are included. As a result the two-dimensional WZ-model is seen to constitute a very interesting laboratory for the study of lattice fermions. If they are included (4.6.1) is by construction an algebraic identity for the improved actions. Any deviations found would hence signal a flaw in the implementation, e.g. an improper sampling of the fermion determinant in the pseudo fermion algorithm. If deviations are found for non-supersymmetric models they should be to interpreted to be systematically and may as such not necessarily vanish in the continuum limit. For that case one could argue, that the specific lattice action will not lead to the correct continuum limit.¹¹⁵ Since in the free theory bosons and fermions decouple and the improvement term vanishes identically, it follows readily, that deviations should become more and more pronounced if the interaction strength is turned on. Since Wilson type

¹¹⁴The extra factor of two is due to the fact, that the scalar field is complex, i.e. has twice as many degrees of freedom, for the two-dimensional theory

¹¹⁵For instance this is expected for quenched but not for the unimproved models. The former lack fermion contributions at all and are thus most naturally not expected to yield the correct continuum limit. The latter differ only by a surface term, which by contrast should vanish in the continuum limit.

fermions¹¹⁶ differ clearly from Slac fermions the outcome of the analysis might also depend on this particular choice.

The continuum limit of the Wess-Zumino model is reached if the bare mass parameter is tuned to zero. For a fixed number of lattice points this means that the actual physical volume also shrinks. However, the presence or absence of supersymmetry is not expected to depend strongly on the physical extension of the studied space-time volume. The actual analysis can hence be done for a fixed lattice size at different values of the bare mass parameter. For the discussion of this section the bare mass was varied from $m_L = 0.1$ to $m_L = 0.6$. At all values of m_L the system was simulated at different coupling strengths λ ranging from $\lambda = 0.8$ to $\lambda = 1.5$. All points (m_L, λ) in the theory's two dimensional parameter space were analyzed with (standard) Wilson and Slac fermions respectively. For each type of fermions the system was simulated both with the improved and unimproved action and with or without the inclusion of dynamical fermions¹¹⁷. Every ensemble comprised of roughly 50,000 independent configurations which was checked explicitly by computing the integrated autocorrelation time for the bosonic action of the model used. The quoted Jack-Knife errors were computed after re-sampling the data into 100 bins.¹¹⁸ Although the error on the error was not computed explicitly consistency was checked by repeating the Jack-Knife method with different bin sizes. All simulations were carried out with the pseudo fermion algorithm using the Four. acc. 4th order integrator. For Slac fermions all data were

obtained from a 15×15 lattice. The quenched results are given in Figure (17a) for the improved and in Figure (17b) for the unimproved model respectively. Both systems clearly deviate from the correct supersymmetric value, which would be here $\langle S_B \rangle = 225$. The deviations amount to at most 7% for the improved action and about 11% for the unimproved model. As expected they increase in size if either λ or m_L become larger.

λ	$S_0^{(\text{impr,quenched})}$	$S_0^{(\text{unimpr,quenched})}$	$S_0^{(\text{unimpr,dyn.})}$
Slac			
0.8	224.76(1)	224.78(2)	224.94(2)
1.0	224.79(3)	224.80(3)	224.94(2)
1.2	224.82(6)	224.83(6)	224.97(2)
1.5	224.90(10)	224.93(12)	224.99(3)
Wilson			
0.8	258.1(6)	258.0(5)	255.88(1)
1.0	258.7(7)	258.5(6)	255.87(1)
1.2	259.2(9)	258.9(6)	255.88(1)
1.5	259.0(5)	259.4(6))	255.92(1)

Table 9: Extrapolation of the bosonic action towards $m_L = 0$. The measurements were fitted against (4.6.1) in the range $0 \leq m_L \leq 0.25$.

Conversely, for small values of m_L the value of $\langle S_B \rangle$

¹¹⁶For the reasoning here there is no substantial difference between standard and twisted Wilson fermions. The latter can be safely subsumed for this discussion.

¹¹⁷In total this sums up to eight different models, i.e. two different types of fermions, two choices for the bosonic action and whether fermions were treated quenched or dynamical.

¹¹⁸Hence every bin contained 500 values.

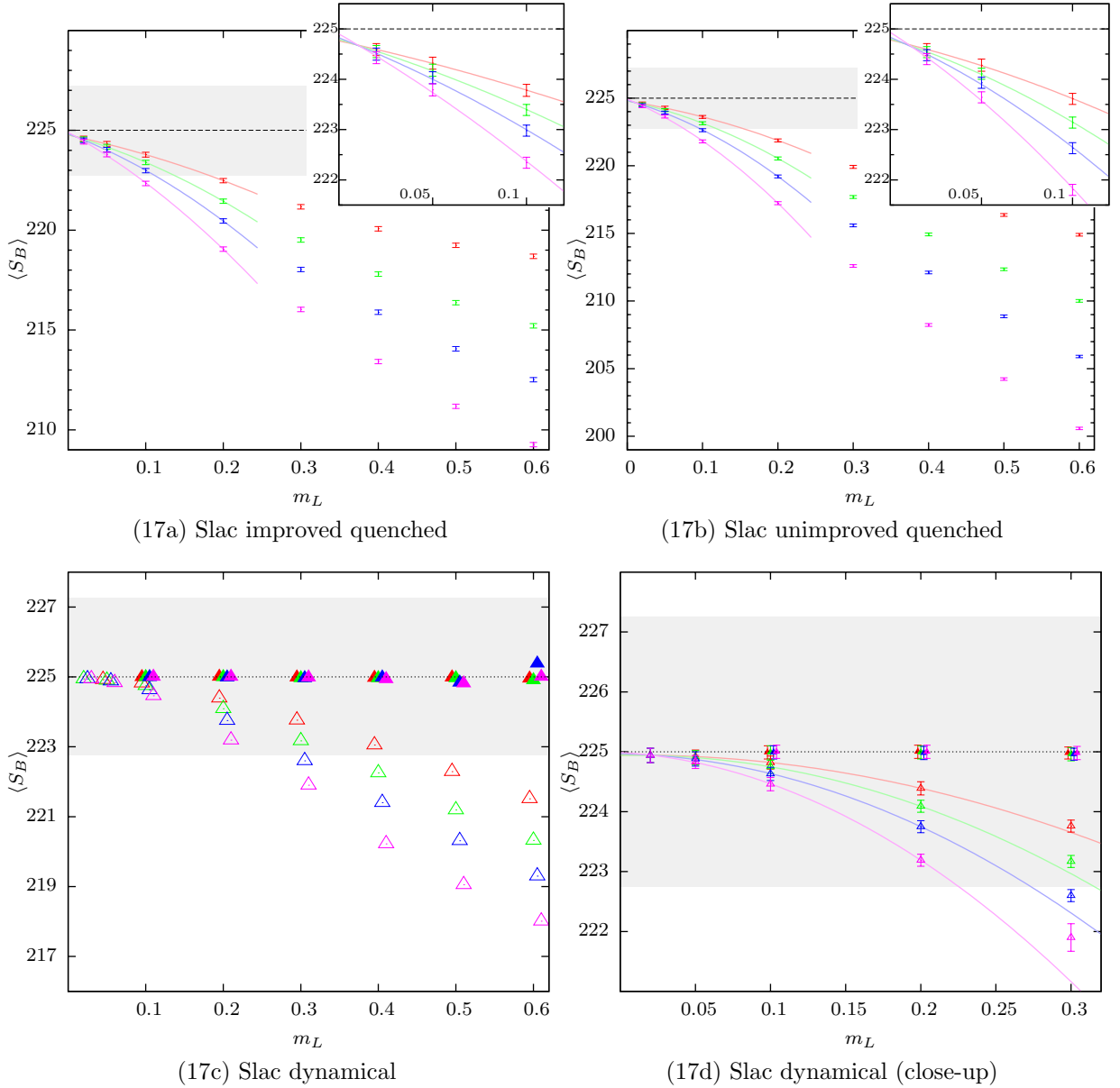


Figure 17: Bosonic action as a function of m_L for Slac fermions. Different colors denote different values of λ according to $\lambda=0.8$ (red), 1.0 (green), 1.2 (blue) and 1.5 (magenta). The extrapolation to $m_L = 0$ (solid lines) was done by fitting (4.6.1) in the range $0 \leq m_L \leq 0.25$. The gray shaded bar visualizes the one percent interval around the supersymmetric value of $\langle S_B \rangle = 225$. In Figs. (17c), (17d) the improved action is depicted with full triangles, the unimproved with empty triangles. For better visibility data points are slightly shifted. The symbols in (17c) are larger than the respective errors.

may be fitted to¹¹⁹

$$S_B(m_L) = S_0 + C_1 m_L + C_2 m_L^2. \quad (4.6.2)$$

The values obtained for S_0 are given in Tab. 9. As to the results for the quenched theory alone, they are in good agreement with each other and indicate that the improved and unimproved lattice models yield the same theory in the continuum limit, although they still deviate from the supersymmetric prediction.¹²⁰ The latter may hence be taken as

¹¹⁹Some care has to be taken with this extrapolation. Since the lattice size is held fixed the physical volume shrinks to zero with $m_L \rightarrow 0$. The quoted values of S_0 are thus not necessarily the true values of S_B in a finite volume, not to speak of the infinite volume limit.

¹²⁰That the extrapolation at larger λ yields a value of S_0 that is closer to this is accidental and stems most probably from insufficient statistics and too few data points close to $m_L = 0$.

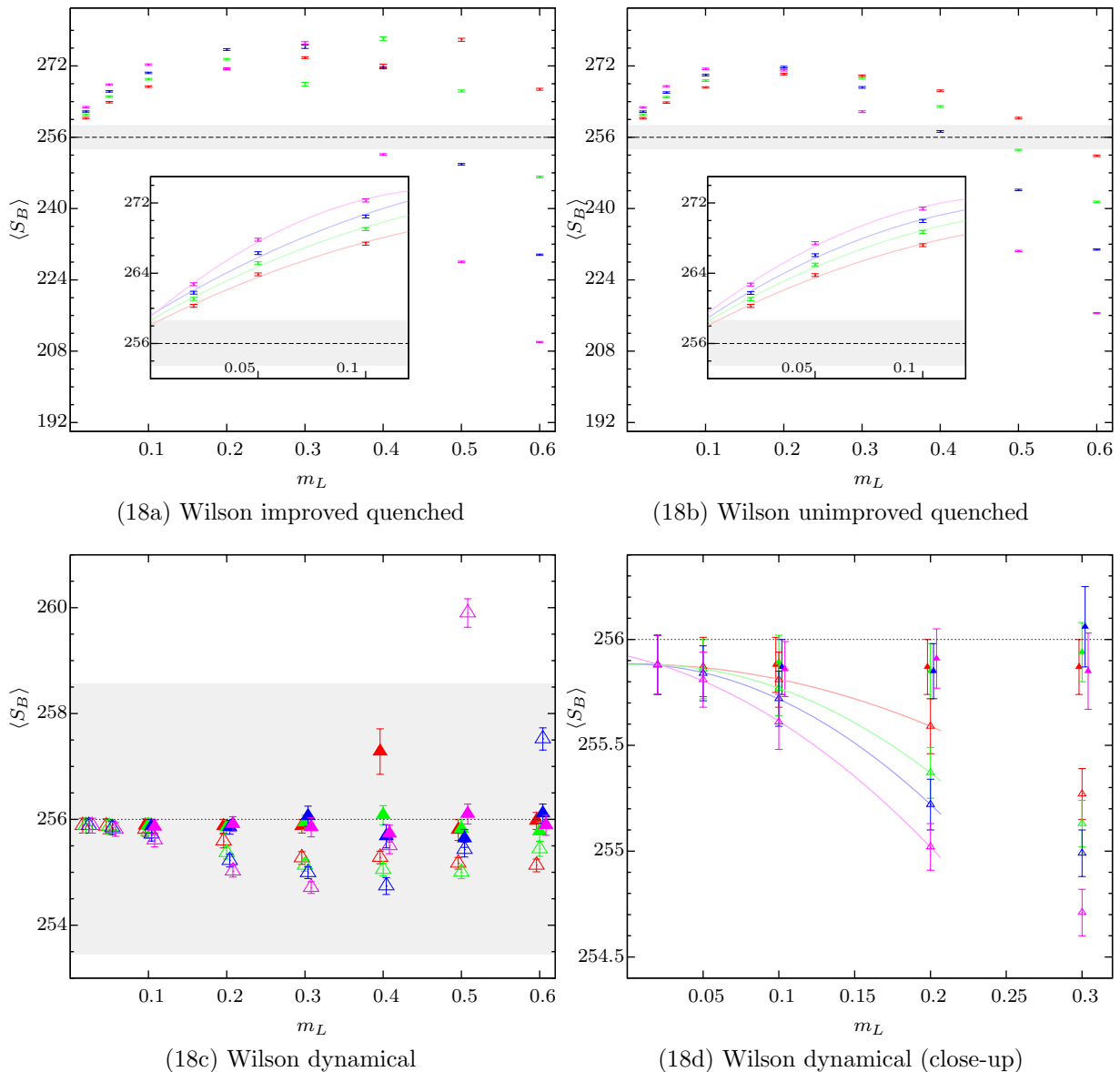


Figure 18: Expectation value of the bosonic action using Wilson fermions. The same conventions as in Fig. 17 are understood.

an indicator for the absence of fermions. Figs. (17c) and (17d) show the results for the analysis using dynamical fermions. The unimproved data still deviates significantly from the improved one, which is found at $\langle S_B \rangle = 225$ as expected. However, the unimproved model is now only 3% off. This is by a factor of three smaller than the quenched results. Furthermore in the limit $m_L \rightarrow 0$ the unimproved model converges to the correct value which is also seen from the extrapolated value S_0 , cf. 3rd column of Tab. 9.

The analysis was repeated for Wilson fermions on a 16×16 . The results from the quenched simulations are depicted in Fig. (18a) (improved) and Fig. (18b) (unimproved). When compared to Slac fermions, the deviations are considerably larger. They amount to about 20% at $m_L = 0.6$ and $\lambda = 1.5$. Also in the limit $m_L \rightarrow 0$ the absence of the fermions remains more visible by one order of magnitude, cf. Tab. 9. Upon the inclusion of fermions the situation changes considerably, which is depicted in Figs. (18c) and (18d). While the improved model is found again to lie on top of the predicted

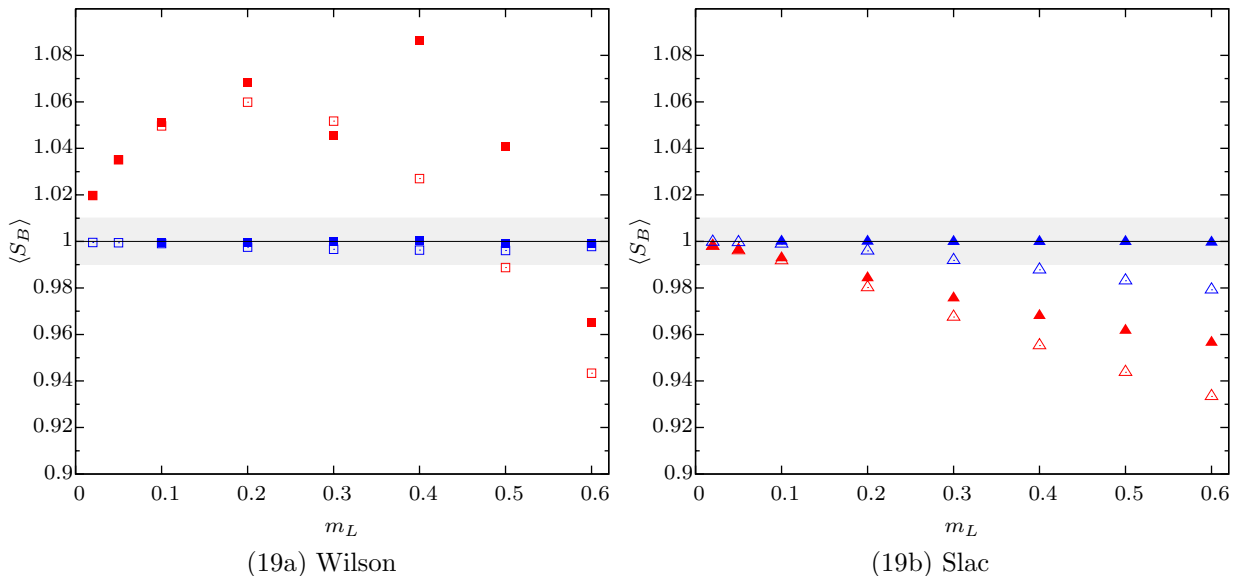


Figure 19: Bosonic action as a function of m_L . Empty symbols refer to unimproved, filled symbols to improved models. Quenched results are shown in red, dynamical fermion results in blue.

value for all m_L and λ , the unimproved model is now much closer by than the respective unimproved model with Slac fermions. Accordingly, in the extrapolation $m_L \rightarrow 0$ both models agree again.

To sum up, the analysis has revealed that the bosonic action is useful to resolve the presence or absence of both dynamical fermions or improvement terms. In Fig. 19 the two fermion types are compared to each other at a fixed coupling strength $\lambda = 1.0$. Especially Slac fermions, cf. Fig.(19b), exhibit a systematic improvement, i.e. unimproved dynamical is closer than improved quenched is closer than unimproved quenched. For Wilson fermions the quenched results are clearly off while the unimproved model with dynamical fermions is almost on top of the respective improved model.

4.6.2 Limitations for the improved models

Concerning the bosonic action S_B only the improved models with dynamical fermions are capable to yield the correct supersymmetric value. However, upon the inclusion of the improvement ΔS , cf. Eq. (4.2.6), new complications arise which are discussed in the following. To begin with, it is useful to recall the definition of the bosonic part of the improved action from (4.2.2):

$$S_B = \frac{1}{2} \sum_x |2(\partial\varphi)_x + \overline{W}_x|^2. \quad (4.6.3)$$

Obviously, the action is bounded from below and minimized for a constant field configuration $\varphi_x = \varphi_0$, where φ_0 minimizes the expression $W'(\varphi_0)$. These configurations may hence be called ground states. But (4.6.3) allows for a multitude of other possible

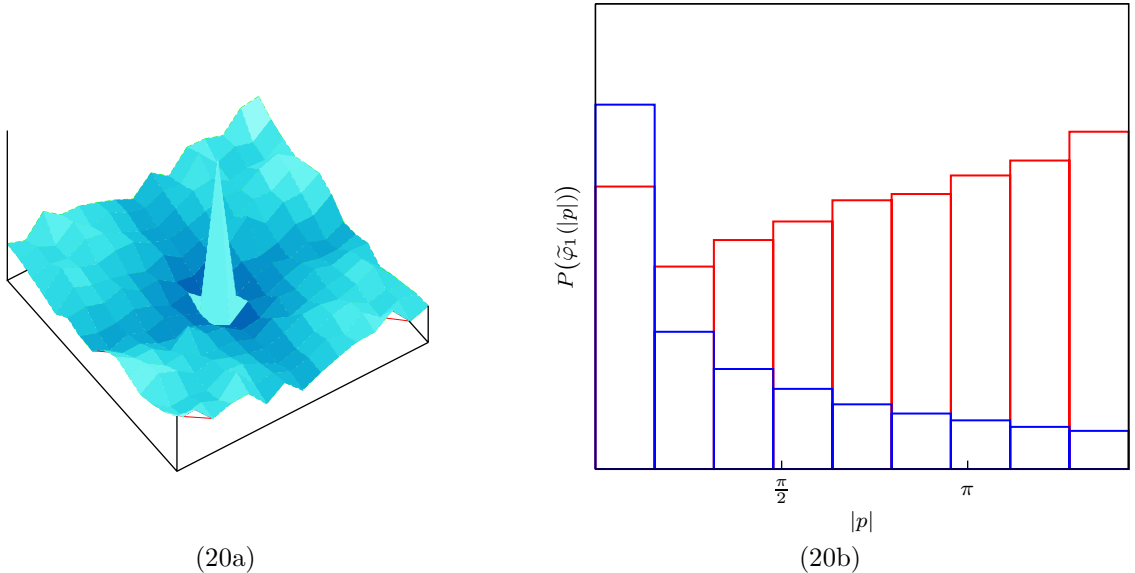


Figure 20: Fourier mode analysis for the improved model in the unphysical region. Fig. (17a) shows the two-dimensional mode content averaged over 25,000 configurations, while Fig. (17b) shows the distribution projected onto the modulus of the (lattice) momentum p . The red bars correspond to what is depicted on the left, the blue bars were obtained from configurations near the physical ground state. The data was obtained from Slac fermions on a 15×15 lattice at $m_L = 0.6$ and $\lambda = \frac{5}{3}$.

solutions, too. Namely, one finds readily that¹²¹

$$S_B = 0 \iff 2(\partial\varphi)_x = -\overline{W}_x. \quad (4.6.4)$$

In particular this means that large fluctuations in φ_x that contribute to $(\partial\varphi)_x$ can compensate for large values of opposite sign in \overline{W}_x . Indicated by the latter the system could be found far away from its aforementioned classical ground state. Writing the improved action in yet a different fashion as

$$S_B^{\text{impr.}} = S_B^{\text{unimpr.}} + \Delta S \quad (4.6.5)$$

one surely wants to find $\langle S_B^{\text{impr.}} \rangle \approx \langle S_B^{\text{unimpr.}} \rangle$, i.e. $\langle \Delta S \rangle \approx 0$. However, the discussion above alludes to the possibility to find the system in a region of configuration space where instead

$$|\langle \Delta S \rangle|, \langle S_B^{\text{unimpr.}} \rangle \gg \langle S_B^{\text{impr.}} \rangle = N^2. \quad (4.6.6)$$

Since $S_B^{\text{unimpr.}}$ is a sum of squares, it can only take positive values and so one must have $\Delta S < 0$. Actual simulations have revealed, that it depends strongly on the actual values of m_L and λ whether the 'physical' configurations around the classical ground states dominate or whether the system is driven towards some other 'unphysical' configurations into what will be called a 'broken' phase for reasons to become clear later on. The nomenclature of 'physical' and 'unphysical' configurations refers to the following

¹²¹More precisely this leads to non-trivial solutions only for superpotentials describing interactions which is of course the interesting case.

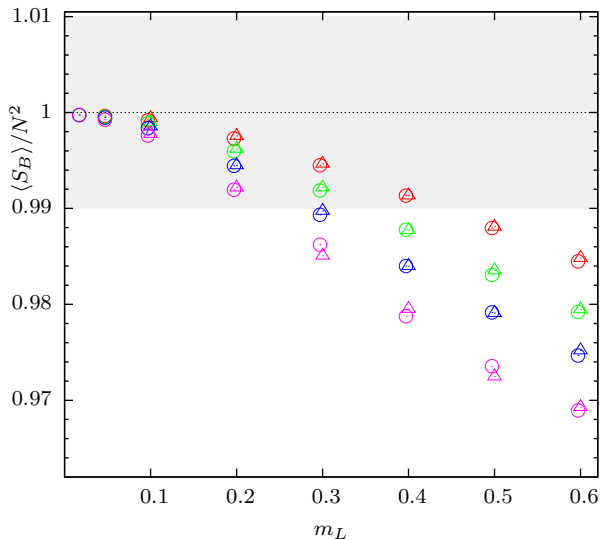


Figure 21: Normalized bosonic action of the unimproved model with Slac fermions from a 15×15 (triangles) and a 25×25 (circles) lattice. Different colors denote $\lambda = 0.8$ (red), 1.0 (green) and 1.5 (magenta)

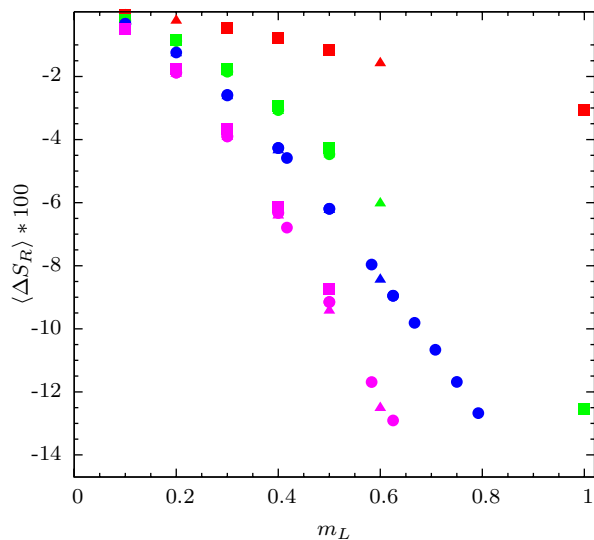


Figure 22: Reduced improvement term for different lattice sizes, i.e. 9×9 (squares), 15×15 (triangles) and 25×25 (circles). The colors are the same as in Fig. 21

interpretation. As already discussed, a large value of ΔS can only be found on very rough configurations. Hence these configurations are dominated by their UV modes prohibiting a sensible continuum limit. A heuristic justification of the reasoning is given in Fig. 20, where an ensemble that comprises such unwanted configurations has been analyzed in terms of its Fourier mode contents and is compared to the same analysis obtained from an improved ensemble without such contributions (both times the Fourier modes were averaged over 10,000 configurations). Clearly, the modes condense at the edges of the Brillouin zone and not (only) around the origin, cf. Fig. (20a). The contributions of such configurations come unwanted and spoil the numerical results. It is thus necessary to learn as much as possible about the actual size of the improvement term in order to assure that results from numerical simulations of the lattice theory are sensible. A convenient observable for this can be defined as

$$\Delta S_R = \frac{\Delta S}{N^2} \quad (4.6.7)$$

and will be called the reduced improvement term in the following. In terms of this, the broken phase is characterized by $|\Delta S_R| \gg 1$, cf. Eq. (4.6.6). That the phenomenon can be described sufficiently with m_L and λ , i.e. irrespective of the lattice size can be deduced from Figs. 21 and 22. Both the (properly normalized) unimproved bosonic action as well as the reduced improvement term scale appropriately with the lattice size. In this sense it is safe to base the further analysis on a single lattice size considering solely the dependence on m_L and λ . Fig. 22 also shows, that $\Delta S_R \rightarrow 0$ when m_L is taken to zero in accordance with the expected behavior. For finite m_L it grows the faster the larger λ is taken. It is interesting to note that ΔS_R can become as large as 13% of the measured improved action. This difference between the improved and unimproved action

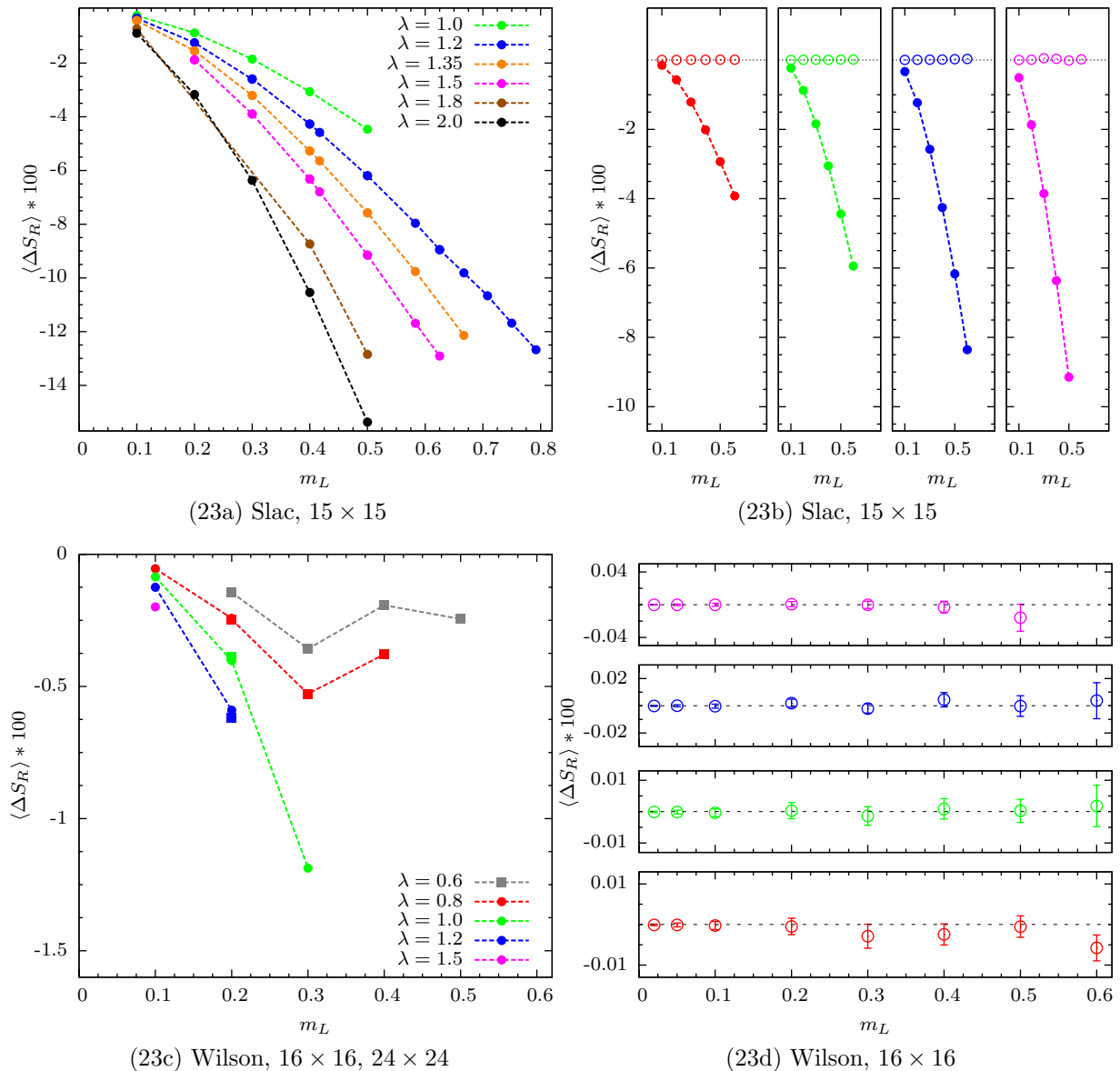


Figure 23: Analysis of the reduced improvement term for Slac and Wilson fermions. The last point in Figs. (23a) and (23b) refers to the last sensible simulation as explained in the text. Note that for Slac fermions improvement works with larger λ and m_L . The improvement term measured from the unimproved ensemble is found to vanish for Slac (empty circles in Fig. (23b)) and Wilson (Fig. (23d)) fermions. The graphs in Fig. (23c) are composed from 16×16 (circles) and a 24×24 (squares) lattices respectively.

should be compared to the deviation of the unimproved action within the unimproved simulation which is less than 3%, cf. Fig. 21.¹²² This confirms the fact that improved and unimproved models sample configuration space in distinct manner.

If ΔS_R is measured on an ensemble generated with the unimproved action the claim made at the end of Sec. 4.3 can now be confirmed numerically. As anticipated there, the improvement term vanishes because of the broken discrete symmetries induced by the improvement term. A direct comparison of the reduced improvement term from both models can be found in Fig. (23b). The outcome of the analysis with Wilson fermions is qualitatively the same and presented in Figs. (23c) and (23d). Yet quantitatively there

¹²²As for Fig. 22 the data for Fig. 21 was collected from different lattice sizes and no significant dependence on the lattice size was found.

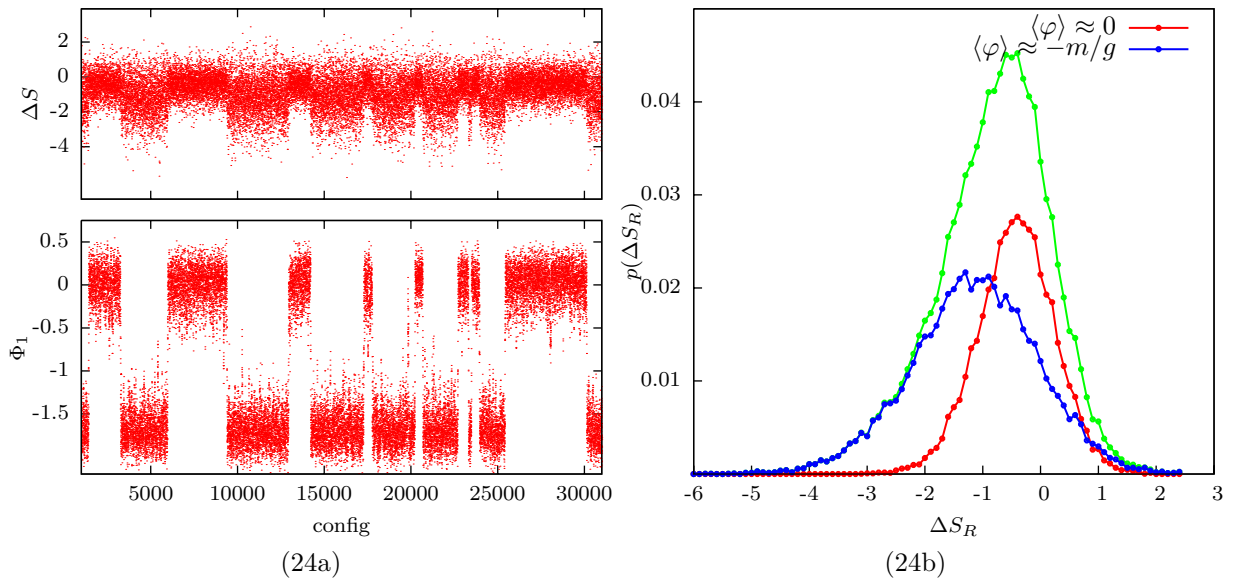
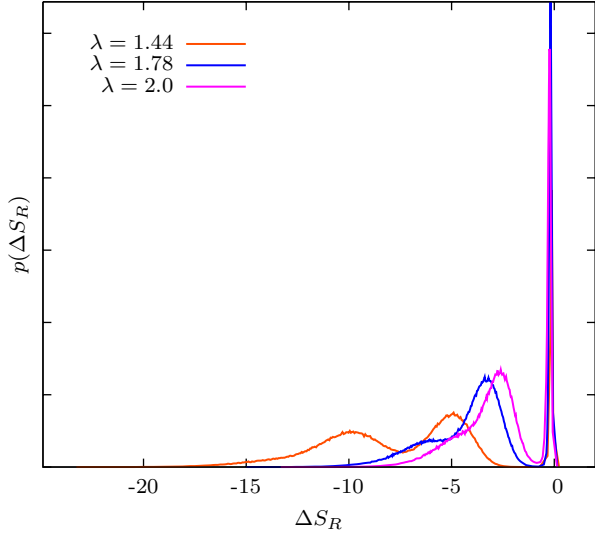


Figure 24: Coupling between Wilson and improvement term ($L = 24 \times 24$, $\lambda = 0.6$, $m_L = 0.3$)

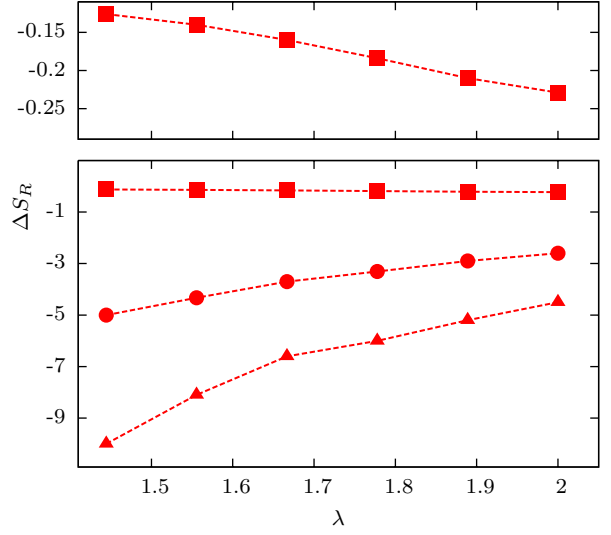
are large discrepancies between the two fermion prescriptions. The overall size of the improvement term is smaller for Wilson fermions as long as the simulation is not driven into the broken phase. Conversely, the simulations with Wilson fermions break down at much smaller values of either λ or m_L . While with Slac fermions even at $\lambda = 2.0$ and $m_L = 0.5$ the simulation remains located around the physical ground states, the system with Wilson fermions gets already broken at $\lambda = 1.2$ and $m_L = 0.2$. From this follows, that to simulate the theory at the same physical parameters m and g with Wilson fermions lattices have to be much larger in size than what were required for Slac fermions. Hence w.r.t. to compatibility with improved lattice actions Slac fermion are more resilient.

A second difference already apparent in Figure (23c) is the fact that the (reduced) improvement term does not decrease monotonously as a function of m_L . This phenomenon can be traced back to the fact that due to the Wilson term the vacuum expectation value of ΔS_R cannot be uniquely defined. In Fig. 24 the improvement term is shown for Wilson fermions at $\lambda = 0.6$ and $m_L = 0.3$. From the MC history on the left a clear correlation between the lattice mean φ_1 and ΔS can be observed. Since the minima are separated clearly, the histogram of ΔS can be evaluated under the constraint that only fluctuations around a distinct minima are included. This analysis is shown in the right and makes clear that depending on the ground state the distribution of the improvement term differs from one another in terms of both its mean and width. This can be explained with the discrete symmetry that is broken due to the Wilson term as mentioned in Sec. 4.3. Logically this has not been observed for Slac fermions.

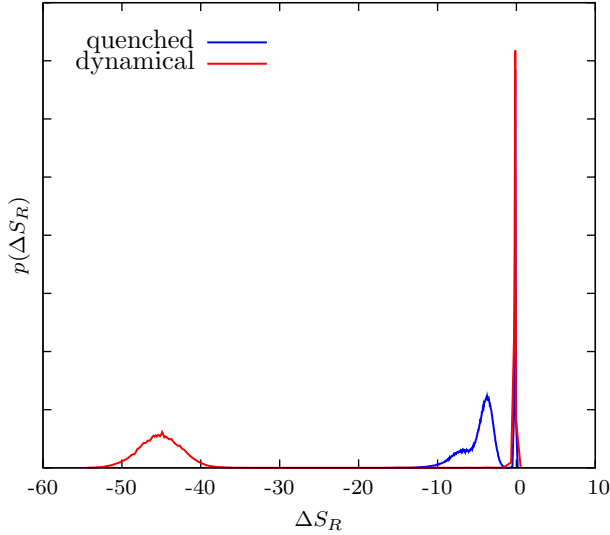
The discussion of the following deals in detail with the previously mentioned broken phase. Here only the results for Slac fermions are given. Nonetheless qualitatively quite similar results were also found for Wilson and twisted Wilson fermions the main difference being the even larger instability. All data was obtained from a 15×15 lattice



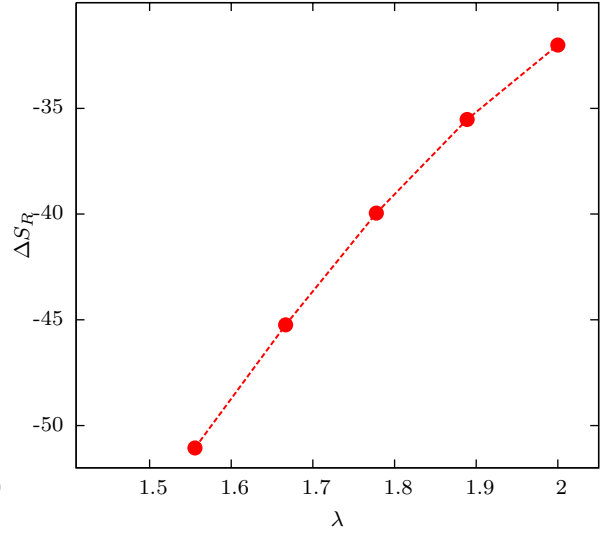
(25a) quenched at three different values of λ



(25b) 1st, 2nd and 3rd peak (quenched)



(25c) quenched vs. dynamical at $\lambda = 4/3$



(25d) 2nd peak from dynamical fermions

Figure 25: Probability distribution of ΔS_R (Slac 15×15 , $m_L = 0.7$). Fig. (25b) shows the positions of the 1st, 2nd and 3rd peak of the distribution from quenched simulations as a function of λ , Fig. (25c) shows the position of the 2nd (unwanted) peak using dynamical fermions.

and about 500,000 quenched and 30,000 configurations with dynamical fermions were evaluated for each distinct value of λ . The bare mass parameter was conveniently set to $m_L = 0.7$. The large statistics were needed to appropriately sample the histograms shown below. In order to understand what happens when the system is driven away from the physical region in configuration space it is useful to consider both quenched and dynamical simulations. This is done in Fig. 25. In the distribution functions of ΔS_R computed from the quenched ensembles and depicted in the upper row two new much broader peaks can be found. The sharpest peak to the very right of Fig. (25a) corresponds to the physical configurations. While the interaction strength is increased the second and third peak draw nearer indicating this problem being more and more important for larger coupling constants, cf. Fig. (25b). Looking at the positions of these peaks one realizes that the improvement term is about five respectively ten times larger than the predicted value of N^2 . In no regard it might then be called a correction to the

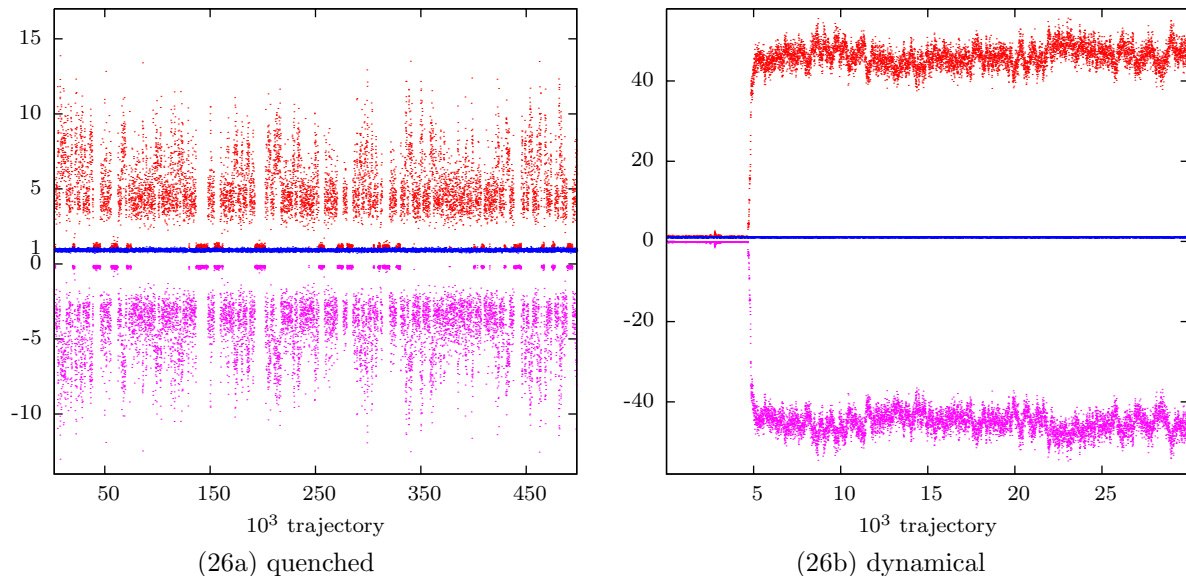


Figure 26: Unimproved bosonic action normalized to N^2 (red) and ΔS_R (magenta) from improved ensemble. The normalized improved bosonic action (blue) is shown for reference. (Slac $L=15 \times 15$, $\lambda = 5/3$, $m_L = 0.6$)

unimproved action.

When dynamical fermions are switched on, the situation changes. The second peak is located much farther to the left, i.e. the improvement term is now found to be 40 to 50 times the size of the improved action. If λ is turned on it draws nearer again easing tunneling events to happen. Hence for larger values of λ improvement becomes more and more unstable. Furthermore, dynamical fermions also influence the way the simulation samples the configuration space. In Fig. 26 the MC history of the improvement term is shown in magenta together with the unimproved (red) and improved (blue) action. The latter serves merely the purpose to provide a scale of reference while as expected the unimproved action is found to be strictly positive and the improvement term hence negative. Comparing the quenched with the dynamical simulation it becomes apparent at once that only in the first tunneling occurs from the physical into the unphysical and from the unphysical into the physical region. With dynamical fermions the system remains for a certain amount of iterations around the physical ground state and jumps on a sudden and only once.¹²³ For practical simulations this poses a real nuisance since it cannot be predicted when this will happen. In particular a very large run with Wilson fermions, that was carried out for the determination of masses, a single ensemble using the improved action broke down after 300,000 iterations. At the same values of m_L and λ fifteen other replicas¹²⁴ did not sample the unphysical region in one out of 10^6 configurations.¹²⁵

Surely then, it should be possible to explain the observed differences from the dynamical

¹²³Note however, that the MC time scales in Fig. 25 do not match. The quenched history comprises more than ten times as many configurations.

¹²⁴Simulations that only differed with the seed of their (pseudo) random number generator from one another

¹²⁵This happened for a 32×32 lattice at $m_L = 0.4$ and $\lambda = 0.4$

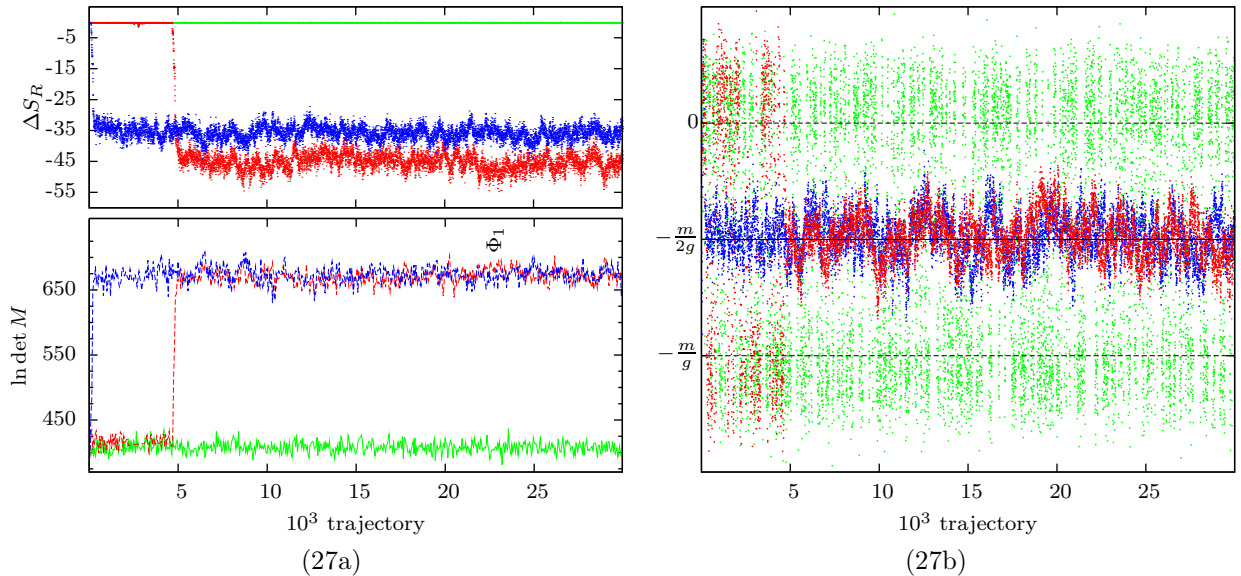


Figure 27: Relation between ΔS_R , the fermion determinant (Fig. (27a)) and the lattice mean of φ_1 (Fig. (27b)). (Slac, 15×15 , $m_L = 0.6$, $\lambda = 1.4$ (green), 1.7 (red), 1.9 (blue))

ical properties of the fermion determinant, which constitutes the only difference between the quenched and dynamical ensemble. Such an analysis is shown in Fig. (27a), which may be interpreted as follows. When the first tunneling event¹²⁶ due to the improvement term in the bosonic action¹²⁷ occurs the fermion determinant accelerates this dynamics further and the system is ever more pushed away, cf. Fig. 26 until the fermion determinant settles around a new equilibrium which is independent of λ . The latter is contrast to what was found earlier for the improvement term, and can also be seen easily from Fig. (27a). Since the logarithm of the determinant enters the action with a relative minus sign the system is now no longer capable to overcome this barrier once more and thus remains in the broken phase.

To shed some light on the mechanism by which the determinant acquires such a large value it is useful to consider the spatial average of φ_1 once more. As with the improvement term and the fermion determinant its behavior undergoes a dramatic change once the system has tunneled into the broken phase. Numerical evidence for this claim may be inferred from Fig. (27b). While in the physical phase the red curve fluctuates around on of the two minima and tunnels inbetween them frequently. It ceases to do so at once when the jump in either the improvement term or the fermion determinant is observed. Afterwards it is drawn near the local maximum of the superpotential, which was given in (4.3.1).¹²⁸ To make the contributions from the large momentum modes visible the

¹²⁶For the blue graph this happens right at the beginning of the MC history and is thus not resolved on the time scale of Fig. 27

¹²⁷This is justified by the fact, the such tunneling events were observed to occur frequently in the quenched simulations.

¹²⁸It is worth to note that the fluctuations are now much more correlated. This can be partly explained with a worsening of the acceptance rate in the broken phase.

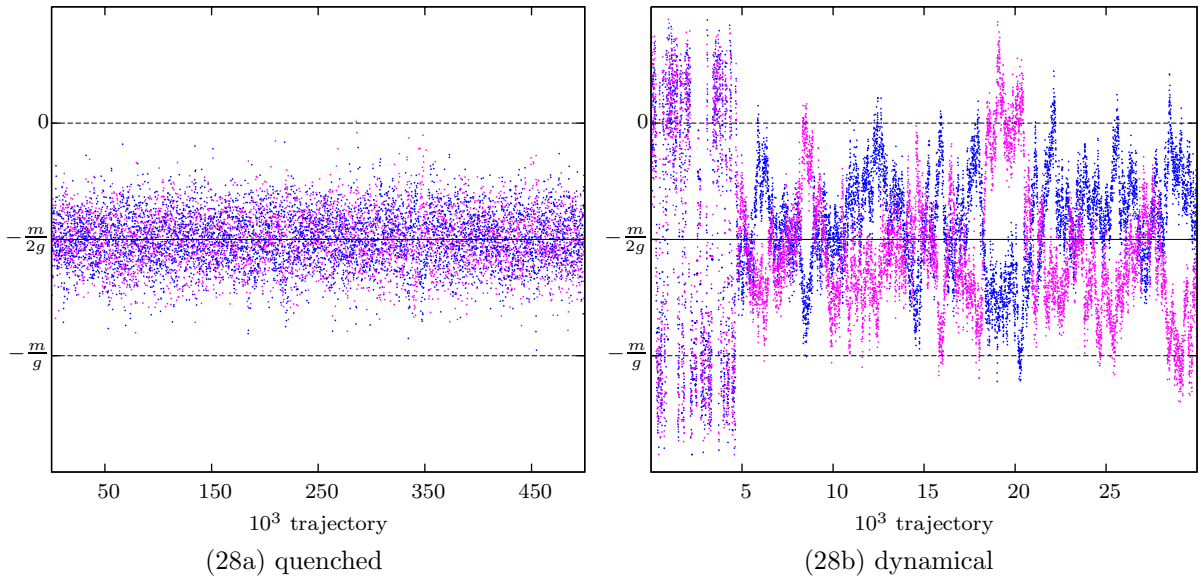


Figure 28: Lattice mean of φ_1 from odd (blue) and even (magenta) sub-lattices obtained from quenched and dynamical simulations (Slac $L=15 \times 15, \lambda = 1.7, m_L = 0.6$).

lattice mean may be decomposed into its odd and even part, i.e.

$$\Phi_{1,o} = \sum_{x \in \Lambda_o} \varphi_{1,x} \quad \text{and} \quad \Phi_{1,e} = \sum_{x \in \Lambda_e} \varphi_{1,x}, \quad (4.6.8)$$

where Λ_o refers in obvious manner to the odd and Λ_e to the even sub-lattice. This analysis is shown in Fig. 28 for both quenched and dynamical fermions at the same set of parameters that were used for the red graphs of Fig. 27. In the quenched ensemble both $\Phi_{1,o}$ and $\Phi_{1,e}$ fluctuate all the time around the locus of local maximum of the classical potential but apart from this show no further correlation or anti-correlation. However, the picture with dynamical fermions is different. Within the physical phase they are again no visible signs of strong correlations but once in the broken phase they are clearly anti-correlated indicating large contributions from UV modes. Coming back to the fermion determinant it seems likely that this reordering into a sort-of anti-ferromagnetic phase is self-enhancing, i.e. the stronger the anti-correlation becomes the larger become the kinetic term and the determinant.

In summary, it was revealed that the proposed improved actions are w.r.t to MC simulations limited. Since other construction schemes arrive at the same improved lattice action this is no particular property of the construction utilizing the Nicolai map as outlined earlier. Whether supersymmetrically improved lattice actions of other models suffer from the same drawbacks is a very interesting question. For the time being it may be stressed that if the models are studied at ever finer lattice spacings the raised problems will eventually loose relevance. But so does also the improvement here since at least for the two-dimensional WZ-model it has been also argued that improved and unimproved actions lead to the same continuum limit. Another question that remains is whether there exists a certain window in parameter space where it is possible to gain practical advantages from improved lattice actions without being trapped in the broken

phase.

4.7 Mass spectrum

In this section the discussion has eventually reached the stage to determine physical observables from the lattice models. Earlier simulations were either confined by small lattice sizes or very small coupling constants λ . Having been able to overcome both these constraints the determination of particle masses in this theory may be readdressed. The observables suggested for the analysis of the previous section can now be employed to judge on the physical plausibility of the MC simulations, and doubtful data can be safely identified and be discarded.

The computation of the bosonic twopoint functions proceeds in straightforward manner. To improve the overlap with the first excited state the correlators are projected onto zero spatial momentum, i.e. the correlators¹²⁹

$$C_{ij}(t) = \sum_{t'} \langle \Phi_i(t+t') \Phi_j(t') \rangle, \quad \Phi_i(t) = \sum_x \varphi_i(t, x) \quad (4.7.1)$$

were analyzed. Since the bosonic kinetic term is diagonal in φ_1 and φ_2 the off-diagonal correlators $C_{12}(t)$ and $C_{21}(t)$ are expected to vanish for all values of their argument. This was checked explicitly and found to be fulfilled to large precision. The masses extracted from the remaining correlators $C_1(t) \equiv C_{11}(t)$ and $C_2(t) \equiv C_{22}(t)$ will be identified by $m_{1,b}$ and $m_{2,b}$ respectively.

Since the correlation functions of the fermion field itself (instead of composites thereof) is needed the spinor degrees of freedom have to be projected out. Starting from the free fermion propagator

$$G_F(p) = \frac{\gamma^\mu p_\mu + m}{p^2 + m^2} \quad (4.7.2)$$

one may infer that for zero spatial momentum ($p_1 = 0$) the propagator can be expanded in γ_0 and the identity matrix. Taking the trace projects out the scalar part which is just the bosonic propagator times the mass m . The fermionic correlator that was studied is hence given by

$$C_F(t) = \sum_\alpha \sum_{t'} \langle \Psi_\alpha(t+t') \bar{\Psi}_\alpha(t') \rangle, \quad \Psi_\alpha(t) = \sum_x \psi_\alpha(t, x). \quad (4.7.3)$$

Masses were extracted from fitting all three correlators to (3.4.10) and for the extrapolation into the continuum (3.4.11) and (3.4.12) were reused.

The precision up to which (fermion) masses can be extracted calls for a careful treatment of systematic errors. These include contributions from higher excited states as well as finite-size effects. Both issues have been assessed as to guarantee that the

¹²⁹The summation over t' is once more employed as to increase the signal to noise ratio. Still, this is allowed due to translational invariance.

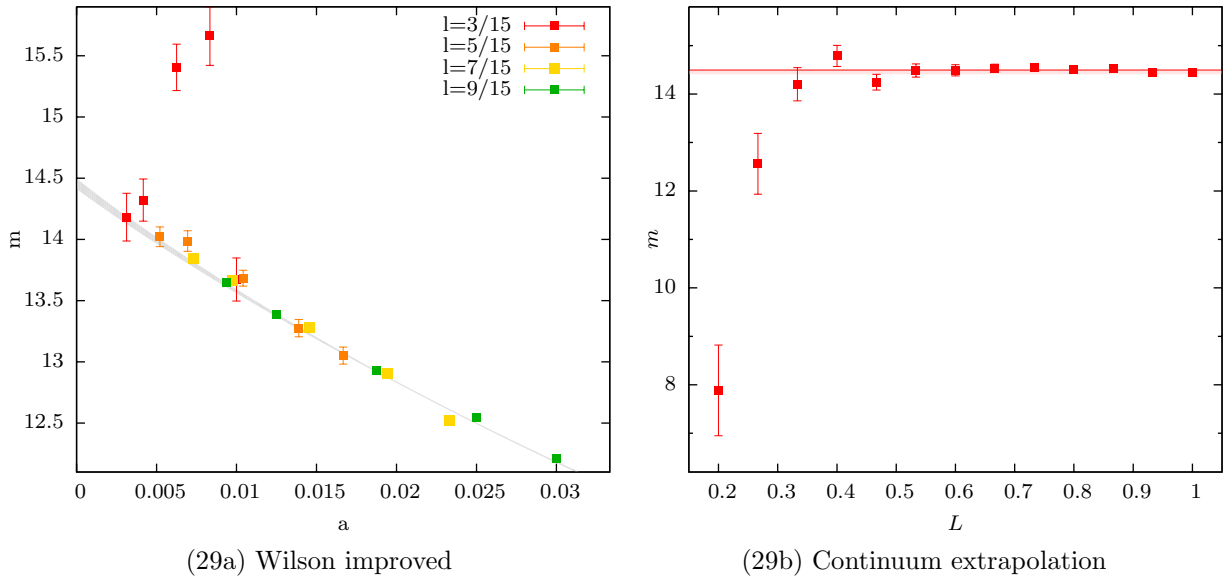


Figure 29: Impact of finite size on the extraction of fermion masses. Shaded areas refer to the extrapolation at $l = 1.0$ (Wilson fermions w. impr. action, $m = 15, \lambda = 0.3$)

data analysis is not influenced by them. Since perturbation theory predicts a decline of the physical mass for ever stronger couplings λ a rather large initial value of $m = 15$ (in physical units) was chosen as to be able to compensate for this. Fig. (29a) shows that scaling violations for this specific choice and $\lambda = 0.3$ are not detectable before the physical volume shrinks to one-half the size that is actually used (gray shaded graph in Fig. (29a)). For all volumes larger than this the continuum extrapolations yield the same result which is shown in Fig. (29b). Higher excitations were seen to be of interest only on the largest lattices, i.e. smallest lattice spacings. Fig. 30 depicts for Wilson (bottom) and twisted Wilson (top) the extracted fermion mass m_f as a function of $t_{\text{skip}} \equiv t_A$, cf. Sec. 3.4.8 and

$$m_{\text{eff}}(t) = \ln \frac{C(t)}{C(t+1)} \quad (4.7.4)$$

which for a purely exponential decay exhibits a plateau its value given by $m_{\text{eff}} \approx m_f$. Clearly from both graphs and for both quantities an insensitivity on t_{skip} (or a plateau) is only reached at later times. All masses quoted in Tab. 11 were determined from the global fitting procedure as described above corresponding to the blue graphs in Fig. 30.

Three different physical questions were investigated. At first it is interesting to see whether the three distinct lattice fermions that were suggested for the simulation yield still the same continuum results once interactions are turned on.¹³⁰ Indeed, this could be confirmed numerically for all values of λ and all (improved and unimproved) models. The presence of lattice artifacts on the other hand turns out to depend very much on the concrete lattice fermion prescription. Fig. 31 compares the extracted fermion masses as a function of the lattice spacing for Wilson, twisted Wilson and Slac fermions to one another. For the value determined with Slac fermions a single lattice of size 45×45 was

¹³⁰Recall, that for the free theory this was seen already in Sec. 4.3

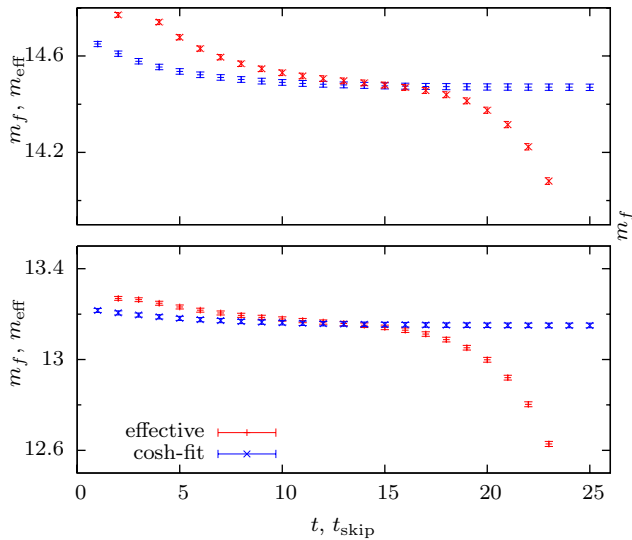


Figure 30: Extracted mass for twisted Wilson (top) and Wilson (bottom) fermions. ($N = 64 \times 64$, $m = 15$, $\lambda = 0.3$)

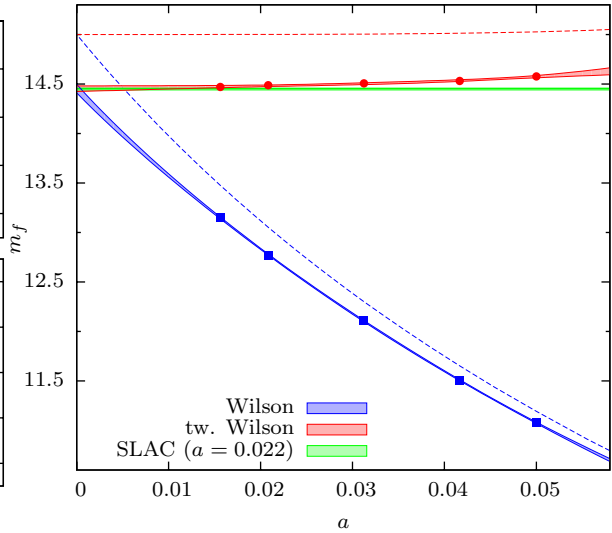


Figure 31: Continuum extrapolation from different lattice fermions ($m = 15$, $\lambda = 0.3$). The shaded areas depict the error of the fit parameters, dashed lines correspond to the resp. free theory.

analyzed. For Wilson and twisted Wilson fermions five different lattices (20×20 , 24×24 , 32×32 and 64×64) were studied. Several things are worth to be mentioned. All three fermions extrapolate to the same continuum value and the data from Wilson fermions are again found being subject to NLO corrections. For twisted Wilson and Slac fermions the continuum value is already reached within an accuracy of 0.5% for a lattice-spacing of about $a = 0.02$. Twisted Wilson fermions have thus been confirmed to yield superior results to standard Wilson fermions and are strongly suggested to substitute the latter in further MC simulations.

Having argued that the correct continuum limit can be obtained from both improved and unimproved lattice models an interesting question that remains is whether they can be discriminated by means of their spectra at finite lattice spacing. At least for the bosonic action it was already argued that this indeed makes a detectable difference. This time however, the analysis is considerably more involved. The reason for this may be traced back to a very problematic signal-to-noise ratio of the bosonic correlators. Comparing the achievable precisions it was found that fermions come out sharper by at least a factor of ten. Furthermore, it has to be added, that for the fermionic correlators about 10,000 (independent) configurations suffice to determine the masses with an remaining uncertainty of about or less than 0.1%. For the computation of the bosonic correlators as many as 1.6×10^7 configurations¹³¹ were needed. As to such large statistics only two distinct values of the coupling strength have been hitherto analyzed. The results are summarized in Tab. 11 and for Wilson fermions also given graphically in Fig. 32. Note that the errors on the fermion masses are much smaller than the symbol sizes. However, a clear distinction of the models cannot be observed. The degeneracy of the mass spectrum is fulfilled for both of them and thus does not serve the purpose of discriminating supersymmetry or its absence on the lattice. More precisely, it has

¹³¹This number comprises 16 independent replicas each containing 1×10^6 independent configurations.

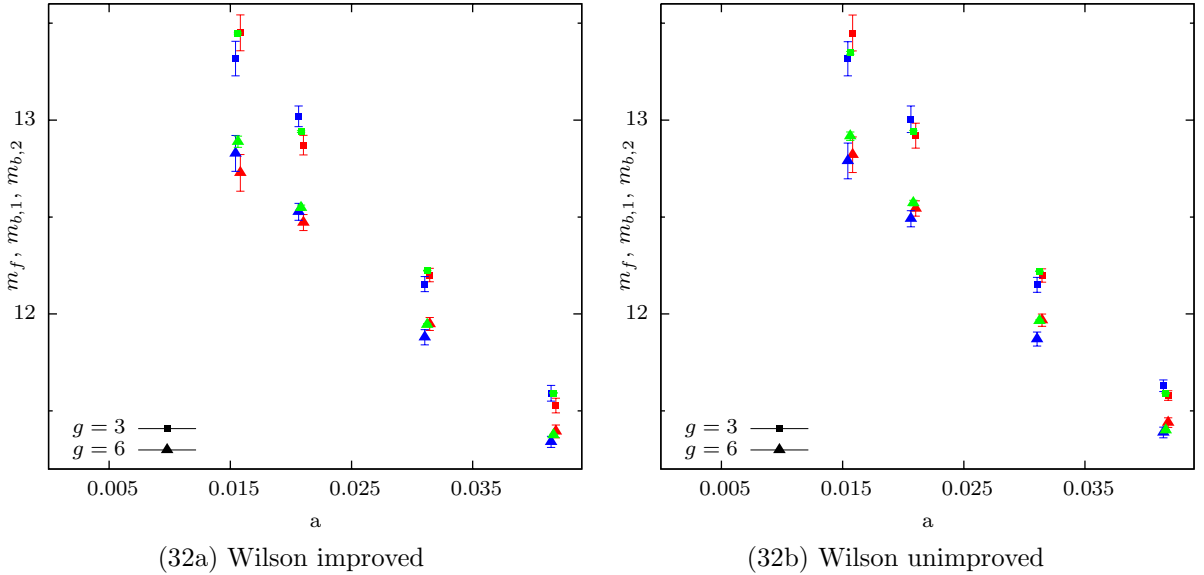


Figure 32: Comparison of mass degeneracy between improved and unimproved model as a function of the lattice spacing. Fermions are plotted in green, boson masses in red (φ_1) and blue (φ_2).

been confirmed that deviations in the mass spectrum due to broken supersymmetry are smaller than 0.1%. The question may be readdressed as soon as results at larger coupling constants are available.

Using the clean signal of the fermionic correlators the continuum extrapolations can be directly compared to perturbative results. The one-loop result for the mass gap is [25, 48]

$$m_{1\text{-loop}}(\lambda) = \sqrt{m \left(1 - \frac{4}{3\sqrt{3}}\lambda^2 \right)} = m \left(1 - \frac{2}{3\sqrt{3}}\lambda^2 \right) + \mathcal{O}(\lambda^2) \quad (4.7.5)$$

and compared to the numerical data in Fig. 33. In the range $\lambda \in [0, 0.3]$ this function was resolved with 15 distinct (subsequent simulations $\delta\lambda = 0.02$ apart) measurements for twisted Wilson and Wilson (both with the improved and unimproved action) fermions. The leading coefficient in perturbation theory was then determined by fitting the numerical data to $m(\lambda) = m_0\sqrt{1 - \lambda^2/\alpha}$, and it was found to be in very good agreement with the analytical prediction, cf. Tab. 10. Going beyond perturbation theory Slac fermions are very convenient choice since they allow for a direct comparison with continuum results. For instance, the numerical data in Fig. (33b) depicting the Slac fermions (red and blue trian-

Model	α	m_0
Wilson improved	1.34(6)	15.007(6)
Wilson unimproved	1.39(7)	15.008(6)
twisted Wilson improved	1.26(4)	14.996(4)
Wilson improved	1.37(5)	fixed to 15
Wilson unimproved	1.42(6)	fixed to 15
twisted Wilson improved	1.25(3)	fixed to 15

Table 10: Fit for the perturbative mass formula with $\mathcal{O}(\lambda^2)$ corrections to be compared with the one-loop results. The analytical calculation yields $\alpha = 3\sqrt{3}/4 \approx 1.299$

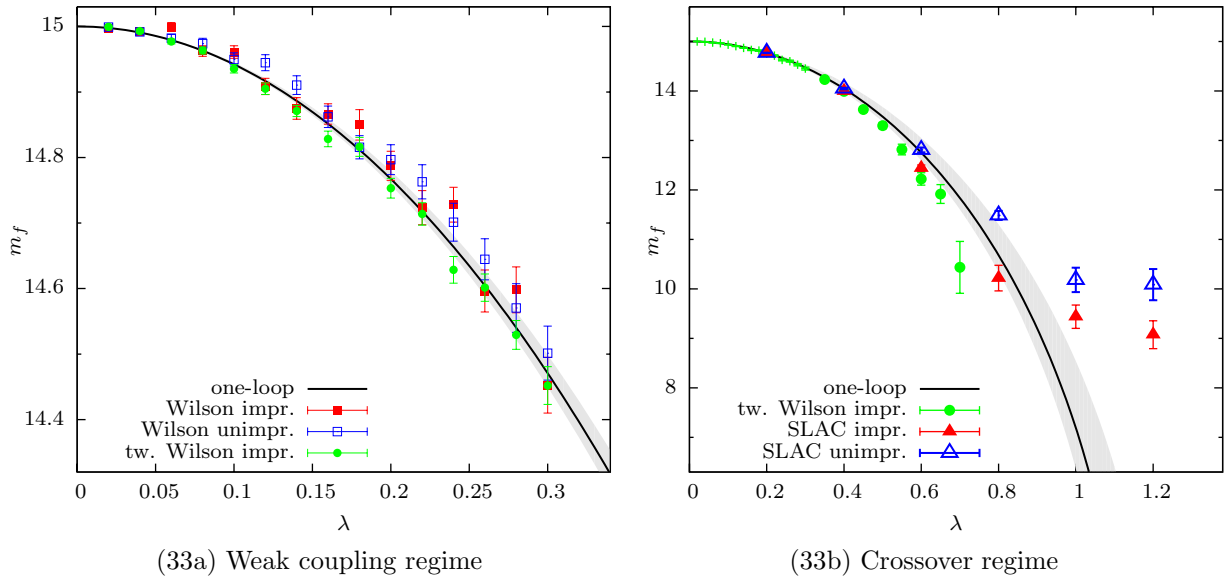


Figure 33: Comparison of lattice results with (continuum) perturbation theory. The black line is the perturbative result, the shaded area corresponds to error bounds from a fit of the numerical data to the one-loop formula for $\lambda \leq 0.3$. The data for Slac fermions is from a single lattice of size 45×45 .

gles) were obtained from a single lattice size and found to lie on top of the continuum extrapolations of the other two lattice fermions as well as the analytical result. Differences between the improved and unimproved model show up from $\lambda = 0.8$. To test lattice artifacts that may become important for Slac fermions only for large couplings the simulation for $\lambda = 1.0$ was repeated on a 63×63 lattice. While the difference amounts to $\delta m = 1.28(35)$ on a 45×45 lattice it reduces to $\delta m = 0.16(34)$ on the 63×63 lattice being mainly due to a significant drop of the unimproved value. One may hence infer that the improved model is (by supersymmetry) much less influenced by lattice artifacts.

For simulations at even larger couplings several issues have to be addressed first. While the number of configurations with a negative determinant can be safely neglected up to $\lambda = 1.0$ and a bare lattice mass parameter of $m_L \leq 0.3$ this issue becomes important for coupling constants larger than that. The more frequent changes of the sign are furthermore accompanied by numerical instabilities due to near-zero eigenmodes of the fermion matrix. The straight-forward employment of the pseudofermion algorithm used so far becomes hence questionable and needs further improvements. Also tunneling between the two vacua at $\varphi_1 = -m/g$ and $\varphi_1 = 0$ become more frequent and lead for the bosonic correlators to connected parts that have to be subtracted off and will lead to additional noise. The proposed projection for the fermionic correlator will eventually also cease to work.

Nonetheless this questions are already under investigation, and it is likely that they will have been solved in the near future. Besides the particle's masses other observables are by now also within reach. Perhaps most interestingly is the study of the constraint effective potential from MC simulations. The large statistics required can be easily provided and due to the large attainable lattice sizes both the thermodynamic and the

continuum limit can be studied. Stimulated by analytical calculations to be published soon the role instantons play for the decay of perturbative ground-states may be numerically confirmed. Also WIs may be reanalyzed if larger coupling constants become feasible and clear signals may be expected. Finally, it is of great interest whether the improved actions can be stabilized as to prohibit (at least practically) the broken phase either by slight modifications to the action itself or algorithmic improvements.

Model	N_s	g	m_f	$m_{b,1}$	$m_{b,2}$
Wilson improved	24	3	11.592(2)	11.53(4)	11.59(4)
	24	6	11.375(4)	11.39(3)	11.34(3)
	32	3	12.224(2)	12.20(3)	12.15(4)
	32	6	11.945(5)	11.95(3)	11.88(4)
	48	3	12.941(5)	12.87(5)	13.02(5)
	48	6	12.548(13)	12.47(4)	12.53(4)
	64	3	13.349(10)	13.45(9)	13.32(9)
	64	6	12.89(3)	12.73(9)	12.83(9)
Wilson unimpr.	24	3	11.591(2)	11.58(2)	11.63(3)
	24	6	11.400(4)	11.44(2)	11.39(3)
	32	3	12.221(2)	12.20(3)	12.15(4)
	32	6	11.965(5)	11.97(3)	11.87(4)
	48	3	12.942(5)	12.92(6)	13.00(7)
	48	6	12.572(14)	12.54(4)	12.49(4)
	64	3	13.347(7)	13.45(9)	13.32(9)
	64	6	12.91(2)	12.82(9)	12.79(9)
twisted Wilson (impr.)	24	3	14.811(7)	14.94(11)	14.91(12)
	24	6	14.13(1)	14.21(9)	14.06(8)
	32	3	14.788(6)	14.61(14)	14.94(12)
	32	6	14.08(1)	14.39(14)	13.68(13)
	48	3	14.789(6)	14.74(11)	14.61(11)
	48	6	14.04(1)	14.16(16)	13.98(15)
Slac improved	45	3	14.768(4)	14.87(10)	14.83(9)
	45	6	13.997(13)	14.08(11)	13.92(10)
Slac unimproved	45	3	14.769(4)	14.75(6)	14.57(6)
	45	6	14.047(16)	13.74(8)	13.75(7)

Table 11: Fermion and bosonic masses at $\lambda = 0.2$ ($g = 3$) and $\lambda = 0.4$, ($g = 6$). The bare lattice mass was computed from $m = 15$, i.e. $m_L = m/N_s$.

5 Summary & Outlook

In this thesis the WZ model in one and two dimensions has been thoroughly investigated. With the help of the Nicolai map it was possible to construct supersymmetrically improved lattice actions that preserve one of several supersymmetries. For the WZ model in one dimension SLAC fermions were utilized for the first time leading to a near-perfect elimination of lattice artifacts. In addition the lattice superpotential does not get modified which in two dimensions becomes important when further (discrete) symmetries of the continuum action are considered. For Wilson fermions two new improvements have been suggested and were shown to yield far better results than standard Wilson fermions concerning lattice artifacts.

In the one-dimensional theory WIs were studied. However, supersymmetry violations due to broken supersymmetry could only be detected at coarse lattices and very strong couplings. For the two-dimensional models a detailed analysis of supersymmetric improvement terms was given, both for Wilson and SLAC fermions. It was found that improvement may lead to a broken phase, where simulations become meaningless. By comparing with quenched results it was shown that this unwanted phase structure is entirely due to the improvement terms albeit dynamical fermions make the situation even worse. By contrast, simulations with either improved or unimproved actions of the WZ model the differences yield only marginal differences in the observed energy spectrum. Even for the immense statistics of 1.6×10^7 independent configurations particle masses remained insensitive and cannot be used as a signal for supersymmetry or its breaking due to lattice artifacts. In the weak coupling regime for instance an upper bound for the violations due to broken supersymmetries was found to be less than 0.2% for the coarsest lattice spacings investigated. If extrapolated to the continuum the numerical data was found to be in very good agreement with the one-loop result of (continuum) perturbation theory, irrespective of the concrete lattice fermions that were used. For SLAC fermions, where the improved action remains stable for a larger range of couplings constants λ , first deviations from the perturbative results set in for $\lambda \geq 1$. In that case at least the fermion masses of the improved and unimproved model can be separated. However, whether the boson mass will now differ from the fermion mass in the unimproved model remains an open and interesting question.

By utilizing a closed form expression for the fermion determinant the simulations of the one-dimensional significantly increased in speed and precision. Substantial progress was also achieved in the two-dimensional theory. Combining Fourier acceleration with a higher order integration scheme the model could be simulated on lattices of up to 128×128 lattice points. Critical slowing down usually quite an issue so close to the critical point was seen to be avoided. Together with the help of higher order integrators the finite time-step size could be kept at a tolerable level.

Of course these results lead to a couple of new and interesting questions which will be briefly addressed below.

For the $\mathcal{N} = (2, 2)$ WZ model in two dimensions the simulations are quite well under

control for values of $\lambda \leq 1.5$. For even larger values simulations become more and more unstable. To some extent this can be traced back to the additional noise of the pseudo fermion fields. It is anticipated that more elaborate techniques such as the PHMC or RHMC algorithm may help in reducing these effects. Then the model could be studied at even larger values of λ , and it is safe to claim that for $\lambda \approx 2.0$ differences between the improved and unimproved models will be large enough to be clearly distinguishable. To accomplish this also the integrator must be studied further. The tuning that was found to work well at comparatively small couplings will not suffice for larger λ . Improving this is the subject of ongoing research.

In addition, the large statistics achieved with the new codes makes the computation of the (constrained) effective potential possible. Thus it seems feasible to confirm the non-renormalization of the superpotential or to investigate the role of instantons numerically.

On a related note the $\mathcal{N} = 1$ WZ model may also be reinvestigated by means of MC simulations. Using the methods developed here it is possible to improve on previously numerical data. From a physical point of view this model is also more interesting since supersymmetry can be broken spontaneously. The manifestation of this in a lattice theory is an interesting subject in its own right. However, additional technical problems have to be overcome as well. For instance, the model requires the inclusion of the Pfaffian (instead of the determinant) of the fermion operator.

It is certainly interesting to study the performance of the new integrator also for non-supersymmetric theories in two, three or four dimensions. Especially for theories without gauge couplings the integrator is believed to yield results as good as for the two-dimensional WZ-model. However it may be necessary to tune the integrator in a somewhat different fashion. Whether numerical integration schemes of even higher order still lead to significant improvements should be investigated as well.

The given code platform that was initially setup for the models of this thesis allows for a straightforward implementation of lattice models. This is due to the highly modularized design of the code, which has been one of the primary intents from the very beginning. Another advantage of the present code is the fact that it runs on both parallel platforms as well as standard office PCs and by now has become a universal tool for the non-perturbative analysis of field theories in Jena.

References

- [1] Sidney Coleman and Jeffrey Mandula. All possible symmetries of the s matrix. *Phys. Rev.*, 159(5):1251–1256, Jul 1967.
- [2] J. Wess and B. Zumino. A Lagrangian Model Invariant Under Supergauge Transformations. *Phys. Lett.*, B49:52, 1974.
- [3] N. Seiberg and Edward Witten. Monopoles, duality and chiral symmetry breaking in $N=2$ supersymmetric QCD. *Nucl. Phys.*, B431:484–550, 1994.
- [4] N. Seiberg and Edward Witten. Electric - magnetic duality, monopole condensation, and confinement in $N=2$ supersymmetric Yang-Mills theory. *Nucl. Phys.*, B426:19–52, 1994.
- [5] Edward Witten. Dynamical Breaking of Supersymmetry. *Nucl. Phys.*, B188:513, 1981.
- [6] Roland Peetz, Federico Farchioni, Claus Gebert, and Gernot Munster. Spectrum of $SU(2)$ SUSY Yang-Mills theory with a light gluino. *Nucl. Phys. Proc. Suppl.*, 119:912–914, 2003.
- [7] Federico Farchioni and Roland Peetz. The low-lying mass spectrum of the $N = 1$ $SU(2)$ SUSY Yang-Mills theory with Wilson fermions. *Eur. Phys. J.*, C39:87–94, 2005.
- [8] G. Veneziano and S. Yankielowicz. An Effective Lagrangian for the Pure $N=1$ Supersymmetric Yang-Mills Theory. *Phys. Lett.*, B113:231, 1982.
- [9] Georg Bergner, Tobias Kaestner, Sebastian Uhlmann, and Andreas Wipf. Low-dimensional supersymmetric lattice models. *Annals Phys.*, 323:946–988, 2008.
- [10] G. Münster I. Montvay. *Quantum Fields on a Lattice*. Cambridge University Press, 1994.
- [11] H.J. Rothe. *Lattice Gauge Theories An Introduction*. World Scientific Lecture Notes in Physics. World scientific, 3rd revised edition edition, 2005.
- [12] *Introduction to Quantum Fields on a Lattice*. Cambridge University Press, 2002.
- [13] T. DeGrand & C DeTar. *Lattice Methods for Quantum Chromodynamics*. World Scientific, 2006.
- [14] Jurgen Berges, Nikolaos Tetradis, and Christof Wetterich. Non-perturbative renormalization flow in quantum field theory and statistical physics. *Phys. Rept.*, 363:223–386, 2002.
- [15] F. J. Wegner. Duality in Generalized Ising Models and Phase Transitions Without Local Order Parameters. *J. Math. Phys.*, 12:2259–2272, 1971.
- [16] Kenneth G. Wilson. Confinement of Quarks. *Phys. Rev.*, D10:2445–2459, 1974.
- [17] Joshua W. Elliott, Joel Giedt, and Guy D. Moore. Lattice four-dimensional $N=4$ SYM is practical. 2008.
- [18] Joel Giedt. Deconstruction and other approaches to supersymmetric lattice field theories. *Int. J. Mod. Phys.*, A21:3039–3094, 2006.
- [19] P. H. Dondi and H. Nicolai. Lattice Supersymmetry. *Nuovo Cim.*, A41:1, 1977.
- [20] Simon Catterall. A geometrical approach to $N = 2$ super Yang-Mills theory on the two dimensional lattice. *JHEP*, 11:006, 2004.
- [21] Simon Catterall. Lattice formulation of $N = 4$ super Yang-Mills theory. *JHEP*, 06:027, 2005.
- [22] Simon Catterall. On the restoration of supersymmetry in twisted two- dimensional lattice Yang-Mills theory. *JHEP*, 04:015, 2007.
- [23] Simon Catterall. Simulations of $N = 2$ super Yang-Mills theory in two dimensions. *JHEP*, 03:032, 2006.
- [24] Simon Catterall and Eric Gregory. A lattice path integral for supersymmetric quantum mechanics. *Phys. Lett.*, B487:349–356, 2000.
- [25] Simon Catterall and Sergey Karamov. Exact lattice supersymmetry: the two-dimensional $N = 2$ Wess-Zumino model. *Phys. Rev.*, D65:094501, 2002.
- [26] Simon Catterall. Lattice supersymmetry and topological field theory. *JHEP*, 05:038, 2003.
- [27] Simon Catterall. Lattice supersymmetry and topological field theory. *Nucl. Phys. Proc. Suppl.*, 129:871–873, 2004.
- [28] Fumihiko Sugino. A lattice formulation of super Yang-Mills theories with exact supersymmetry. *JHEP*, 01:015, 2004.
- [29] Fumihiko Sugino. A lattice formulation of super Yang-Mills theories with exact supersymmetry. *Nucl. Phys. Proc. Suppl.*, 140:763–765, 2005.
- [30] Fumihiko Sugino. Super Yang-Mills theories on the two-dimensional lattice with exact supersymmetry. *JHEP*, 03:067, 2004.

- [31] Fumihiko Sugino. Various super Yang-Mills theories with exact supersymmetry on the lattice. *JHEP*, 01:016, 2005.
- [32] Fumihiko Sugino. Two-dimensional compact $N = (2,2)$ lattice super Yang-Mills theory with exact supersymmetry. *Phys. Lett.*, B635:218–224, 2006.
- [33] Hermann Nicolai. On a New Characterization of Scalar Supersymmetric Theories. *Phys. Lett.*, B89:341, 1980.
- [34] K. G. Wilson and John B. Kogut. The Renormalization group and the epsilon expansion. *Phys. Rept.*, 12:75–200, 1974.
- [35] F.A. Berezin. *The Method of Second Quantization*. Academic Press, 1966.
- [36] M.E.J. Newman & G.T. Barkema. *Monte Carlo Methods in Statistical Physics*. Oxford University Press, 1999.
- [37] S. Duane, A. D. Kennedy, B. J. Pendleton, and D. Roweth. Hybrid Monte Carlo. *Phys. Lett.*, B195:216–222, 1987.
- [38] Philip Argyres. Introduction to supersymmetry. Online available from <http://www.physics.uc.edu/~argyres/661/susy1996.pdf>.
- [39] Andreas Wipf. Non-perturbative methods in supersymmetric theories. 2005.
- [40] Maarten F. L. Golterman and Donald N. Petcher. A Local Interactive Lattice Model With Supersymmetry. *Nucl. Phys.*, B319:307–341, 1989.
- [41] Alessandro D’Adda, Issaku Kanamori, Noboru Kawamoto, and Kazuhiro Nagata. Twisted superspace on a lattice. *Nucl. Phys.*, B707:100–144, 2005.
- [42] Alessandro D’Adda, Issaku Kanamori, Noboru Kawamoto, and Kazuhiro Nagata. Exact extended supersymmetry on a lattice: Twisted $N = 2$ super Yang-Mills in two dimensions. *Phys. Lett.*, B633:645–652, 2006.
- [43] Falk Bruckmann, Simon Catterall, and Mark de Kok. A critique of the link approach to exact lattice supersymmetry. *Phys. Rev.*, D75:045016, 2007.
- [44] Falk Bruckmann and Mark de Kok. Noncommutativity approach to supersymmetry on the lattice: SUSY quantum mechanics and an inconsistency. *Phys. Rev.*, D73:074511, 2006.
- [45] Wolfgang Bietenholz. Exact supersymmetry on the lattice. *Mod. Phys. Lett.*, A14:51–62, 1999.
- [46] S. Catterall and S. Karamov. A two-dimensional lattice model with exact supersymmetry. *Nucl. Phys. Proc. Suppl.*, 106:935–937, 2002.
- [47] S. Cecotti and L. Girardello. Local Nicolai Mappings in Extended Supersymmetry. 1982. IC/82/105.
- [48] Matteo Beccaria, Giuseppe Curci, and Erika D’Ambrosio. Simulation of supersymmetric models with a local Nicolai map. *Phys. Rev.*, D58:065009, 1998.
- [49] Simon Catterall and Sergey Karamov. A lattice study of the two-dimensional Wess Zumino model. *Phys. Rev.*, D68:014503, 2003.
- [50] Holger Bech Nielsen and M. Ninomiya. No Go Theorem for Regularizing Chiral Fermions. *Phys. Lett.*, B105:219, 1981.
- [51] A. Kirchberg, J. D. Lange, and A. Wipf. From the Dirac operator to Wess-Zumino models on spatial lattices. *Ann. Phys.*, 316:357–392, 2005.
- [52] S. D. Drell, Marvin Weinstein, and S. Yankielowicz. Variational Approach to Strong Coupling Field Theory. 1. Φ^4 Theory. *Phys. Rev.*, D14:487, 1976.
- [53] S. D. Drell, Marvin Weinstein, and S. Yankielowicz. Strong Coupling Field Theories. 2. Fermions and Gauge Fields on a Lattice. *Phys. Rev.*, D14:1627, 1976.
- [54] Luuk H. Karsten and Jan Smit. The Vacuum Polarization with SLAC Lattice Fermions. *Phys. Lett.*, B85:100, 1979.
- [55] Joel Giedt, Roman Koniuk, Erich Poppitz, and Tzahi Yavin. Less naive about supersymmetric lattice quantum mechanics. *JHEP*, 12:033, 2004.
- [56] P. West. *Introduction to Supersymmetry and Supergravity*. World Scientific, 1990.
- [57] Joel Giedt. R-symmetry in the Q-exact $(2,2)$ 2d lattice Wess-Zumino model. *Nucl. Phys.*, B726:210–232, 2005.
- [58] Roberto Frezzotti, Pietro Antonio Grassi, Stefan Sint, and Peter Weisz. Lattice QCD with a chirally twisted mass term. *JHEP*, 08:058, 2001.
- [59] D. H. Weingarten and D. N. Petcher. Monte Carlo Integration for Lattice Gauge Theories with Fermions. *Phys. Lett.*, B99:333, 1981.

- [60] Roberto Frezzotti and Karl Jansen. A polynomial hybrid Monte Carlo algorithm. *Phys. Lett.*, B402:328–334, 1997.
- [61] M. A. Clark and A. D. Kennedy. The RHMC algorithm for 2 flavors of dynamical staggered fermions. *Nucl. Phys. Proc. Suppl.*, 129:850–852, 2004.
- [62] Roberto Frezzotti and Karl Jansen. The PHMC algorithm for simulations of dynamical fermions. I: Description and properties. *Nucl. Phys.*, B555:395–431, 1999.
- [63] Roberto Frezzotti and Karl Jansen. The PHMC algorithm for simulations of dynamical fermions. II: Performance analysis. *Nucl. Phys.*, B555:432–453, 1999.
- [64] M. A. Clark and A. D. Kennedy. Accelerating dynamical fermion computations using the rational hybrid Monte Carlo (RHMC) algorithm with multiple pseudofermion fields. *Phys. Rev. Lett.*, 98:051601, 2007.
- [65] Lapack, linear algebra package. Online available from <http://www.netlib.org/lapack/>.
- [66] Hestenes M. R. and E. Stiefel. Method of Conjugate Gradients for Solving Linear Systems. *NBS J. Res.*, pages 409–436, 1952.
- [67] C. Davies et al. Langevin simulations of lattice field theories using Fourier acceleration. *J. Stat. Phys.*, 43:1073–1075, 1986.
- [68] Raul Toral and A. L. Ferreira. Generalized hybrid Monte Carlo. 1994.
- [69] Simon Catterall and Sergey Karamov. Testing a Fourier accelerated hybrid Monte Carlo algorithm. *Phys. Lett.*, B528:301–305, 2002.
- [70] R. Folk I. P. Omelyan, I. M. Mryglod. Symplectic analytically integrable decomposition algorithms: classification, derivation, and application to molecular dynamics, quantum and celestial mechanics simulations. *Computer Physics Communications*, 151:272–314, 2003.
- [71] Tetsuya Takaishi and Philippe de Forcrand. Testing and tuning new symplectic integrators for hybrid Monte Carlo algorithm in lattice QCD. *Phys. Rev.*, E73:036706, 2006.
- [72] P. C. Hohenberg and B. I. Halperin. Theory of Dynamic Critical Phenomena. *Rev. Mod. Phys.*, 49:435–479, 1977.
- [73] Fftw, a library for computing the discrete fourier transform (dft) in one or more dimensionslinear. Online available from <http://www.fftw.org>.

A Summary (in german)

Das Standardmodell der Elementarteilchenphysik stellt einen herausragenden Erfolg für die Physik des 20. Jahrhunderts dar. Es erlaubt eine umfassende Beschreibung aller physikalischen Erscheinungsformen bis zu einer Energieskala von einigen 100 GeV. Bei der Klassifikation der Elementarteilchen und Beschreibung ihrer Wechselwirkungen spielen Symmetrien eine wichtige Rolle. Für ein Verständnis der nicht mehr durch das Standardmodell beschreibbaren Physik ist es daher naheliegend neue Symmetrien heranzuziehen. Eine solche Möglichkeit wurde bereits Ende der 70er Jahre in Form der Supersymmetrie gefunden. Diese erweitert den Begriff der Raumzeit-Symmetrie in entscheidender Weise und verknüpft Teilchen oder Felder von ganz- und halbzahligen Spin, d.h. Bosonen und Fermionen miteinander. Bei der Untersuchung resultierender supersymmetrischer Quantenfeldtheorien hat sich früh gezeigt, dass in diesen ein Verständnis ihrer Dynamik in einem sonst unbekanntem Maße möglich ist. Insofern sind sie neben ihrer Rolle für mögliche Theorien jenseits des Standardmodells ebenso für konzeptionelle Fragen im allgemeinen Rahmen von Quantenfeldtheorien von hohem Belang.

Die vorliegende Arbeit setzt sich mit der Konstruktion und numerischen Simulation niedrigdimensionaler supersymmetrischer Feldtheorien auseinander. Motiviert wird diese Fragestellung durch das Ziel mehr über die dynamischen Mechanismen zu erfahren, die zur Brechung der Symmetrie auf Niederenergieskalen führen können. Für die Phänomenologie von entscheidender Bedeutung – das bisher bekannte Teilchenspektrum weist keine Anzeichen von Supersymmetrie auf – ist die spontane Symmetriebrechung ein genuin nicht-perturbativ zu beschreibender Effekt. Sein Verständnis ermöglicht Einblicke in die Dynamik einer Quantenfeldtheorie jenseits einer störungstheoretischen Definition. Um allerdings bis dahin zu gelangen, müssen wesentliche technische Hürden genommen werden. Letztgenannte führen wiederum zu Fragen konzeptioneller Natur und bilden für ein spezifisches supersymmetrisches Modell den Inhalt dieser Arbeit im engeren Sinn. Ziel ist es, durch die Diskretisierung der das Modell beschreibenden Kontinuumstheorie auf ein Raumzeitgitter die Dynamik desselben einer numerischen Simulation zugänglich zu machen. Im Falle der Gittereichtheorie hat sich gezeigt, dass diese Anstrengungen außerordentlich erfolgreich gewesen sind. Anhand einer Vielzahl von Argumenten kann dieser Erfolg der Tatsache zugeschrieben werden, dass eine Gitterformulierung der Kontinuumseichtheorie gefunden wurde, die die Eichsymmetrien vollständig respektiert. Im Fall der Supersymmetrie ist bereits bekannt, dass dies nicht ohne Weiteres gelingen kann.

Zunächst werden in dieser Arbeit am Beispiel der supersymmetrischen Quantenmechanik, die auch als eindimensionales Wess-Zumino Modell interpretiert werden kann, die diesbezüglichen Probleme herausgearbeitet. Als wesentlich stellt sich dabei das Fehlen der Leibniz- oder Produktregel für die Differentiation von Gitterfunktionen heraus. Mit Hilfe einer speziellen Vorschrift – der Nicolai-Abbildung – wird gezeigt, wie eine Gittertheorie konstruiert werden kann, die jeweils eine der ursprünglich zwei Su-

persymmetrien respektiert. Eine weitere Schwierigkeit auf dem Weg zu einer supersymmetrischen Gittertheorie liegt ferner in der Behandlung von Fermionen auf dem Gitter. Die für Supersymmetrie unbedingt notwendigen Fermionen führen erneut auf konzeptionelle und – vor allem die Numerik betreffende – technische Herausforderungen. Beides wird ebenfalls am Beispiel der supersymmetrischen Quantenmechanik diskutiert. Neben den in der Gitterfeldtheorie weit verbreiteten Wilson-Fermionen werden auch sogenannte Slac-Fermionen behandelt. Es stellt sich heraus, dass die für Gittereichtheorien völlig ungeeigneten Slac-Fermionen für die in dieser Arbeit besprochenen Theorien herausragende Eigenschaften aufweisen. Da z.B. mit diesen das Problem der Fermionverdopplung nicht auftritt, ist auch – anders als im Falle der Wilson-Fermionen – keine Modifikation des die Wechselwirkungen beschreibenden Superpotentials notwendig. Für sechs verschiedene Gittermodelle werden die Ergebnisse numerischer Simulationen präsentiert und miteinander verglichen. Sie umfassen die Bestimmung der Energien der leichtesten angeregten Zustände und die Auswertung von Ward-Identitäten, die die An- bzw. Abwesenheit von Supersymmetrie auf dem Niveau der Korrelationsfunktionen anzeigen. Es zeigt sich, dass die speziell konstruierten Gittertheorien bereits bei endlichem Gitterabstand in Bezug auf diese Observablen supersymmetrisch sind. Ebenso wird deutlich, dass eine naive Umschreibung nicht zu dem gewünschten Resultat führt. Darüber hinaus kann gezeigt werden, dass Slac-Fermionen in Bezug auf die Kontinuumsextrapolation weit weniger von Gitterartefakten betroffen sind als die zum Vergleich herangezogenen Wilson-Fermionen.

Im Anschluss daran werden die gewonnenen Erkenntnisse auf das zweidimensionale $\mathcal{N} = (2, 2)$ -Wess-Zumino-Modell übertragen. Erneut können supersymmetrische Gittertheorien konstruiert werden, die hier jedoch nur noch eine der ursprünglich vier Supersymmetrien respektieren. Anschließend wird gezeigt, dass aufgrund dieser Konstruktion ein Teil der in der Kontinuumstheorie ebenfalls vorhandenen diskreten Symmetrien verloren geht. Durch die für Wilson-Fermionen notwendige Einführung des Wilsonterms werden die verbleibenden diskreten Symmetrien noch einmal halbiert. Diese Beobachtungen lassen Slac-Fermionen damit auch für die Untersuchung dieses Modells geeigneter erscheinen. Neben den üblichen Wilson-Fermionen werden des Weiteren sogenannte Twisted-Wilson-Fermionen eingeführt, die im direkten Vergleich mit Wilson-Fermionen zu wesentlich geringeren Gitterartefakten führen. Für eine spezielle Wahl des Wilsonparameters r kommen diese den Slac-Fermionen sehr nahe.

Da bereits im Falle zweidimensionaler Theorien die numerische Behandlung durch die Berechnungsgeschwindigkeit der Fermiondeterminante limitiert ist, sind hierzu eine Reihe von Untersuchungen durchgeführt wurden, deren Ergebnisse vorgestellt werden. Im Einzelnen wird hierbei das Leistungsvermögen von zwei exakten und einem approximativen Algorithmus miteinander verglichen. Es wird deutlich, dass der approximative Ansatz, die Fermiondeterminante mit Hilfe sogenannter Pseudofermionen auszudrücken, den beiden anderen Algorithmen in hohem Maße überlegen ist. Durch die Kombination desselben mit iterativen Lösungsverfahren zur Bestimmung linearer Gleichungs-

systeme wird es möglich, das Modell zum einen auf sehr fein auflösenden Gittern und zum anderen mit einer extrem hohen Statistik zu untersuchen. Beides wäre unter Verwendung der direkten Verfahren unmöglich. Eine weitere wesentliche Verbesserung stellt sich durch die Verwendung hier zum Einsatz gekommener numerischer Integrationsverfahren höherer Ordnung ein. Diese erlauben größere Zeitschritte und damit insgesamt kürzere Berechnungszeiten pro Konfiguration und führen dennoch auf höhere Akzeptanzraten. Wird dieses Integrationsschema mit einem Fourierbeschleunigung genannten Verfahren kombiniert, können einstellige Autokorrelationszeiten auch noch nahe des kritischen Punktes eingestellt werden. Dies verbessert die Auswertung von Korrelationsfunktionen bei gegebener Ensemblegröße erneut deutlich und führt im Weiteren zu einer entscheidenden Verbesserung gegenüber den in der Literatur bereits veröffentlichten Resultaten.

Im numerischen Abschnitt dieses Teiles der Arbeit werden fünf verschiedene Gittermodelle analysiert. Neben den drei supersymmetrischen Gitterwirkungen mit Wilson-, Twisted-Wilson- oder Slac-Fermionen werden auch die nicht supersymmetrischen Modelle mit Wilson- oder Slac-Fermionen mitsimuliert. Der erste Teil der numerischen Analyse widmet sich der eingehenden Untersuchung des sogenannten Improvementterms, der die supersymmetrischen von den nicht supersymmetrischen Gitterwirkungen unterscheidet. Es wird gezeigt, dass dieser bei endlichem Gitterabstand tatsächlich zu diskriminierbaren Unterschieden zwischen der super- und nichtsupersymmetrischen Formulierung führt und gleichzeitig als Oberflächenterm im Kontinuumslimit verschwindet. Andererseits wird deutlich, dass dieser Term bei größer werdender Kopplung das Gittermodell destabilisiert und in einen unphysikalischen Bereich des Konfigurationsraumes drängt. Insofern werden diese Formulierungen im numerischen Kontext dann bedeutungslos. Allerdings sind erhebliche Unterschiede zwischen Wilson- und Slac-Fermionen vorhanden, wobei letztere eine Simulation bei weitaus stärkeren Kopplungswerten zulassen. Als eines der Hauptresultate dieser Arbeit lassen sich hiervon Implikationen für die numerische Relevanz supersymmetrischer Gitterwirkungen anderer supersymmetrischer Theorien ableiten. Im Weiteren werden als physikalische Observablen die Massen der Bosonen und Fermionen bestimmt. Es zeigt sich, dass alle fünf Modelle in der Kontinuumsextrapolation zum gleichen Resultat gelangen. Bezüglich des Massenspektrums sind keine Unterschiede zwischen den super- und nichtsupersymmetrischen Modellen nachweisbar. Jedoch ist die Beantwortung dieser Frage erheblich durch die Bestimmung der Bosonmassen erschwert. Die hingegen sehr exakt mögliche Bestimmung der Fermionmassen führt bei schwacher Kopplung zu einer ausgezeichneten Übereinstimmung mit dem störungstheoretischen Resultat in niedrigster Ordnung. Darüber hinaus ist es möglich zu bestimmen, wann die Störungstheorie ihre Gültigkeit verliert.

Diesen beiden Hauptteilen der Arbeit sind eine kurze allgemeine Einführung sowie eine Einführung in die in der Arbeit verwandten Methoden vorangestellt.

B Own Publications

- [1] Tobias Kästner, Georg Bergner, Sebastian Uhlmann, Andreas Wipf, and Christian Wozar. Supersymmetric lattice models in one and two dimensions. *PoS, LATTICE2007*:265, 2007.
- [2] Christian Wozar, Tobias Kästner, Sebastian Uhlmann, Andreas Wipf, and Thomas Heinzl. Z_3 Polyakov Loop Models and Inverse Monte-Carlo Methods. *PoS, LATTICE2007*:341, 2007.
- [3] Georg Bergner, Tobias Kästner, Sebastian Uhlmann, and Andreas Wipf. Low-dimensional supersymmetric lattice models. *Annals Phys.*, 323:946–988, 2008.
- [4] Christian Wozar, Tobias Kästner, Andreas Wipf, and Thomas Heinzl. Inverse Monte-Carlo determination of effective lattice models for SU(3) Yang-Mills theory at finite temperature. *Phys. Rev.*, D76:085004, 2007.
- [5] A. Wipf, T. Kästner, C. Wozar, and T. Heinzl. Generalized Potts-models and their relevance for gauge theories. *SIGMA*, 3:006, 2007.
- [6] Christian Wozar, Tobias Kästner, Andreas Wipf, Thomas Heinzl, and Balazs Pozsgay. Phase structure of Z(3) Polyakov loop models. *Phys. Rev.*, D74:114501, 2006.
- [7] Thomas Heinzl, Tobias Kästner, and Andreas Wipf. Effective lattice actions for finite-temperature Yang- Mills theory. 2005.
- [8] Thomas Heinzl, Tobias Kästner, and Andreas Wipf. Effective actions for the SU(2) confinement-deconfinement phase transition. *Phys. Rev.*, D72:065005, 2005.

Danksagung

Während der Erstellung dieser Dissertationsschrift habe ich den Zuspruch und die Unterstützung vieler Menschen erfahren. Ihnen allen gilt mein tief empfundener Dank.

Für die gute Zusammenarbeit möchte ich mich ganz besonders bei Prof. Dr. A. Wipf meinem betreuenden Hochschullehrer bedanken. Seine Erfahrung und seine Anregungen haben manchen Irrweg erkennen und manche Sackgasse überwinden geholfen.

Von ebenso großer Bedeutung ist mir stets die gute Zusammenarbeit mit all den anderen Mitarbeitern der Arbeitsgruppe gewesen. Im Einzelnen danke ich ganz besonders Georg Bergner und Christian Wozar. Viele Ideen und Umsetzungen neuer ProgrammROUTINEN, die Suche nach Programmierfehlern und die Wartung des Codes gelang durch ihre Hilfe. Dafür herzlichen Dank. Sebastian Uhlmann und Ulrich Theis danke ich für alle Fragen die ich stellen durfte und alle Antworten die mich in meinem Verständnis der Physik ein großes Stück vorangebracht haben. Tom Heinzl fühle ich mich ferner für das Lesen des Manuskriptes und dem Anbringen unzähliger Korrekturvorschläge in tiefem Dank verbunden.

Meinen herzlichen Dank auch allen Lehrern, Professoren und Seminarleitern, die mich in meiner Ausbildung bis zum heutigen Tag durch die von ihnen erworbenen Kenntnisse begleitet haben und immer noch begleiten. Das ich die Wunder und Errungenschaften der Physik verstehen lernen durfte, habe ich ihrer ausgezeichneten Arbeit zu verdanken.

Mein herzlicher Dank gilt auch der Konrad-Adenauer-Stiftung für das mir gewährte Graduiertenstipendium, durch das ich mich für die Zeit meiner Promotion von wirtschaftlichen Nöten entbunden fühlen durfte. Mir von gleichbedeutender Wichtigkeit schließe ich daran meinen Dank für die von mir besuchten Seminare, das dort Erfahrene und Gelernte und ganz besonders die wunderbaren Begegnungen mit meinen Koststipendiaten an.

Meinen Eltern und Schwiegereltern danke ich in mit meinem ganzen Herzen für die Hilfe, Unterstützung und Liebe die ich und vor allem auch meine eigene junge Familie in dieser nicht immer ganz leichten Zeit durch sie erfahren haben. Sehr viel ist demjenigen bereits geschenkt, der sich so aufgehoben und angenommen wissen darf.

Dieser nun mein größter Dank gilt Euch beiden, meiner kleinen Familie. Euch um mich zu wissen und von Euch geliebt zu sein, war mir jeden Tag und jede Stunde jeden Augenblick Kraft und Antrieb. Ohne Eure unerschütterliche Liebe hätte all dies niemals gelingen können. Danke.

Lebenslauf

Name Tobias Kästner
geboren am 18. Juli 1979 in Eisenach
Familienstand verheiratet, eine Tochter

Schule

1986 - 1991 Polytechnische Oberschule Karl Liebnecht, Seebach
1991 - 1998 Staatliches Gymnasium Salzmannschule, Waltershausen
Juli 1998 Abitur

Studium

1999 - 2004 Physikstudium, FSU Jena
Nov. 2004 Diplom,
Thema der Diplomarbeit: "Effektive Theorien auf dem
Raumzeitgitter, Die inverse Monte-Carlo-Methode
für Yang-Mills Theorien"
seit Dez. 2004 Doktorand am Theoretisch-Physikalischen Institut der FSU Jena,
betreuender Hochschullehrer: Prof. Dr. A. Wipf

Jena, den 29.06. 2008

Ehrenwörtliche Erklärung

Ich erkläre hiermit ehrenwörtlich, dass ich die vorliegende Arbeit selbstständig, ohne unzulässige Hilfe Dritter und ohne Benutzung anderer als der angegebenen Hilfsmittel und Literatur angefertigt habe. Alle Ergebnisse, die in unmittelbarer Zusammenarbeit mit anderen Mitgliedern der Arbeitsgruppe am Lehrstuhl für Quantentheorie entstanden, sind entsprechend gekennzeichnet. Die aus anderen Quellen direkt oder indirekt übernommenen Daten und Konzepte sind unter Angabe der Quelle gekennzeichnet.

Weitere Personen waren an der inhaltlich-materiellen Erstellung der vorliegenden Arbeit nicht beteiligt. Insbesondere habe ich nicht die entgeltliche Hilfe von Vermittlungs- bzw. Beratungsdiensten (Promotionsberater oder andere Personen) in Anspruch genommen. Niemand hat von mir unmittelbar oder mittelbar geldwerte Leistungen für Arbeiten erhalten, die im Zusammenhang mit dem Inhalt der vorgelegten Dissertation stehen. Die Arbeit wurde bisher weder im In- noch im Ausland in gleicher oder ähnlicher Form einer anderen Prüfungsbehörde vorgelegt.

Die geltende Promotionsordnung der Physikalisch-Astronomischen Fakultät ist mir bekannt. Ich versichere ehrenwörtlich, dass ich nach bestem Wissen die reine Wahrheit gesagt und nichts verschwiegen habe.

Jena, den 29.06.2008